A VERBAL-COMMAND ROBOT TO CONTROL A LAPAROSCOPE IN AID OF SURGERY : A PROTOTYPE DESIGN

CHOOKIET NAKORNNARATHORN

A THESIS SUBMITTED IN PARTIAL FULFILLMENT
OF THE REQUIREMENTS FOR
THE DEGREE OF MASTER OF ENGINEERING
(BIOMEDICAL ENGINEERING)
FACULTY OF GRADUATE STUDIES
MAHIDOL UNIVERSITY
2003

ISBN 974-04-1208-4

Thesis
entitled

A VERBAL-COMMAND ROBOT TO CONTROL A LAPAROSCOPE IN AID OF SURGERY : A PROTOTYPE DESIGN

Mr. Chookiet Nakornnarathorn
Candidate

Admiral Dr. Paibul Nacaskul,
B.Sc. 1st Hons., Ph.D.
Major-Advisor

Prof. Prasit Wattanapa, Ph.D.
Co-Advisor

Mr. Taweedej Siritanapipat, Ph.D.
Co-Advisor

Assst. Prof. Werasak Kurutach, Ph.D.
Co-Advisor

Assoc. Prof. Rassmidara Hoonsawat,
Ph.D.
Dean
Faculty of Graduate Studies

Asst. Prof. Pirojana Suvannasuthi,
M.Eng
Chair
Master of Engineering
Programme in Biomedical Engineering
Faculty of Engineering

Thesis
entitled

A VERBAL-COMMAND ROBOT TO CONTROL A LAPAROSCOPE IN AID OF SURGERY : A PROTOTYPE DESIGN

was submitted to the Faculty of graduate Studies, Mahidol University
for the degree of Master of Engineering (Biomedical Engineering)

on
25 Sep, 2003

.....
Mr. Chookiet Nakornnarathorn
Candidate

.....
Admiral Dr. Paibul Nacaskul,
B.Sc. 1st Hons., Ph.D.
Chair

.....
Prof. Prasit Wattanapa, Ph.D.
Member

.....
Assst. Prof. Werasak Kurutach, Ph.D.
Member

.....
Asst. Prof. Pirojana Suvannasuthi,
M.Eng
Member

.....
Mr. Paweedej Siritanapipat,
Ph.D.
Member

.....
Assoc. Prof. Rassmidara Hoonsawat,
Ph.D.
Dean
Faculty of Graduate Studies
Mahidol University

.....
Asst. Prof. Piya Rattanasuwan,
B. Eng. (Civil), M. Eng.
Dean
Faculty of Engineering
Mahidol University

ACKNOWLEDGEMENT

I would like to express my sincere gratitude and deep appreciation to Admiral Dr. Paibul Nacaskul, my principal advisor, for his guidance, invaluable advice, supervision and encouragement throughout. He was never lacking in kindness and support. I am equally grateful to Dr. Prasit Wattanapa, my associate supervisor, for his constructive comments, supervision and encouragement. He was always nice and friendly.

I wish to thank the Department of Surgery, Siriraj Hospital for the needed co-operation and generous assistance.

I am particularly indebted to the staff of Tool and Facility department, SVI Co., Ltd. for their general assistance, which enables me to undertake this study.

Mr. Chookiet Nakornnarathorn

A VERBAL-COMMAND ROBOT TO CONTROL A LAPAROSCOPE IN AID OF SURGERY : A PROTOTYPE DESIGN

CHOOKIET NAKORNNARATHORN 4137947 EGBE/M

M.Eng.(BIOMEDICAL ENGINEERING)

THESIS ADVISORS: PAIBUL NACASKUL, Ph.D., PRASIT WATTANAPA, Ph.D., WERASAK KURUTACH, Ph.D., TAWEEDEJ SIRITANAPIPAT, Ph.D.

ABSTRACT

Nowadays, robot assisted surgery is highly developed. There exist some efforts to use a surgical robot under a voice command. In this study, a voice command robot for virtually real time manipulation of laparoscope was designed to hold a laparoscope with one arm and to move it in the required direction under the voice command of the surgeon to view a particular area inside the patient. Another robotic arm was added to hold the retractor to manipulate the cut area. The results obtained show that the system works quite closely to the design which, as a prototype design, can be further developed into a practical and safe medical tool in aid of surgery by using Kinematics.

KEY WORDS: AESOP LAPAROSCOPE / VERBAL-COMMAND ROBOT / SURGRY ROBOT / TELESURGICAL WORKSTATION

103 P. ISBN 974-04-1208-4

การบังคับกล้องส่องตรวจภายใน ในงานศัลยกรรม ด้วยการใช้เสียงบังคับหุ่นยนต์ :เครื่องต้นแบบ (A VERBAL-COMMAND ROBOT TO CONTROL A LAPAROSCOPE IN AID OF SURGERY : A PROTOTYPE DESIGN).

ชูเกียรติ นาครนราธร 4137947 EGBE/M

วศ.ม. (วิศวกรรมชีวการแพทย์)

คณะกรรมการควบคุมวิทยานิพนธ์ : ไพบูลย์ นาคสกุล, Ph.D., ประสิทธิ์ วัฒนาภา, Ph.D. วีระศักดิ์ คุรุธัช, Ph.D., ทวีเดช ศิริธนาพิพัฒน์, Ph.D.

บทคัดย่อ

ในปัจจุบัน เทคโนโลยีทางด้านการแพทย์ได้พัฒนาไปอย่างรวดเร็ว มีการทดลองใช้เสียงบังคับเครื่องมือเพื่อช่วยในการผ่าตัด ผู้วิจัยจึงได้ออกแบบหุ่นยนต์ที่ใช้เสียงบังคับให้สามารถควบคุมกล้องส่องตรวจภายใน โดยหมอผู้ทำการผ่าตัดสามารถที่จะสั่งกล้องส่องตรวจภายใน ให้เคลื่อนที่ได้ตามต้องการ เพื่อที่จะดูอวัยวะภายในของผู้ป่วย นอกจากนี้ยังมีแขนกลที่ใช้ในการถ่างแผลช่องท้องของผู้ป่วยได้อีกด้วย ผลงานที่ได้นับว่าเป็นไปตามข้อกำหนดในการออกแบบเป็นส่วนใหญ่ การออกแบบนี้ถือได้ว่า เป็นต้นแบบที่สามารถพัฒนาขึ้นมาในอนาคตให้เป็นเครื่องมือแพทย์ที่เหมาะสมและปลอดภัยในการใช้เป็นเครื่องมือช่วยผ่าตัด โดยพัฒนาในแนวทางที่เสนอไว้ในบทส่งท้าย

103 P. ISBN 974-04-1208-4

CONTENTS

	Page
ACKNOWLEDGEMENT	**iii**
ABSTRACT	**iv**
LIST OF TABLES	**viii**
LIST OF FIGURES	**ix**
CHAPTER I INTRODUCTION	**1**
1.1 BACKGROUND	**1**
1.2 PROJECT OBJECTIVES	**1**
1.3 PROJECT BENEFITS	**1**
1.4 SCOPE OF THIS PROJECT	**2**
CHAPTER II LITERATURE REVIEW	**4**
2.1 AN OVERVIEW OF OPERATING ROOM	**4**
2.2 STERILIZATION	**6**
2.3 GENERAL REMARK	**6**
CHAPTER III MATERIALS AND METHODOLOGY	**7**
3.1 MATERIALS	**7**
3.1.1 SOFTWARE UNIT	**7**
3.1.2 VERBAL COMMAND UNIT	**7**

CONTENTS (Cont.)

3.1.3 SURGICAL ROBOT 9

3.2 METHODOLOGY 11

3.2.1 VERBAL COMMAND SYSTEM 11

3.2.2 SURGICAL ROBOT SYSTEM 22

3.2.3 VERBAL COMMAND CIRCUIT 23

3.2.4 VERBAL COMMAND TABLE 36

3.2.5 VERBAL COMMAND CHART 37

3.2.6 SET UP SEQUENCE OF SURGICAL ROBOT 38

3.2.7 TRAIN AND TEST ROBOT WITH VOICE CONTROL SYSTEM 39

3.3 TEST AND EVALUATION 39

3.3.1 TEST OF LAPAROSCOPE UNIT 40

3.3.2 TEST OF RETRACTOR UNIT 41

CHAPTER IV RESULTS AND DISCUSSION 42

REFERENCES 45

APPENDICES 53

APPENDIX A 53

APPENDIX B 78

APPENDIXC 83

APPENDIX D 96

BIOGRAPHY 103

LIST OF TABLES

		Page
Table 1	Comparison of human and robotic characteristics and limitation	3
Table 2	The command description	18
Table 3	Test Results of Laparoscope Unit	42
Table 4	Test Results of Retractor Arms Unit	43

LIST OF FIGURES

	Page
Figure 1 The patient is the focus of attention of the entire health care team	5
Figure 2 Hardware of Verbal Command Unit	8
Figure 3 Hardware of Laparoscope Robot	9
Figure 4 Hardware of Retractor Robot	10
Figure 5 Program of Verbal Command for User Initial	11
Figure 6 The Verbal Command Program required to setup Com2 Communication Ports	12
Figure 7 Diagram of Verbal Command System	12
Figure 8 The Editor Program	15
Figure 9 Loading Program	15
Figure 10 Inside of Editor Program	16
Figure 11 The Training Program	20
Figure 12 The Number of Training Passes	21
Figure 13 The Recognition Mode	22
Figure 14 Laparoscope and Retractor Units in Surgical Robot System	23
Figure 15 Verbal Command Circuit	23
Figure 16 Decoder 74HCT138 circuit	24

LIST OF FIGURES (Cont.)

Page

Figure 17(a) Decoder 74HCT154 circuit 25

Figure 17(b) Decoder 74HCT154 circuit 26

Figure 17(c) Decoder 74HCT154 circuit 27

Figure 17(d) Decoder 74HCT154 circuit 28

Figure 17(e) Decoder 74HCT154 circuit 29

Figure 18(a) High-Voltage Hight-Current Darlington Transistor ULN2003AN circuit 30

Figure 18(b) High-Voltage Hight-Current Darlington Transistor ULN2003AN circuit 31

Figure 18(c) High-Voltage Hight-Current Darlington Transistor ULN2003AN circuit 32

Figure 18(d) High-Voltage Hight-Current Darlington Transistor ULN2003AN circuit 33

Figure 18(e) High-Voltage Hight-Current Darlington Transistor ULN2003AN circuit 34

Figure 19 Motor circuit of Laparoscope Robot 35

Figure 20 Motor circuit of Retractor Robot 35

Figure 21 Verbal Command Table 36

Figure 22 Verbal Command Chart 37

Figure 23 Reliability Index of Voice Command 39

LIST OF FIGURES (Cont.)

Page

Figure 24 Laparoscope Robot Position **40**

Figure 25 Laparoscope Robot PositionDecoder **41**

CHAPTER I
INTRODUCTION

1.1 BACKGROUND

It has been felt by a number of medical doctors that certain medical aids and devices may possibly be developed by Thai people. Simple robots are among such devices that could have been developed in country for uses in medical fields.

It is thus proposed to design, construct and test a certain robotic device as an aid to surgery in specific manners.

Over the past decade, robots have started to appear in hospital operating rooms. Surgical applications have been progressing rapidly due to the technology base that has been developed in robotics researches during the last three decades. Results in mechanical designs, kinematics, control algorithms, and programming that were developed for industrial robots are directly applicable to many surgical applications. Robotic researchers have also worked to enhance robotic capabilities through adaptability (the use of sensory information to respond to changing conditions) and autonomy (the ability to carry out tasks without human supervision). The resulting sensing and interpretation techniques that are proving useful in surgery include methods for image processing, spatial reasoning and planning, and real-time sensing and control.

1.2 PROJECT OBJECTIVES

(i) To use verbal command to control a laparoscope for a view inside the patient stomach while the surgeon hands are busy manipulating the surgery.

(ii) To use verbal command to control a retractor for opening the cutting area of the body.

(iii) To develop an equipment that should be a fair help to the surgeon.

1.3 PROJECT BENEFITS

To understand the advantages of using robots in surgery, it is helpful to consider the differences between human and machine characteristics,as summarized in Table 1.

Many promising applications are based on unique robotic capabilities. One key difference is precision and accuracy, or more generally, the ability to use copious, detailed quantitative information. The combination of three dimensional imaging data, computers, and intrasurgical sensors, for example, can allow robot to accurately guide instruments into pathological structures deep within the body. Another important difference is that specialized manipulation designs allow robots to work through incisions much smaller than would be required for human hands, or to work at small scales where hand tremor poses fundamental limitations.

The prototype design of robotic system is best described as "**extending human capabilities**" rather than "**replacing human surgeon**".

In case of emergency, an assisting surgeon in the surgery team will be free perform other functions.

The project is aimed at the reduction of imports of medical equipment by suitable in-country products. If this project were successful and the equipment could be developed to pass the Food and Drug Authority, there would be a chance to open up a manufacture and sale of another line of Thailand's own products.

1.4 SCOPE OF THIS PROJECT

The scope of this project is to design a prototype of a verbal-command robot for virtually real time manipulation of laparoscope. The robot is expected to hold a laparoscope with one arm and to be moved in the direction under the voice command of the surgeon to view a particular area inside the patient. Another robotic arm is used to hold the retractor to manipulate the cut area whenever required by the same surgeon.

Table 1 Comparison of human and robotic characteristics and limitations. (Adapted from Taylor and Stulberg).

	Characteristics	Limitations
Humans	Strong hand-eye coordination	Limited dexterity outside natural scale
	Very dexterous (at "human" scale)	Prone to tremor and fatique
	Very flexible and adaptable	Limited geometric accuracy
	Can integrate extensive and diverse information	Limited ability to use quantitative information
	Able to use quantitative information	Large operating room space requirement
	Good judgement	Limited sterility
	Easy to instruct and debrief	Susceptible to radiation and infection
Robots	Good geometric accuracy	Poor judgment
	Stable and untiring	Limited dexterity and hand-eye coordination
	Can be designed for a wide range of scales	Limited to relatively simple procedures
	May be sterilized	Expensive
	Resistance to radiation and infection	Technology in flux
	Can use diverse sensors (chemical, force, acoustic, etc.) in control	Difficult to instruct and debug

CHAPTER II
LITERATURE REVIEW

2.1 AN OVERVIEW OF OPERATING ROOM

Patients are submitted to surgical intervention for a variety of reasons, including:

1. To preserve life, e.g., relief of internal obstruction or decompression of a skull fracture.
2. To maintain dynamic bodily equilibrium, e.g., removal of a diseased kidney.
3. To undergo diagnostic procedures, e.g., breast biopsy, branchoscopy.
4. To prevent infection and to promote healing e.g., burn debridement.
5. To obtain comfort and to ensure the ability to earn a living, e.g., elective herniorrhaphy.

Not all operations are performed in hospitals. Many are performed in surgeons' offices or in independent, nonhospital-based, freestanding surgical facilities if they are not complex enough to require hospitalization of the patients. Not all patients are operated on in a hospital-contained operating room until they are admitted to the hospital. Surgeons view postoperative activity as beneficial rather than hazardous for surgical patients. Consequently, operation on an ambulatory care or an outpatient basis is feasible and safe for carefully selected patients.

The types of operations performed in a hospital or other facilities vary according to the expertise of the surgeon on the staff, the community in which the facility is located, and the equipment availability. The daily schedule of operations is as variable as the type of facility and the types of operations performed. Regardless of the circumstances that bring patients to the operating room (OR), the intraoperative phase of care becomes an integral part of nursing service, filling a need that cannot be met by the individual patient or his or her family. Nursing care of patients undergoing surgical intervention as the therapeutic modality of choice is carried out at two levels, professional and technical.

A person facing an impaired health status strives for wellness. As a patient, this person looks to health care providers to fulfill his or her multiplicity of diversified needs. A patient-centered approach to total surgical care involves meeting all the patient's basic needs during the preoperative, intraoperative, and postoperative phases. The health care team is dedicated to maintaining optimal health and/or restoring it when altered by disease, injury, or deformity. Although the team members may vary with the situation and the patient, the goal is for a favorable outcome from surgical intravention.

In viewing the team in its broadest scope, one can consider the patient as the central part or hub of a wheel with many persons and departments as the supporting frame work. All focus their efforts at the hub, meaning that the patient is the center of attention always , not only when under the OR spotlight. The ultimate beneficiary of teamwork is the patient. Imperfection in any one part of the wheel imperils the performance and security of all. Each team member makes a unique contribution in reaching the goals. The patient care is a doctor's reason for existence as a health care team member.

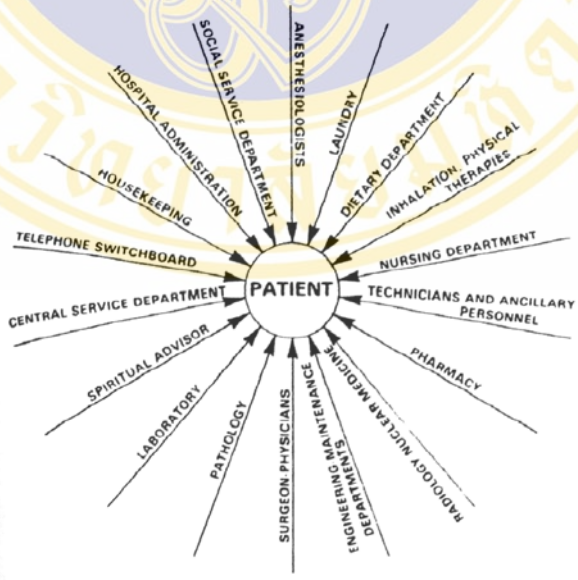

Figure 1 The patient is the focus of attention of the entire health care team

2.2 STERILIZATION

All items (instruments, supplies, equipment, etc.) that come in contact with the sterile field and the wound must be sterile. As soon as possible following use, soiled instruments are cleaned in the washer-sterize. Following terminal decontamination in the washer-sterilizer, the instruments are cleaned in an ultrasonic cleaner to remove any remaining soil.

The three most commonly used methods of sterilization employed in the operation room (or central supply) include :

1. Saturated steam under pressure,
2. Gas chemical sterilization,
3. Liquid chemical sterilization,

2.3 GENERAL REMARK

It is necessary that all equipments used in surgery must be well sterilized before and after usage, if they were to be medical tools for doctors to use and manipulate successfully in sustaining life and / or maintaining health of a patient.

The robot planned for this project is to be designed with th above remark in mind. Any parts of robot which cannot be directly sterilized will be well sealed against contamination. Moreover, since the robot is an electrical device, the design for it to be electrically safe to both the patients and doctors is an important factor to be taken into account.

CHAPTER III
MATERIALS AND METHOD

3.1 MATERIALS

3.1.1 Software Unit

The software for verbal command is written in Visual Basic and C language: DOS (Disk Operating System) version 6.22.

3.1.2 Verbal Command Unit

The hardware needed for verbal command, as shown in Figure 2, comprises the flowing characteristics:

CPU	:	Pentium 120 MHz
RAM	:	At least 32 MB
Hard Disk	:	80 MB
Monitor	:	14-inch VGA (Colour)
Peripherals	:	Keyboard, microphone
Verbal Unit	:	Micro Intro Voice II, a product of Voice Connection, Inc. in U.S.A.
Selector and Decoder	:	4 decoders and 64 ports, to be designed for purposes as part of the project.
Driver	:	Drive power from 12 to 50 V.
Relay	:	32 units for a 12-contact set with 24 VDC, 5 A. Coil.
Expanded 32 Ports	:	For future use.
Display Status	:	Display Status for Selector and Decoder
Power supply	:	+3, +4.5, +5, -5, +6, +7.5, +9, +12, -12, +24, +50 VDC 220 AC
Control Box	:	H66*L70.5*W31 cm
Control Unit Weight	:	41 Kg, gross

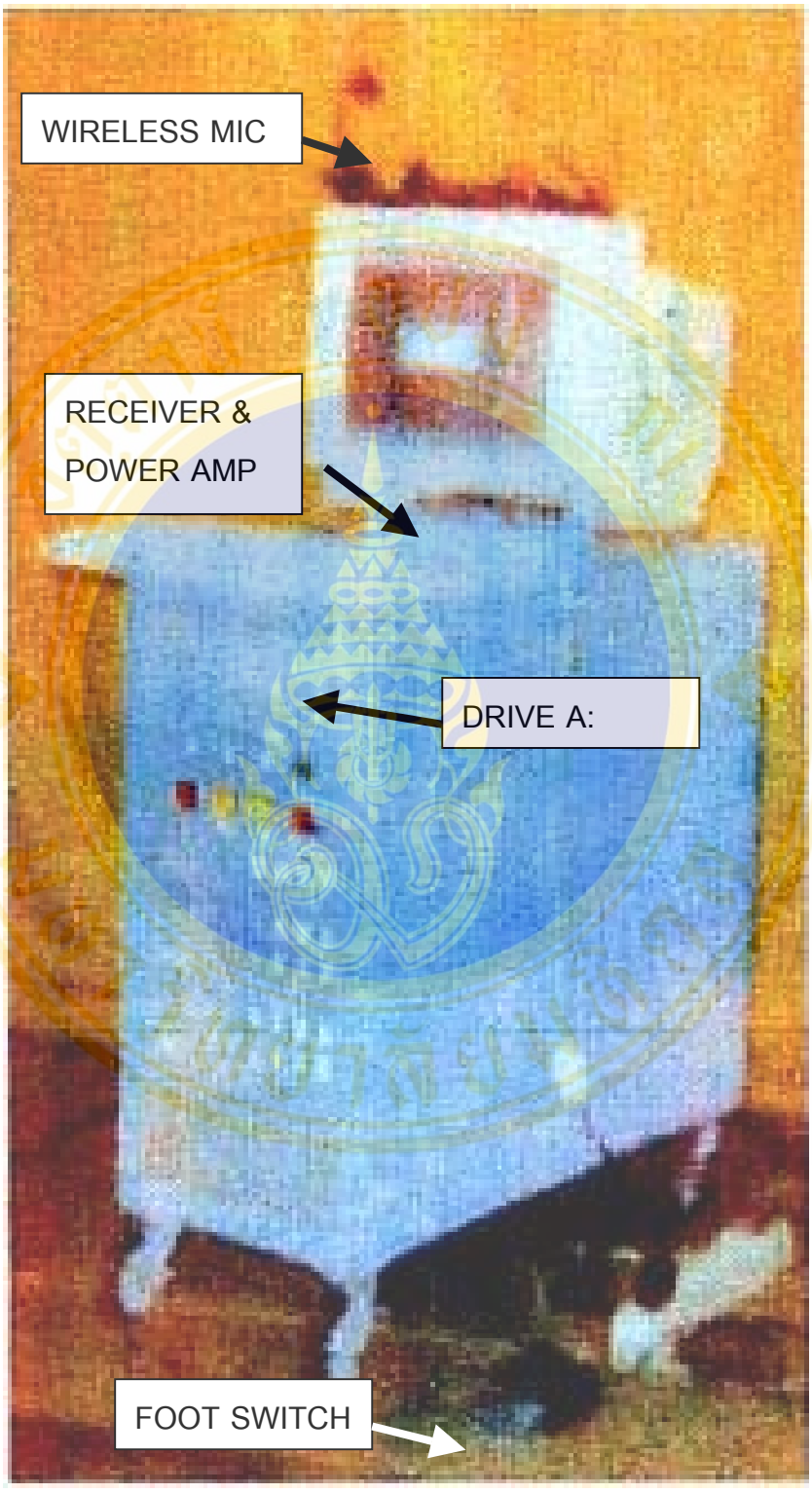

Figure 2 Hardware of Verbal Command Unit

3.1.3 Surgical Robot

The surgical robot as shown in Figures 3 and 4 has the following features:

(i) Laparoscope Robot

4-Axis Control	:	Control Laparoscope
Robot Dimensions	:	H130*L60*W70 cm
Joy Stick	:	H15*L20*W25 cm
Flexible Pipe	:	For ease of positioning the Laparoscope Holder
Robotic Weight	:	23.7 Kg, gross.
Speed	:	Up-Down(20 mm/s),
		Collar Rotate CCW-CW (5 mm/s)
		Collar Up-Down (5 mm/s),
		Collar Left-Right (5mm/s)

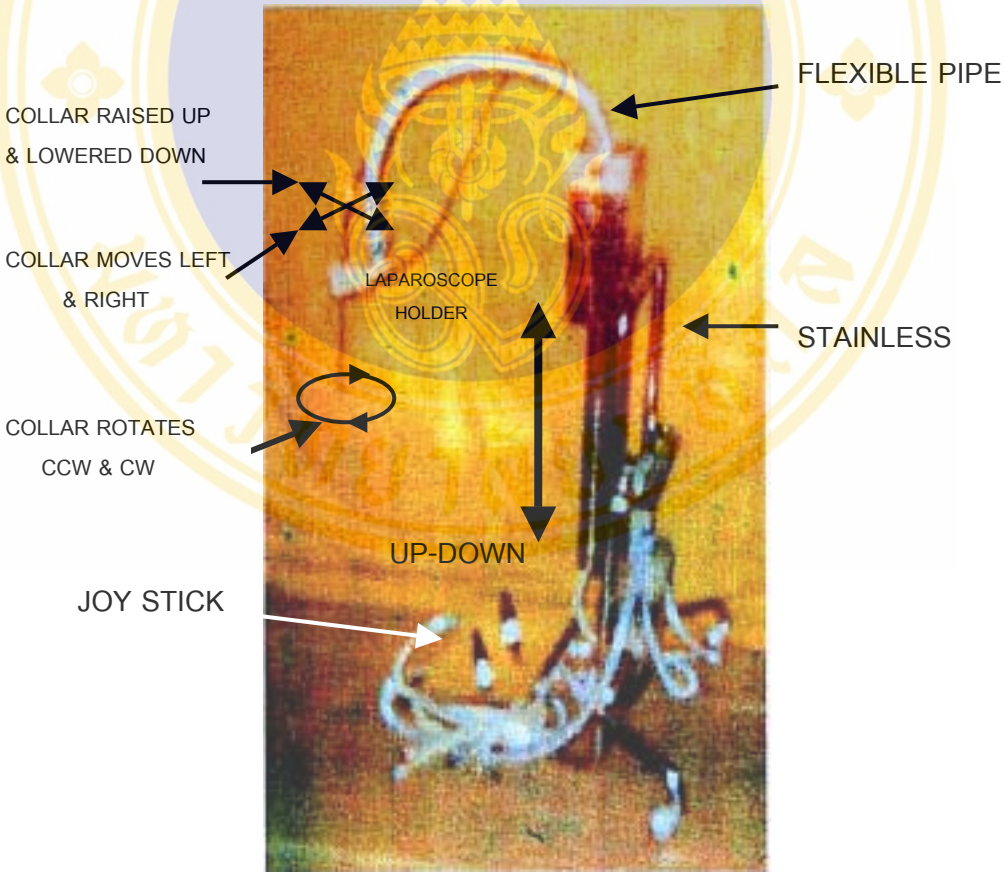

Figure 3 Hardware of Laparoscope Robot

(ii) Retractor Robot

2-Axis Control	:	Control Retractor
Stanless Tray	:	H1.9*L30*W48 cm
Hight Adjust	:	Manually adjustable 100~160 cm.
Foot Switch	:	H6*L35*w16 CM For raising / lowering the Retractor Arm and moving the Retractor Arm left / right
Robot Dimensions	:	H150*L80*W70 CM
Robotic Weight	:	18.3 Kg, gross.
Speed	:	Up-Down (20 mm/s), Left-Right (1 mm/s)

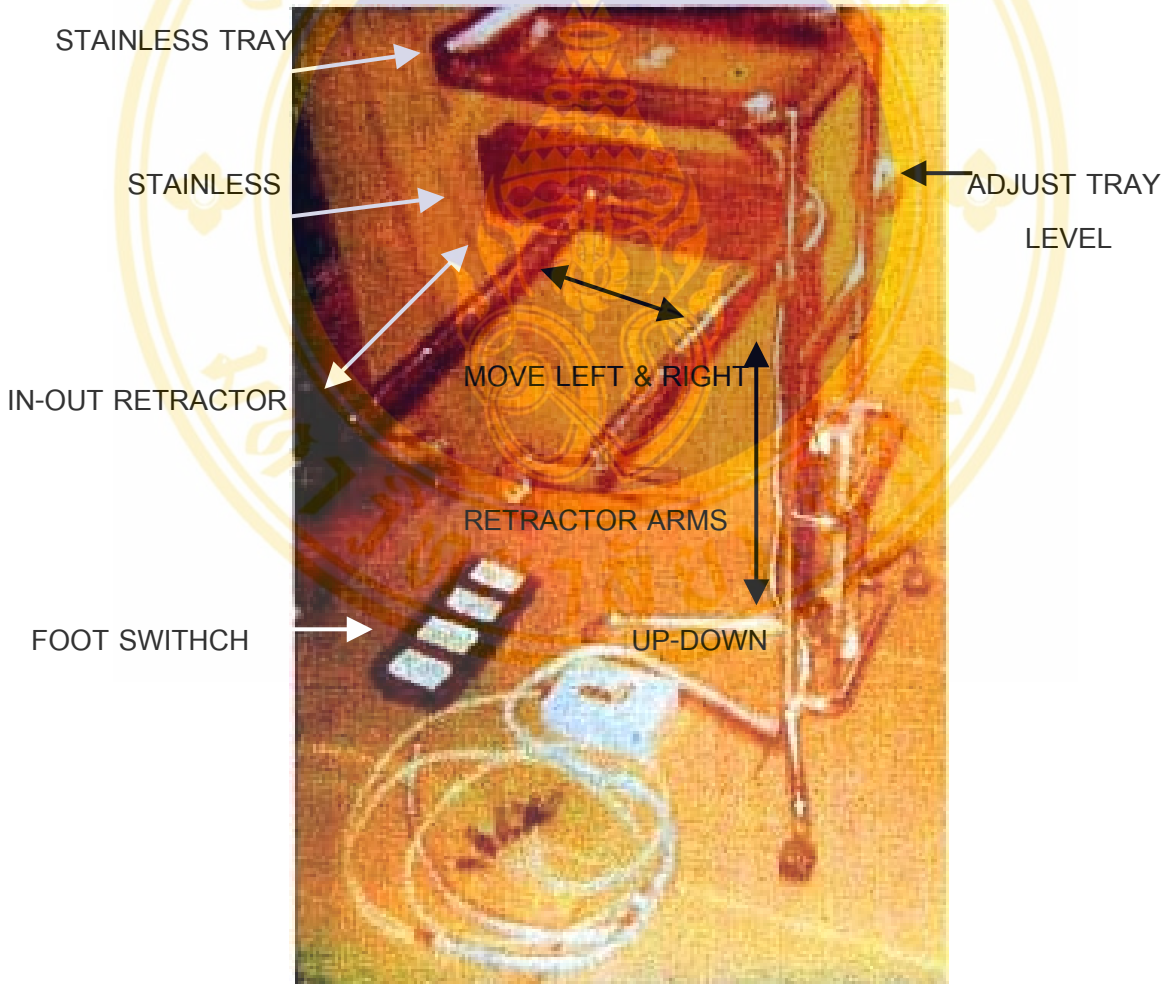

Figure 4 Hardware of Retractor Robot

3.2 METHODOLOGY

Verbal command on surgical robot is designed principally as 2 systems at workas described below:

3.2.1 Verbal Command System

The control program facilitates operation through the PC's RS-232 asynchronous communication port. This program will be designed to make it easy to take full advantages of the outstanding voice recognition and robotic text-to-speech synthesis features of Verbal Command Unit (VCU).

First, the user edits his or her own words for uttering a certain set of commands, and then trains those words 7 times to the VCU. After that, the voice commands are saved in a hard disk. Finally, user switches the VCU to Recognition Mode ready for manipulating operations. The VCU will be able to show the command signal on its monitor screen, whenever a command is uttered via the microphone hidden behind the mask of user.

Figures 5 and 6 below show the start of software program, requesting for user initial and will show "Error" when communications port (COM 2) has not yet been setup. Figure 7 shows the diagram of Verbal Command System.

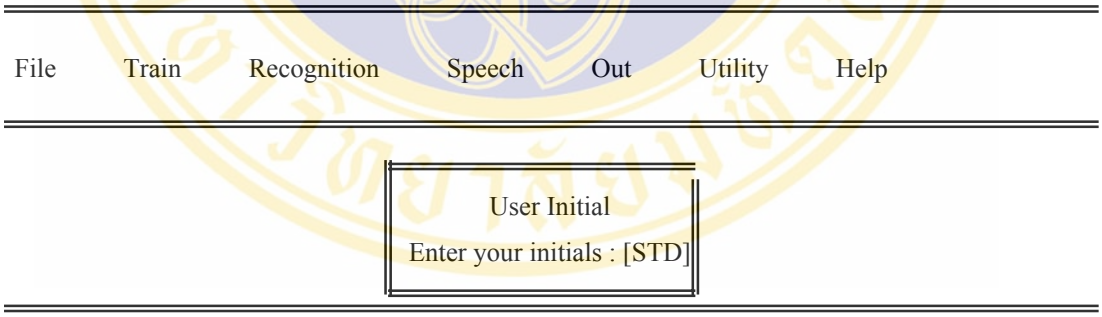

Figure 5 Program of Verbal Command for User Initial

File Train Recognition Speech Out Utility Help

Error
Unable to setup communicattions port: COM2
OK

Enter initials of the person whose voice patterns you wish to work with

Figure 6 The Verbal Command Program requiring the Setup of COM 2 Communication Ports.

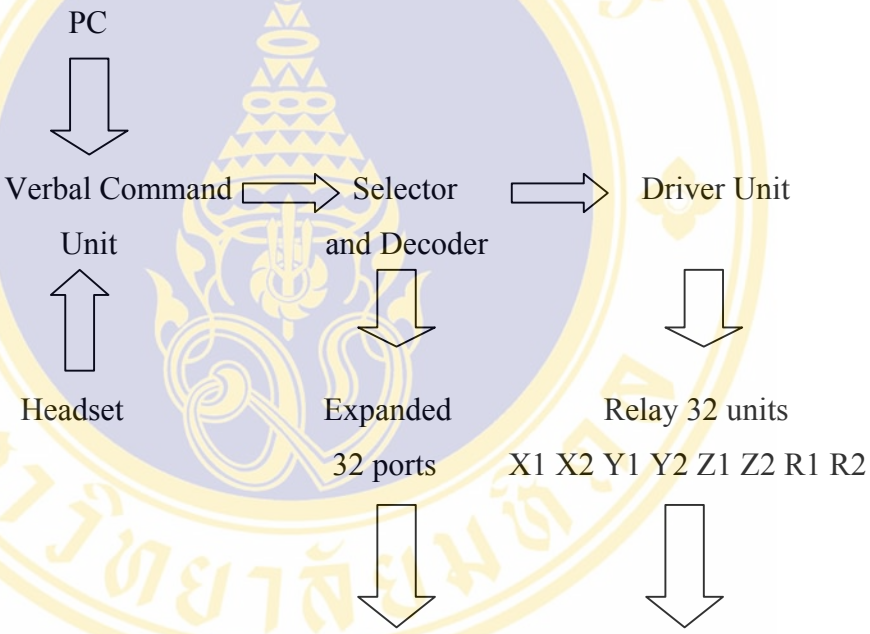

Figure 7 Diagram of Verbal Command System

A set of vocabularies define the words that are to be spoken into the microphone and recognized by the verbal command program. Vocabularies also define what the Verbal Command Unit does when it recognizes a specific word. The verbal command program provides all the tools one needs to easily create, edit, save and print vocabularies (which are stored in vocabulary files).

Each word in a vocabulary consists of 3 fields (or elements): the spoken word field, the key replacement field and the next vocabulary field. Each of these fields is described below.

The Spoken Word field contains the words or phrases to be spoken into the microphone to cause commmands or data to be inputted to a program. These are the words that will be recognized by the VCU when the verbal command is in voice recognition mode. These are also the words or phrases that one will be prompted to speak to train the VCU to recognize the command by its specific voice pattern.

When the VCU recognizes a word or phrase, the characters and/or commands of the key replacement field associated with the recognized spoken word are sent to the computer and/or processed by the Verbal Command Unit. Also, the subvocabularies specified in the next vocabulary field become the new active subvocabularies.

The first word in th spoken word list (normally “Begin”), is a “dummy” word that does not get trained, but VCU behaves as if this word was spoken when the recognition mode is first activated. That is, data in the corresponding key replacement field is processed and the subvocabularies specified in the corresponding next vocabulary field become the active subvocabularies. This allows the user to include a start-up message or command when the verbal command enters Recognition Mode, and to specify the initial active subvocabulary (the next vocabulary field corresponding to “Begin” must specify at least 1 subvocabulary).

The spoken word list also includes subvocabulary labels. A spoken word becomes a subvocabulary label when it is placed within the (main) parenthesis-like subvocabulary label defined in the test vocabulary. (Note that subvocabulary labels cannot contain embedded spaces.) All words or phrases following “Begin” are part of the subvocabulary names in the label unit. Large vocabularies are generally divided into subvocabularies and the spoken word list must contain at least one subvocabulary label.

The Key Replacement field defines the response for the corresponding spoken word when that word is recognized by the Verbal Command Unit. The response can include data that is sent from the verbal command to PC computer and/or commands that are processed by verbal command. Data includes regular text and non-printable key strokes (such as F! or Backspace). Commands are special non-printable characters that provide access to things such as the verbal command text-to-speech synthesizer.

The Key Replacement field can contain up to 255 characters. The verbal command reserves 40,000 bytes (a byte is equal to one character) for all the key replacement fields of the entire vocabulary.

The Next Vocabulary Field contains the subvocabularies that become active after the corresponding spoken word has been recgnized.This feature allows the user to limit the words that are “active” at any one time and change the active subvocabulary based on which words are spoken. If the next vocabulary in the field is blank, then the subvocabulary becomes active when the corresponding word is recognized.

When recognition is first activated, the active subvocabularies are determined by the first word in the spoken word list (the first word must specify at least one defined subvocabulary). Vocabularies can be specified as a subvocabulary label that has been defined in the spoken word list, a word range (such as 5-21), or the previous subvocabulary. The previous subvocabulary specifier indicates that the subvocabulary active before the current one will again become active once the corresponding spoken word is recognized. The previous subvocabulary is entered into the Next Vocabulary Window of the vocabulary editor by pressing “F2” following by “Enter”. If the next vocabulary field contains the previous subvocabulary specifier, it can contain no other data.

Note that when the user saves an edited vocabulary to disk, the verbal command program will check that any subvocabulary labels defined in the next vocabulary fields are indeed labels that were defined in the spoken word list, and will display a descriptive error message if any vocabulary is not found. In contrast, no checking is performed on word ranges.

The Verbal Command Control program features a powerful vocabulary editor that enables the user to create and edit vocabulary files.

The vocabulary editor is accessed when the user creates a new vocabulary with the File/New command (ALT, F, N) and when an existing vocabulary is edited with the File Edit command (ALT, F, E). When the user creates a new vocabulary, the display appears as shown in Figures 8, 9 and 10.

File Train Recognition Speech Out Utility Help

New	F2
Edit	F3
Load	F4
Save	Ctrl-S
Import	
Reset	Ctrl-R
User Initials	Ctrl-I
Print	F9
Exit	F10

Create and edit a new vocabulary

Figure 8 The Editor Program

File Train Recognition Speech Out Utility Help

File Edit

EXAMPLE.STD ROBOT1.STD ROBOT2.STD

ROBOT3.STD ROBOT4.STD

Select vocabulary to be edited <Escape>=Cancel

Figure 9 Loading Program

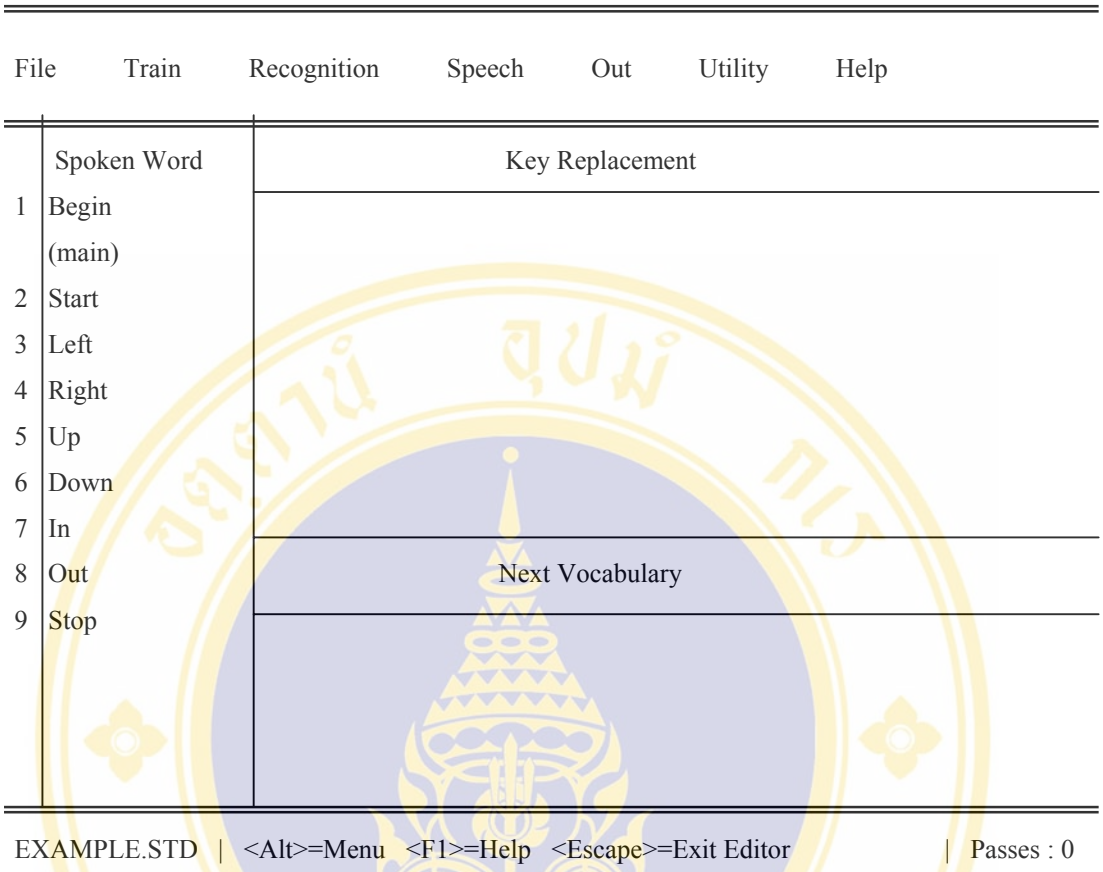

Figure 10 Inside of Editor Program

The menu bar in loading program shown in Figure 9 contains only the commands related to the vocabulary editor. Commands are selected from the vocabulary editor menu in the same way they were selected from the main menu. There is detail on line help available for all of the items in the vocabulary editor menu.

Basically, the vocabulary editor display in Figure 10 is divided into 3 windows. Each of these windows corresponds to the 3 fields of the vocabulary as previously described. Note that the Spoken Word window lists as many spoken words as will fit in the window. In contrast, the Key Replacement and Next Vocabulary windows display only the information corresponding to the currently selected spoken word. One can change the selected spoken word by using the arrow keys to move the

highlight bar up and down in the spoken word list. The cursor can be moved to the different windows by using the TAB and SHIFT+ TAB keys.

When the user creates a new vocabulary, the vocabulary editor automatically inserts the word “Begin” at the start of the spoken word list. As previously explained, this word is not trained but does serve as “special purpose”. The information in the Key Replacement window that corresponds to the first word in the spoken word list is processed when the verbal command first enters voice recognition mode. In addition, the vocabularies specified in Begin’s Next Vocabulary window determine the initial active subvocabularies.

To append a new spoken word to the spoken word list, move the highlight bar to the last word in the list and press the down arrow key or Enter to create a new blank entry. Then type the new word or phrase. With the highlight bar still on the newly created spoken word, tab to the Key Replacement window. Type in the text/or non-printable characters (described below) to define the response when the corresponding spoken word is recognized. If the user would like the active subvocabulary to change when this word is recognized, type the new subvocabulary in the Next Vocabulary window.

In addition to regular text characters, the Key Replacement and Next Vocabulary fields can contain special non-printable characters. Non printable characters are entered by pressing “F2”, or by selecting the Edit/Insert Non-printable Character command (ALT, E, N), and then pressing the key associated with the desired keystroke or command.

The Key Replacement window supports 2 types of non-printable characters. The first type is for non-printable keystrokes. For example, to enter the ESCAPE key, tab the cursor to the Key Replacement window and type F2, ESCAPE. To enter CTRL+HOME, press F2, CTRL+HOME. The second type of non-printable character is for the verbal commands. Commands are entered by typing F2, followed by the key associated with the command. For example, to enter the “Again”

command, tab the cursor to the Key Replacement window and type F2, A. The following table lists the available verbal commands, which keystrokes enter those commands and a description of instruction to VCU.

Table 2 The command description.

Command	Keystroke	Description
Again	F2, A	Cause the key replacement string of the most recently recognized word to be repeated until another utterance is detected by the verbal command.
Toggle Speech	F2, G	This command toggles the voice output enable state. If voice output is enable, the Quit, Speak, Echo and Voice command work together to send text to verbal command text-to-speech synthesizer. If voice output is disable, these command have no effect.
Rubout	F2, J	Cause the verbal command to transmit n BACKSPACE characters (ASCII 8). Where n is the length of the command sent for the most recently recognized word. This has the effect of erasing the text of the last command in most programs. If this command is repeated with no other interventing command, a single BACKSPACE is transmitted.
Help menu	F2, M	Causes the verbal command to send the first 36 words of the active subvocabulary across the serial port. If the user is using the VKEY program, this command will display a window with the list of active words, thereby aiding the user by displaying available commands.
Quit	F2, Q	This command works in combination with the ECHO, Voice and Speak commands. It indicates the end of the text that is to be placed into the speech synthesis buffer (which was started with the ECHO or Voice command). Note that the text is not spoken until the Speak command is Encountered.

Table 2 The command description. (Cont.)

Command	Keystroke	Description
Speak	F2, S	This command works in combination with the ECHO, Voice and Quit commands. It causes the text currently in the speech synthesis buffer to be spoken by the verbal command's text-to-speech synthesizer.
Echo	F2, T	Cause the verbal command to place the text that follows this command into the speech synthesis buffer in addition to being transmitted across the serial port to the PC. This continues until either the Speak or Quit command is encountered.
Voice	F2, V	Cause the verbal command to place the text that follows this command into the speech synthesis buffer only. This allows the spoken text to be completely independent of the data transmitted across the serial port to the PC. This continues until either the Speak or Quit command is encountered.

In the case of the Next Vocabulary window, there is only one possible non-printable character: the previous vocabulary specifier (F2, ENTER). Note that when the Next Vocabulary field contains the previous vocabulary specifier, it can obtain no other data.

Importing voice patterns, as set out to create one's own vocabulary files, the user will discover that many vocabularies will use the same words. For examples, many vocabularies contain the alphabet and/or the digits 0-9. Since retraining these words in a large vocabulary can be very time consuming, the vocabulary editor allows you to import voice patterns from other vocabulary files; thereby, eliminating the need to train previously trained words.

To use this command, one must have the destination file (with the untrained words) loaded in the vocabulary editor. Select the Edit/Import Voice patterns command (ALT, E, V) and the user will be prompted to select the source file (with the already-trained voice patterns) from a list box. The Import Voice Patterns Command will compare each spoken word of the source file with each spoken word of the

destination file. If a match is found and the source file contains trained voice patterns for that word, those voice patterns are copied to the matching word(s) in the destination file. The words do not need to match grammatical case, but must match spelling exactly character for character. After the Import Voice Patterns command is complete, a message box displays how many matches were found.

Voice training, once a vocabulary is created, one must train the verbal command to understand user's own voice as the user speaks each word in the spoken word list. A new feature of this version of verbal command control program allows the user to bypass the training step for words that have already been trained in other vocabularies. (See the import voice patterns command described above.) In addition to topics discussed here, be sure to view the on line help for additional information about voice training. Important topics include Training Parameters that can be modified to enhance the training process and/or to solve any training problems.

Training a single word, from time to time the user may find he is getting poor recognition of a particular word, or find that two words are being confused with each other by the verbal command voice. The Single Word train command (ALT, T, W) allows the user to train a single word form a vocabulary with the use of Training menu in Figures 11 and 12.

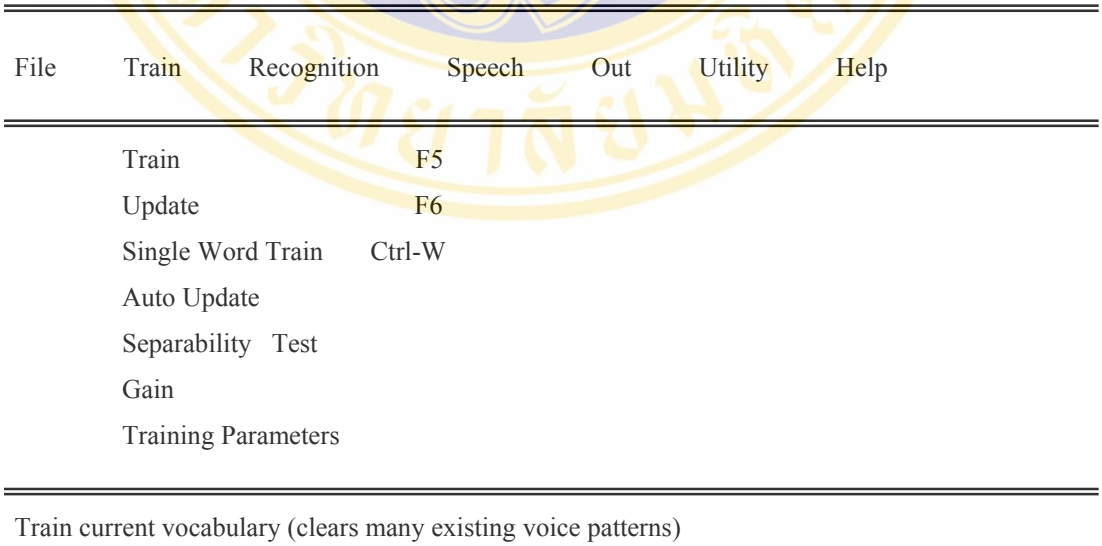

Figure 11 The Training Program

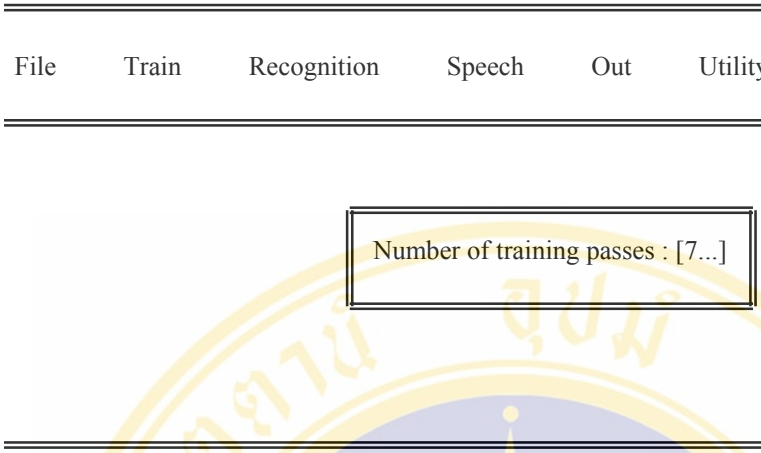

Figure 12 The Number of Training Passes

The auto-update command, to get the best possible recognition from the verbal command, it is important that each word in a given vocabulary has the same number of training passes. The auto-update command insures they do by scanning all of the words currently loaded in the verbal command voice and automatically performing the correct number of training and/or update passes required. If all words currently loaded in the verbal command voice already have an equal number of training passes, the auto-update command displays a message box that informs the user of this and shows how many training passes each of the words have. Note that the vocabulary editor invokes the auto-update command if changes to a vocabulary result in words with a mixed number of training passes.

Voice recognition, once a vocabulary has been trained with the user's voice patterns, the user will be able to make use of verbal command voice recognition features. In addition to the topics discussed here, be sure to review the on-line help for additional information about voice recognition. Important topics include recognition parameters that can be modified to enhance voice recognition and/or to solve any recognition problems.

Voice recognition mode is activated form verbal command program and unit by selecting the recognition/recognition mode command (ALT, R, R). the verbal

command control program's recognition window displays the data received from the verbal command. To close the recognition window and disable recognition mode, press ESCAPE. To exit to DOS with recognition still active, press CTRL+F10.

Test mode is the train mode (ALT, R, T). It is similar to recognition mode except that test mode gives more detailed information regarding the recognized words. Test mode can be useful for determining the quality of a trained vocabulary and for detecting similar sounding words that could result in ambiguity.

While recognition mode as shown in Figure 13 displays the data from the recognized word's key replacement field, test mode instead displays the recognized spoken word, the runner-up, the recognition scores and whether or not the recognition score exceeded the reject threshold. Note that test mode does not use any defined subvocabularies and instead leaves the entire vocabulary active.

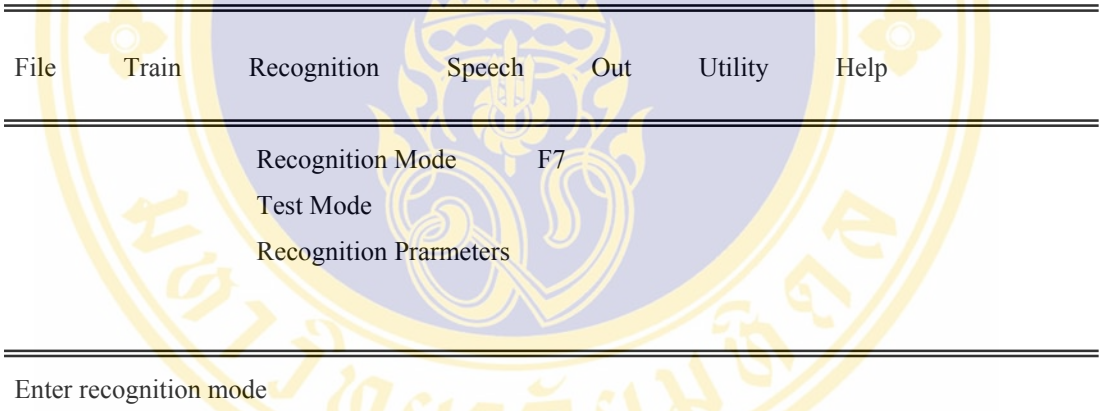

Figure 13 The Recognition Mode

3.2.2 Surgical Robot System

The surgical robot have 2 units. The first unit is used to control and hold the laparoscope to view inside the patient stomach while the surgeon hands are busy manipulating the surgery. The second unit is used to control a retractor for opening the cutting area of the body. Please see the Figure 14 for all Surgical Robot System.

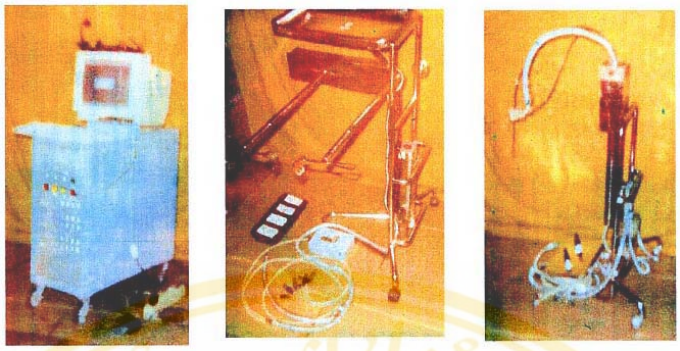

VERBAL COMMAND SYSTEM RETRACTOR ROBOT LAPAROSCOPE ROBOT

Figure 14 Laparoscope and Retractor Units in Surgical Robot System

The laparoscope unit can move in, out, up, down, turn-left, turn-right and rotate-left, rotate –right by the use of Verbal Command Unit.

The retractor unit can only move in, out and up, down by the use of Verbal Command Unit.

3.2.3 Verbal Command Circuit

The Verbal Command Circuit comprising decoder section, relay section and motor section is shown in detail in Figures 15-20 below:

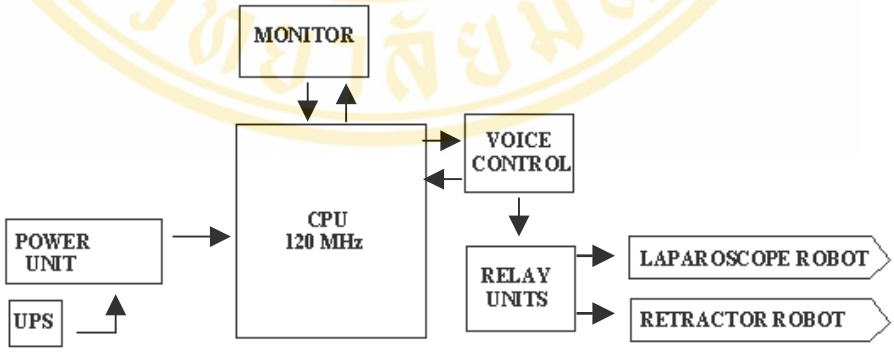

Figure 15 Verbal Command Circuit

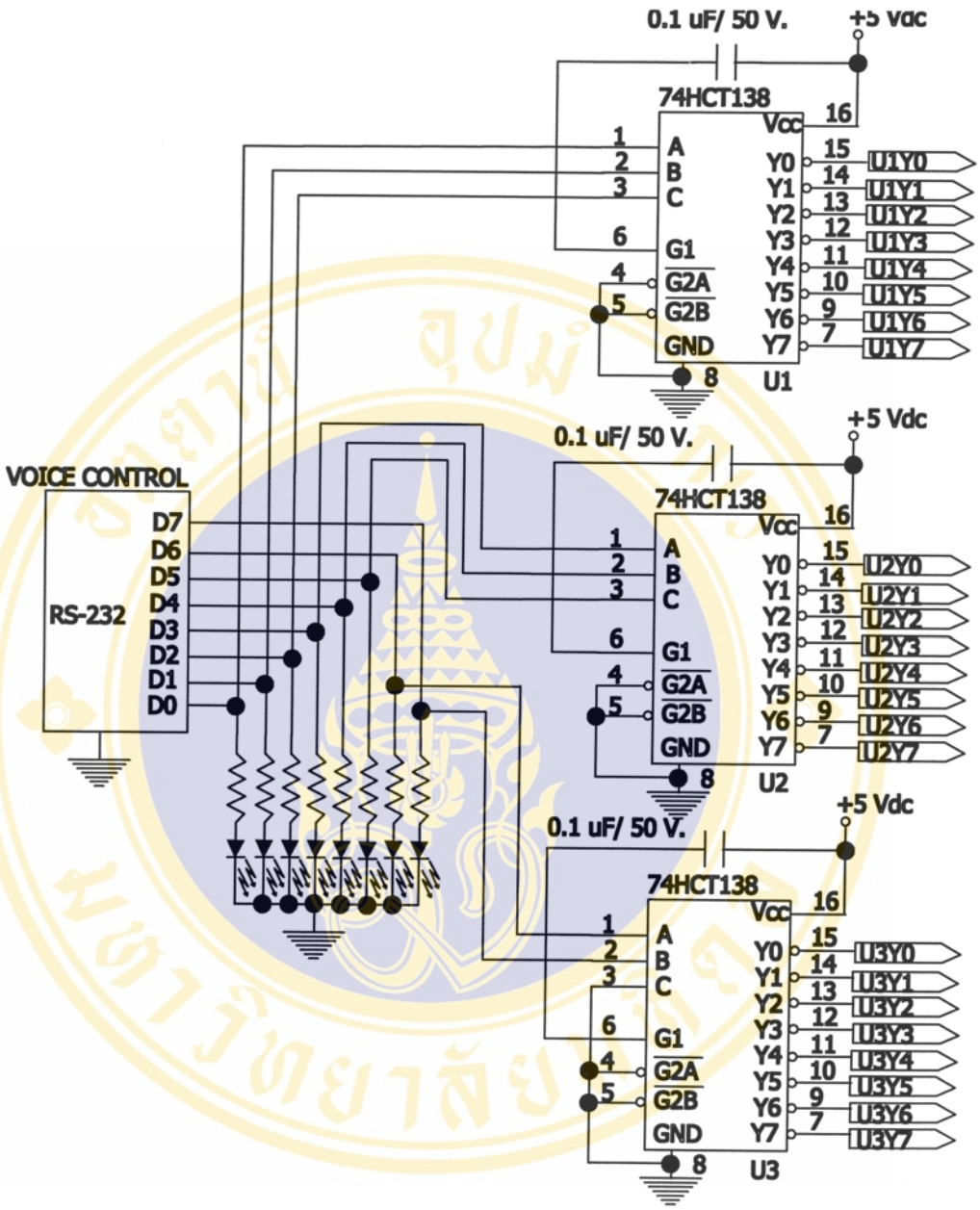

Figure 16 Decoder 74HCT138 circuit

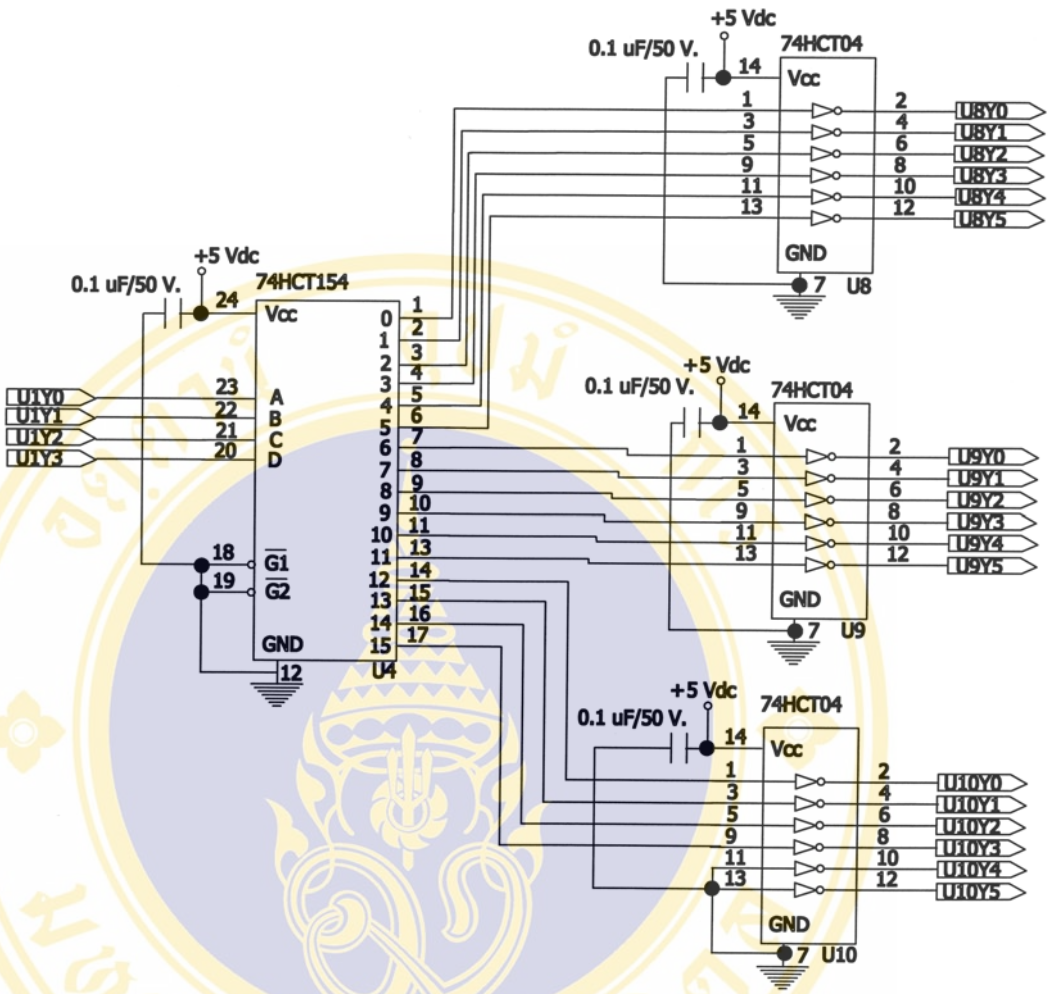

Figure 17(a) Decoder 74HCT154 circuit

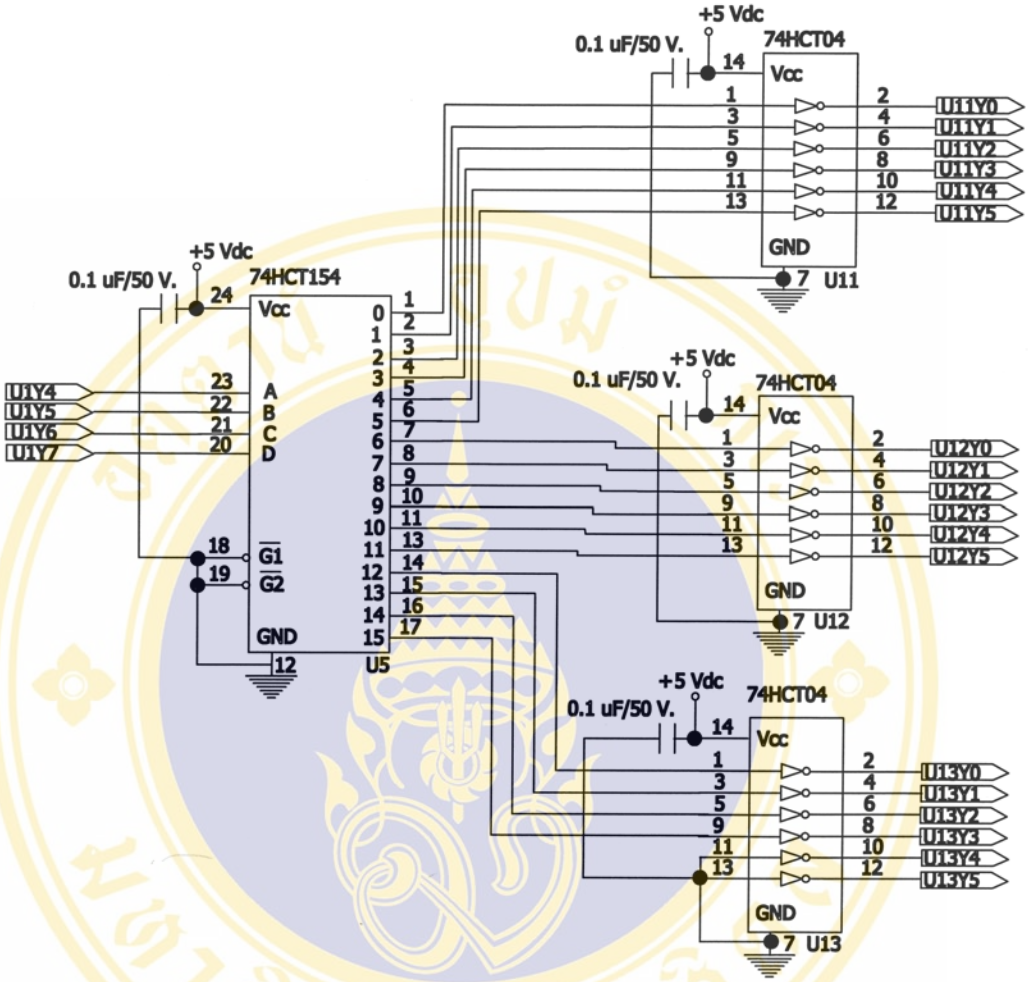

Figure 17(b) Decoder 74HCT154 circuit

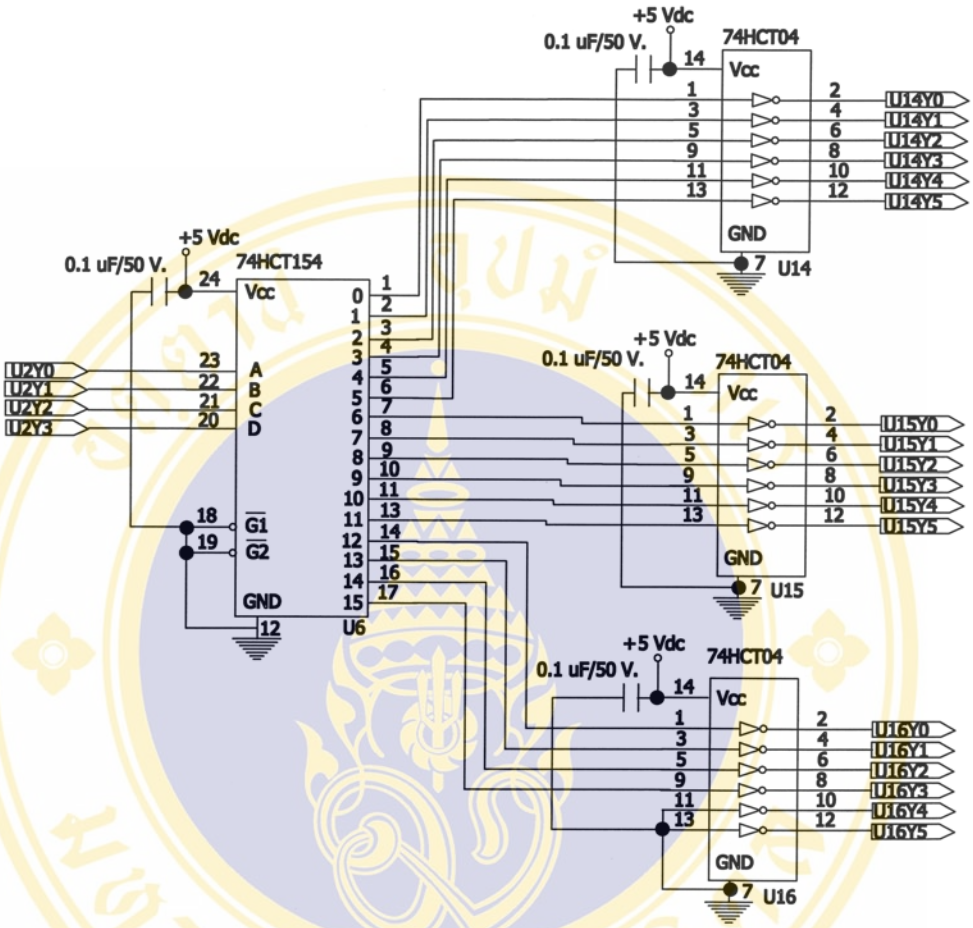

Figure 17(c) Decoder 74HCT154 circuit

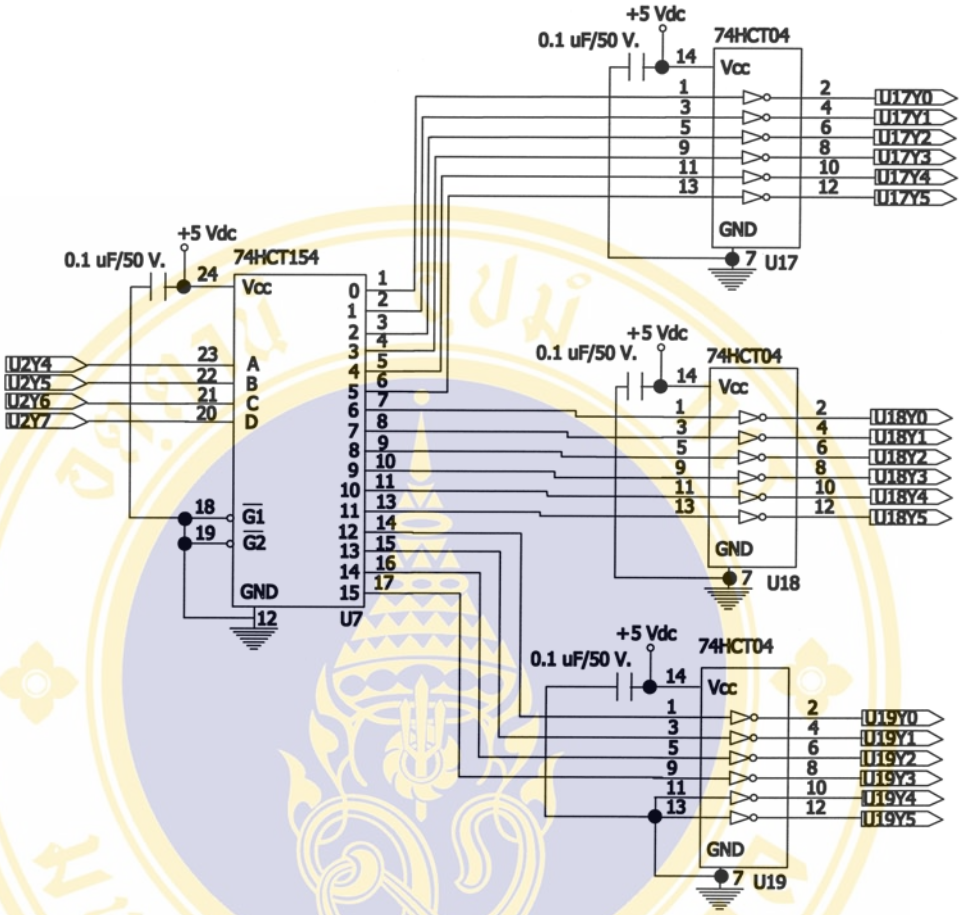

Figure 17(d) Decoder 74HCT154 circuit

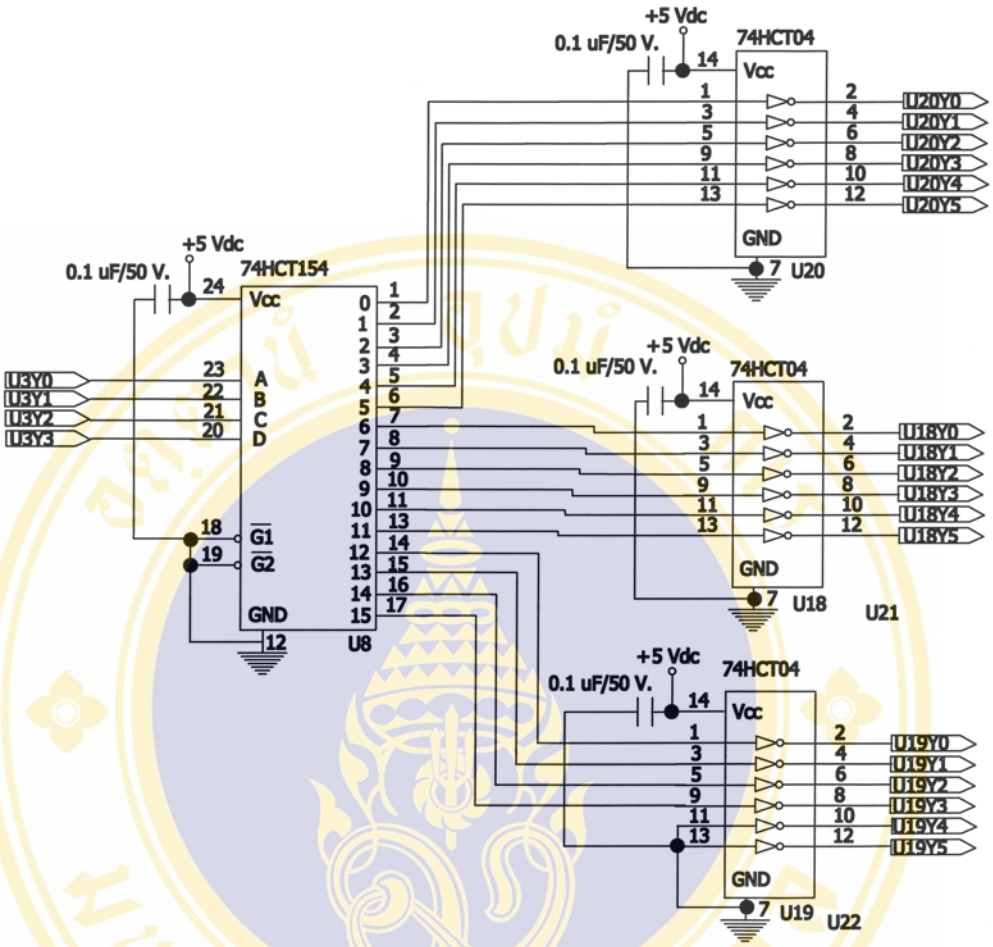

Figure 17(e) Decoder 74HCT154 circuit

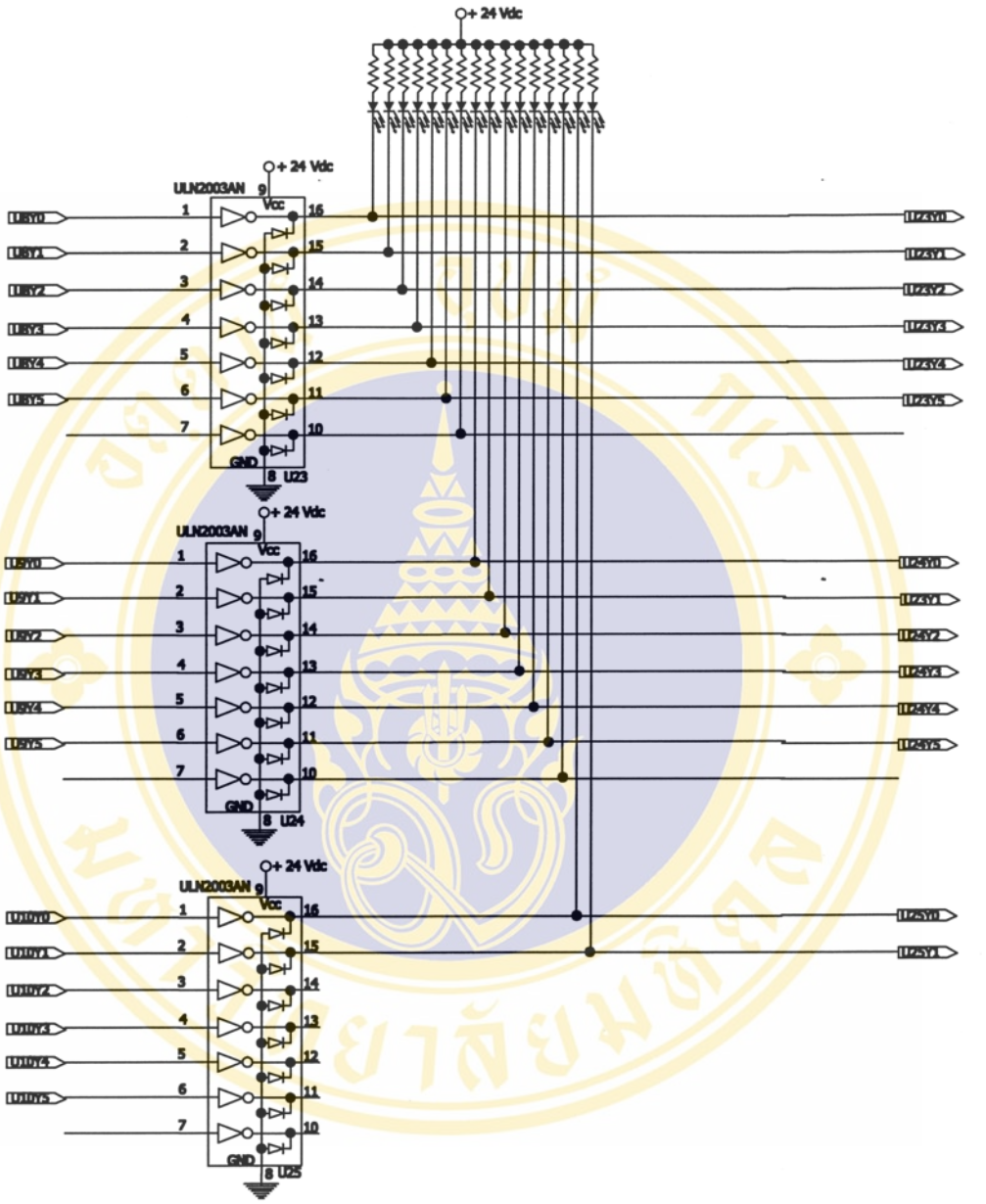

Figure 18(a) High-Voltage High-Current Darlington Transistior ULN2003AN circuit

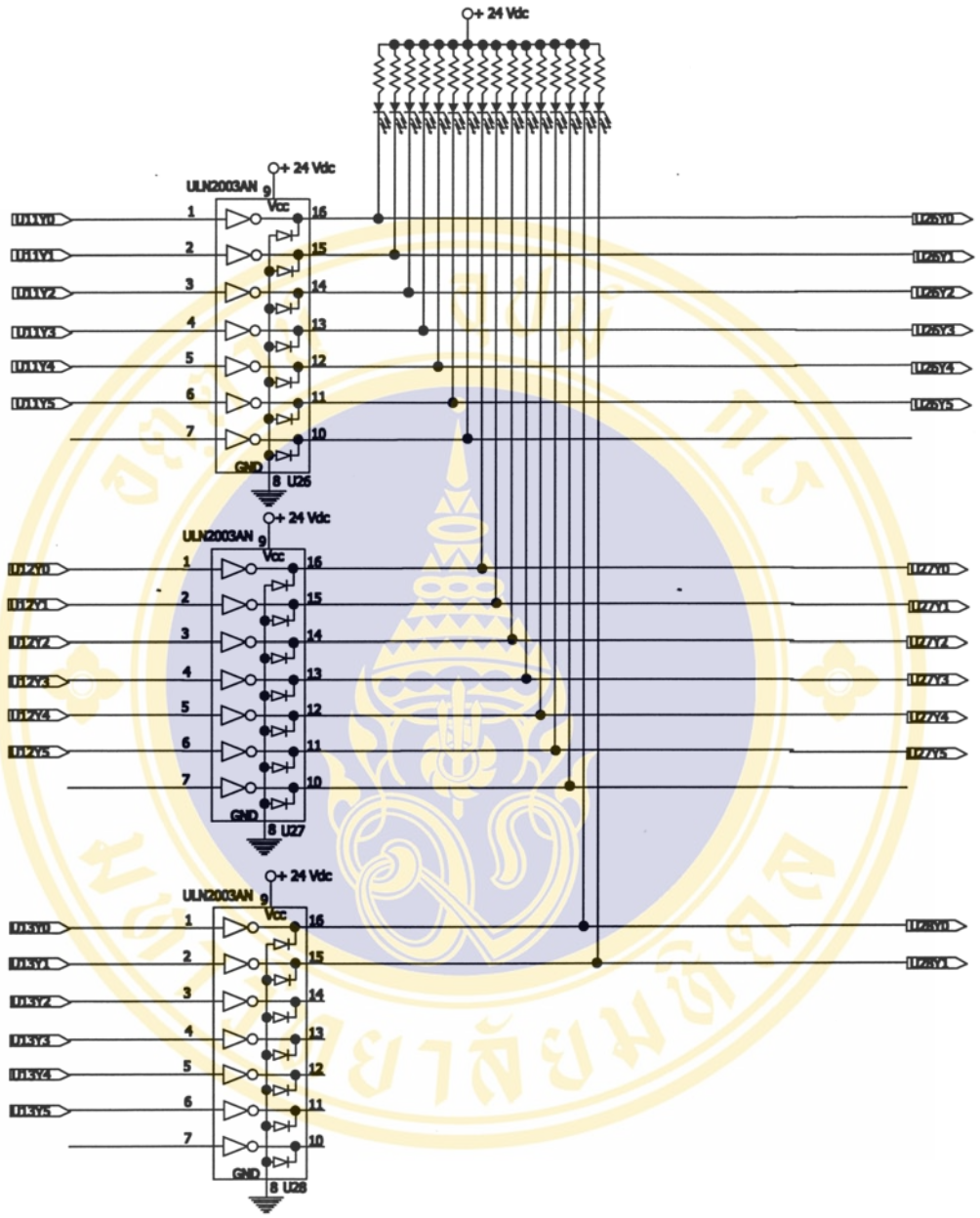

Figure 18(b) High-Voltage High-Current Darlington Transistior ULN2003AN circuit

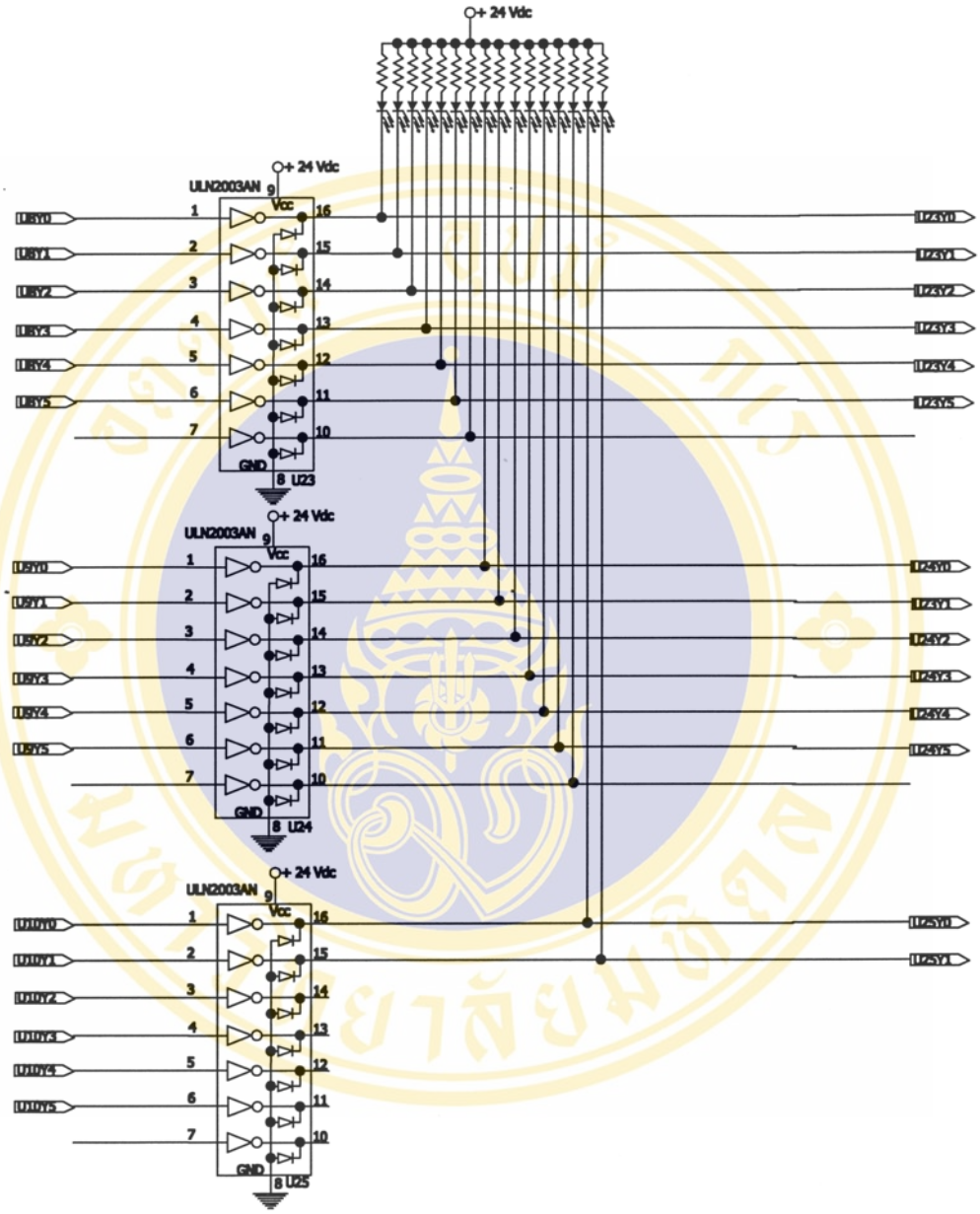

Figure 18(c) High-Voltage High-Current Darlington Transistior ULN2003AN circuit

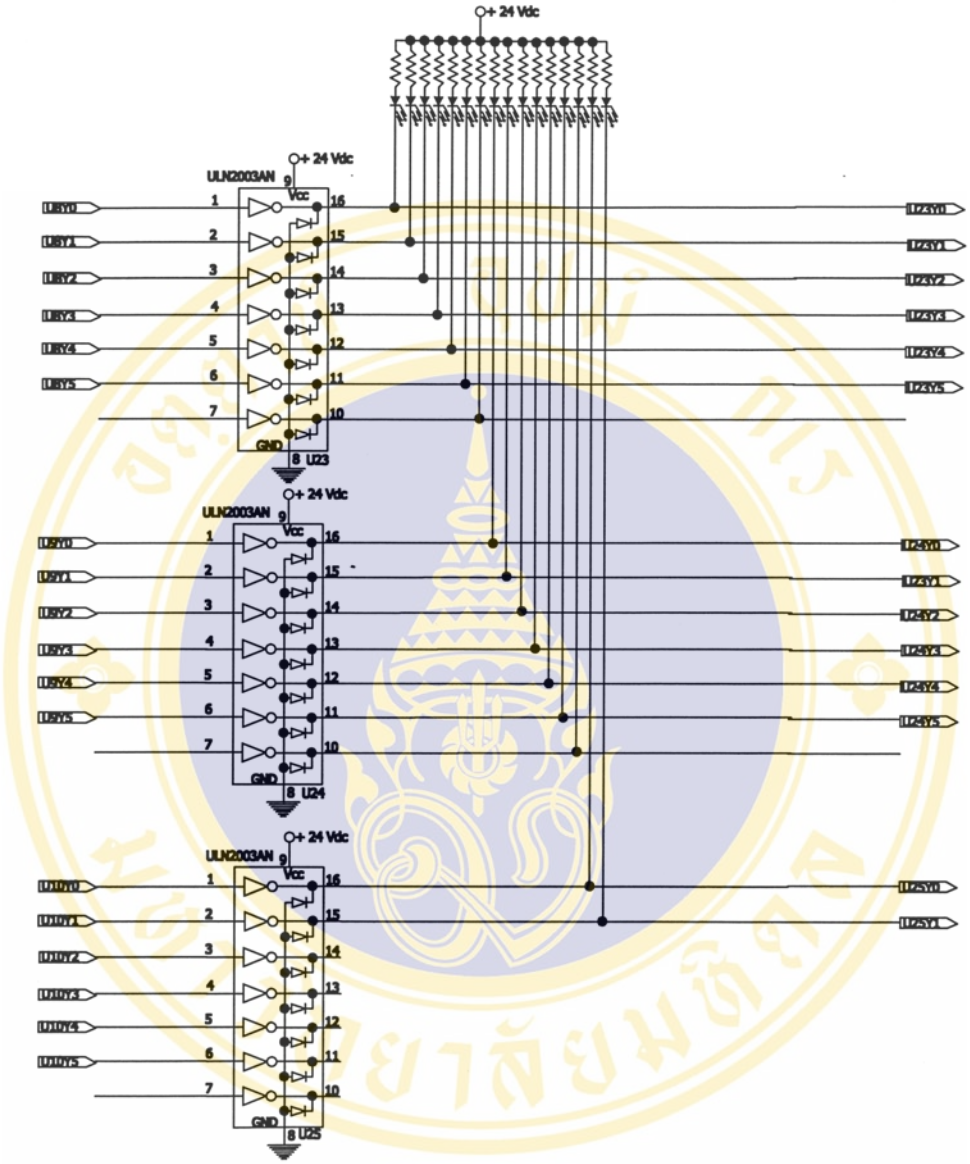

Figure 18(d) High-Voltage High-Current Darlington Transistior ULN2003AN circuit

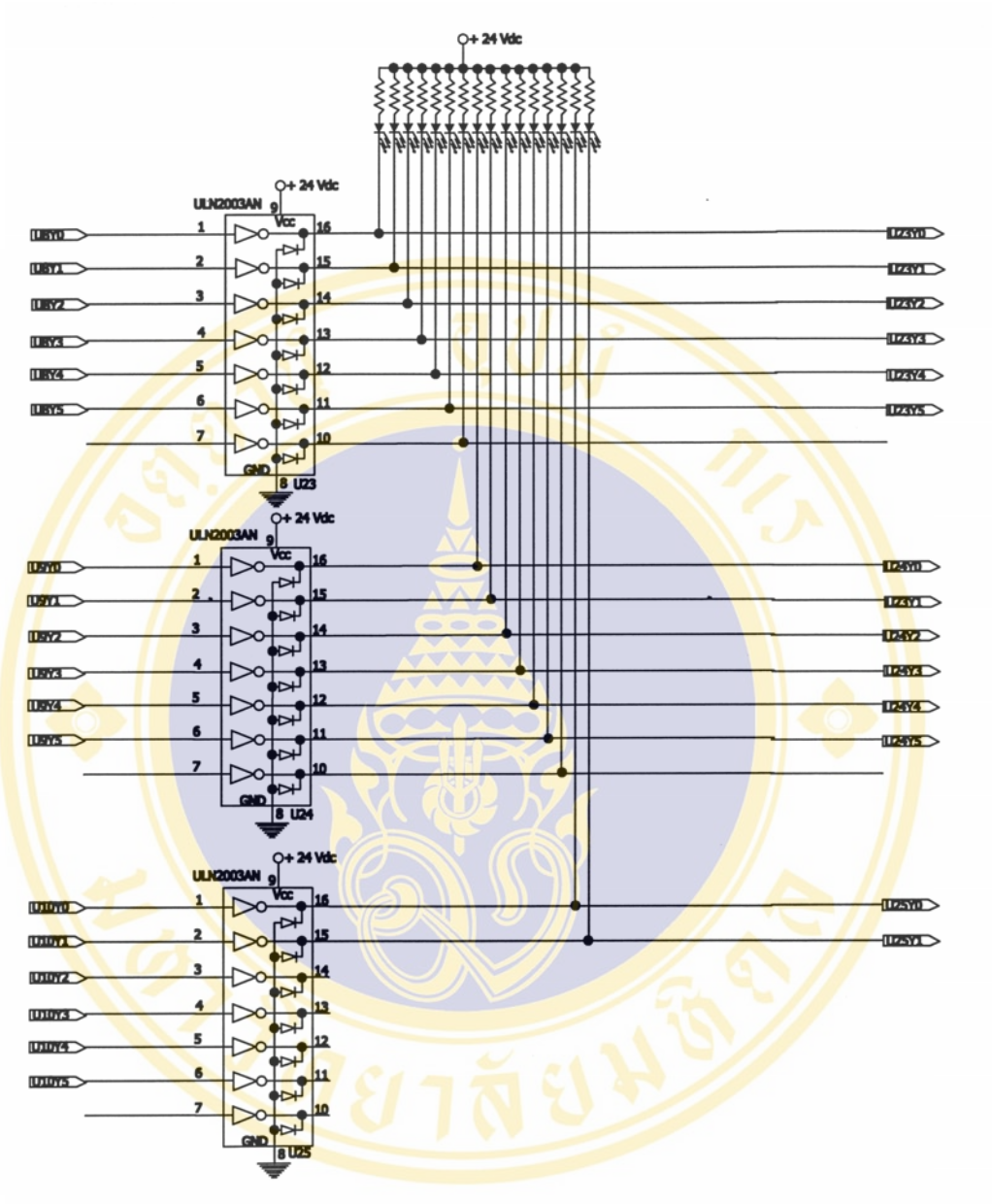

Figure 18(e) High-Voltage High-Current Darlington Transistior ULN2003AN circuit

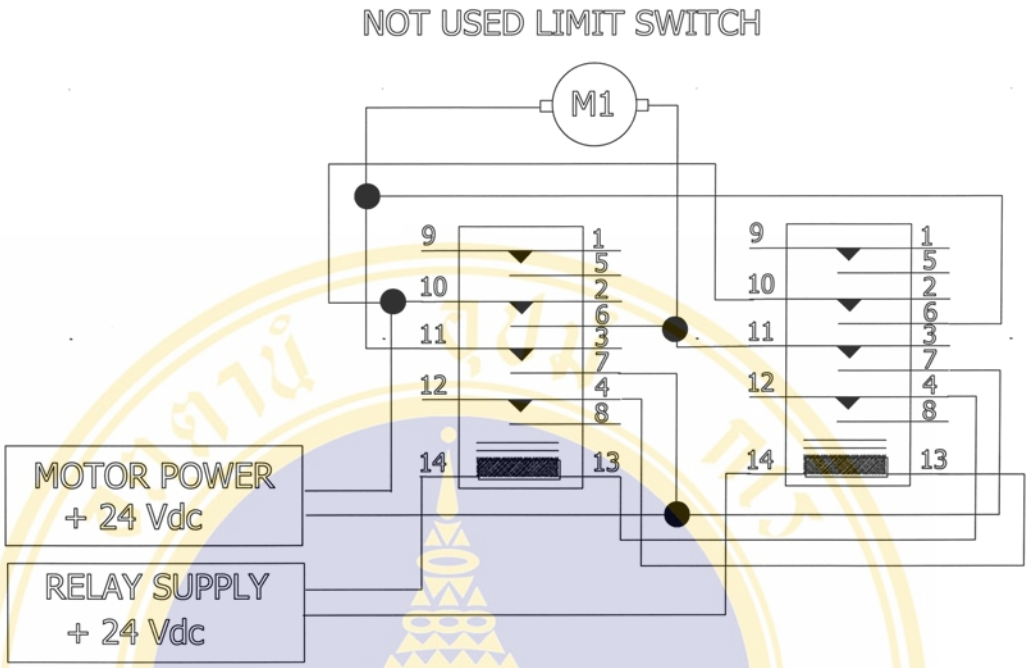

Figure 19 Motor circuit of Laparoscope Robot

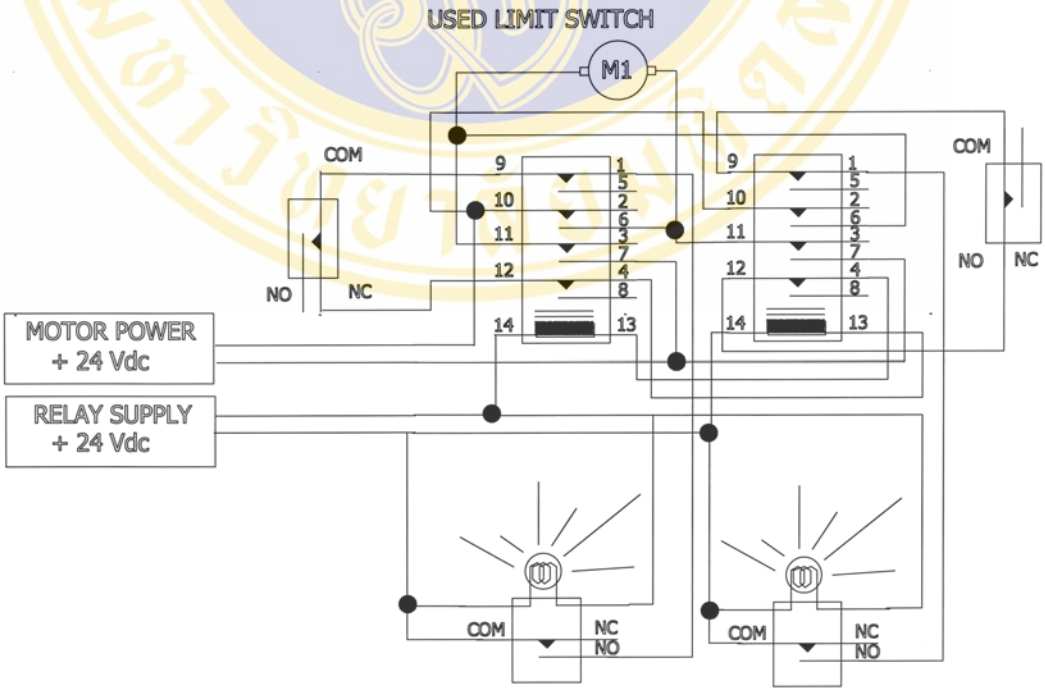

Figure 20 Motor circuit of Retractor Robot

3.2.1 Verbal Command Table

The Verbal Command Table in Figure 21 shows all command words and the binary digits to control the movement of the robot.

Spoken Command		Voice Command as shown at monitor	Decoder D7 D6 D5 D4 D3 D2 D1 D0		Action
Thai	English				
เริ่ม	Start	Robot Start	0000	0000	Start Up the system, showing Menu at Monitor
หยุด	Stop	Robot Stop	0000	0001	Ending the command program
ขึ้น	Robot up	Robot Up	0000	0010	Move arm Up
ลง	Robot dodwn	Robot Down	0000	0100	Move arm Down
ควงซ้าย	Robot Left	Collar Rotate CCW	0000	1000	Rotate collar counter-clockwise
ควงขวา	Robot Right	Collar Rotate CW	0001	0000	Rotate collar clockwise
กล้องขึ้น	Up	Collar Up	0010	0000	Move collar holding Laparoscope Up
กล้องลง	Down	Collar Down	0100	0000	Move collar holding Laparoscope Down
กล้องซ้าย	Left	Collar Left	1000	0000	Rotate Laparoscope to Left
กล้องขวา	Right	Collar Right	0000	0011	Rotate Laparoscope to Right

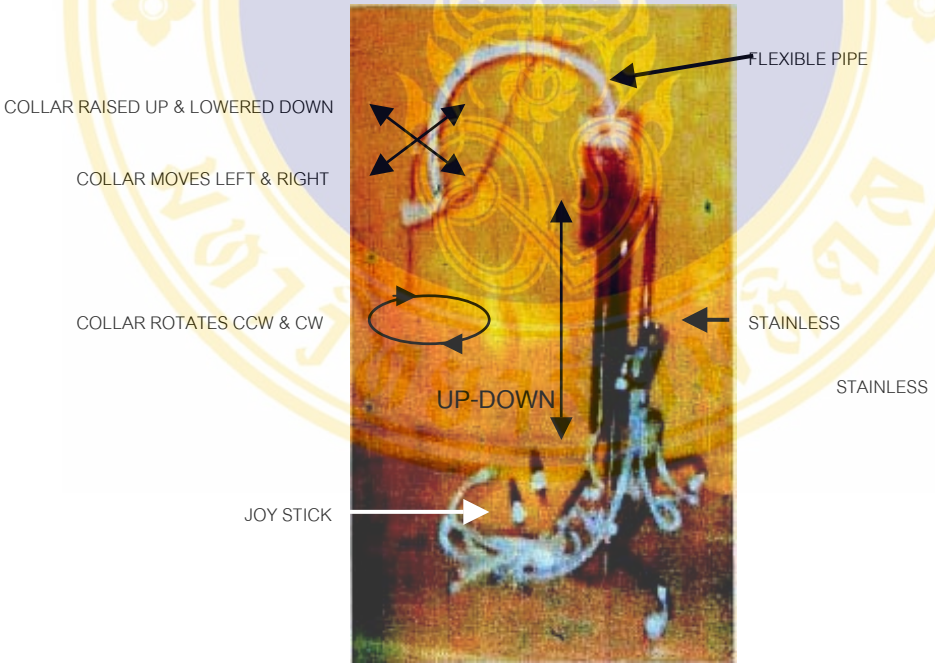

Figure 21 Verbal Command Table

3.2.5 Verbal Command Chart

The Verbal Command Chart in Figure 22 shows the words of voice command and the direction of the movement of the robot.

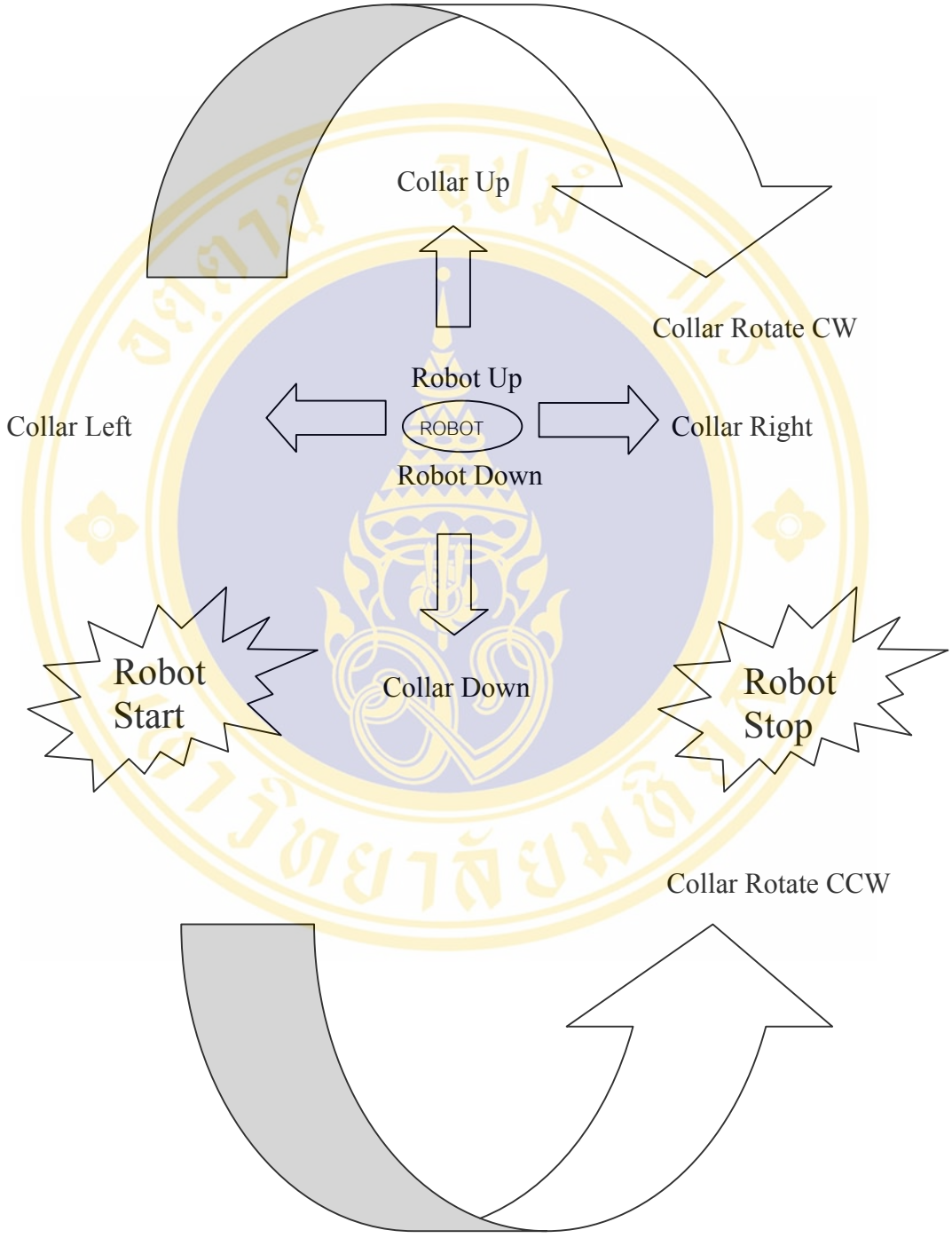

Figure 22 Verbal Command Chart

3.2.6 Set-Up Sequence of Surgical Robot

The set-up sequence of Surgical Robot is divided for 2 functions. First is set-up sequence for Retractor Robot. Second is set-up sequence for Laparoscope Robot.

Set-Up Sequence for Retractor Robot

STEP 1 Position the arm

Mount on the table rail or place the unit near the table, Control the position by pressing the button Up, Down, Check that the arm is secured.

STEP 2 Put retractor arm in the operating position.

STEP 3 Drop the system.

STEP 4 Attach retractor, either Richardson or Dever.

STEP 5 Press button left or right to move the retractor to the left hand side or right hand side.

Note that: STEP1 AND STEP2 must be done before sterile process.

Set-Up Sequence for Laparoscope Robot

STEP 1 Position the arm

Mount on the table rail or place the units near the table, Check position by pressing the button Up, Down, Check that the arm is secured.

STEP 2 Put the Laparoscope arm in operating position.

STEP 3 Drop the system.

STEP 4 Attach Laparoscope collar and collar holder.

STEP 5 Enable Voice control System.

Note that: STEP 1 and STEP 2 must be done before sterile process.

3.2.7 Train and test Robot with Voice Control System

STEP1 Turn on the system and enable Voice Control Interface

Adjust headset and clip, Turn on the Voice Control System, Turn on the PC Auto open program.

STEP 2 Train and test with Recognition Mode

Train the user voice at least 5 times or more, Save the voice pattern in the file name as you want in the hard-disk, Go to Recognition Mode (Move the robot before operation and check the voice command.), Error or not clear of the voice command will go to STEP 1 again.

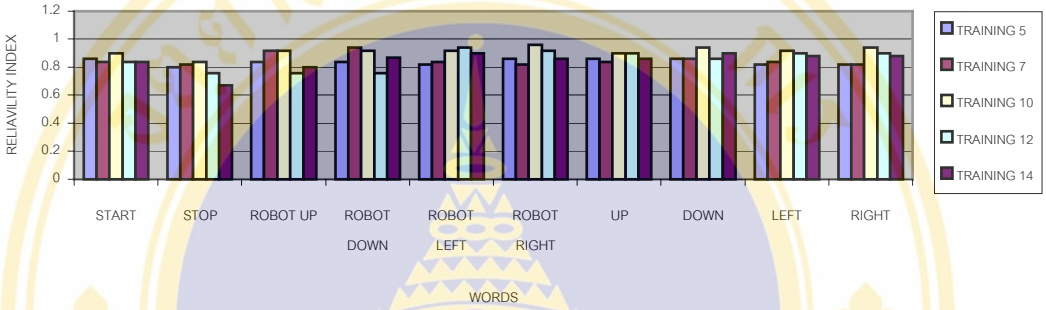

(a) English Voice Command

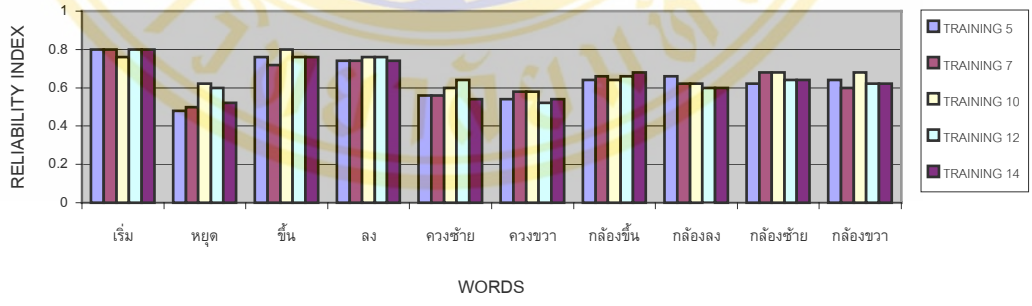

(b) Thai Voice Command

Figure 23 Reliability Index of Voice Command

Reliability Index = Number of Success / Number of Command Inputs is plotted for both English and Thai as shown above in Figure 23 for each Voice Command Training pass.

3.3TEST AND EVALUATION

The Surgical Robot System was tested with the author's own voice for the commands given separately to the Laparoscope Unit and the Retractor Unit as follows:

3.3.1 Test of Laparoscope Unit

The Laparoscope Unit as shown in Figure 24 was tested with the following voice commands:

Robot Start : To start up the Robot System with Menu shown at the Monitor.

Robot Up/Down Command : To lift or lower the Laparoscope arm to the level required to manipulated the Laparoscope into the patient's opening.

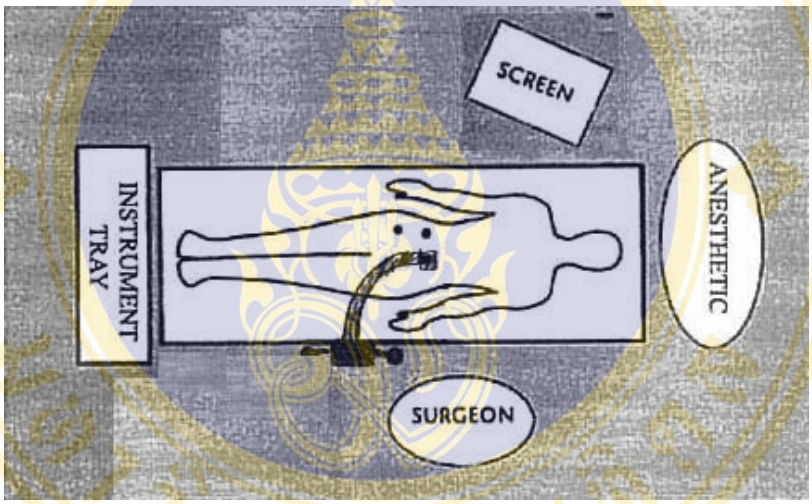

Figure 24 Laparoscope Robot position

The Laparoscope was assumed attached to the Robot Collar and then inserted into the patient's opening. The Robot Collar with the Laparoscope was then inserted into the axis of Collar Motor, which was then subjected to the following Voice Commands:

Collar Up/Down and Collar Left/Right : To direct the Laparoscope into the desired direction for viewing inside the patient's organ.

Collar Rotate CCW/ CW : To rotate the Laparoscope counter-clockwise or clockwise as required to examine the patient's organ in detail.

Robot stop : To end the command program.

The overall responses to the above 10 Voice Commands were shown to perform as stated in the Verbal Command Table in Figure 21.

3.3.2 Test of Retractor Unit

The Retractor Unit as shown in Figure 25 was tested for its ability to be raised up or lowered down by pressing the  switch or the 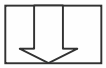 switch (see Figure 4 for switch positions), respectively.

The  and  switches were tested for the Retractor Unit to spread out the cut or the patient's openning and to make the cut /opening smaller, respectively.

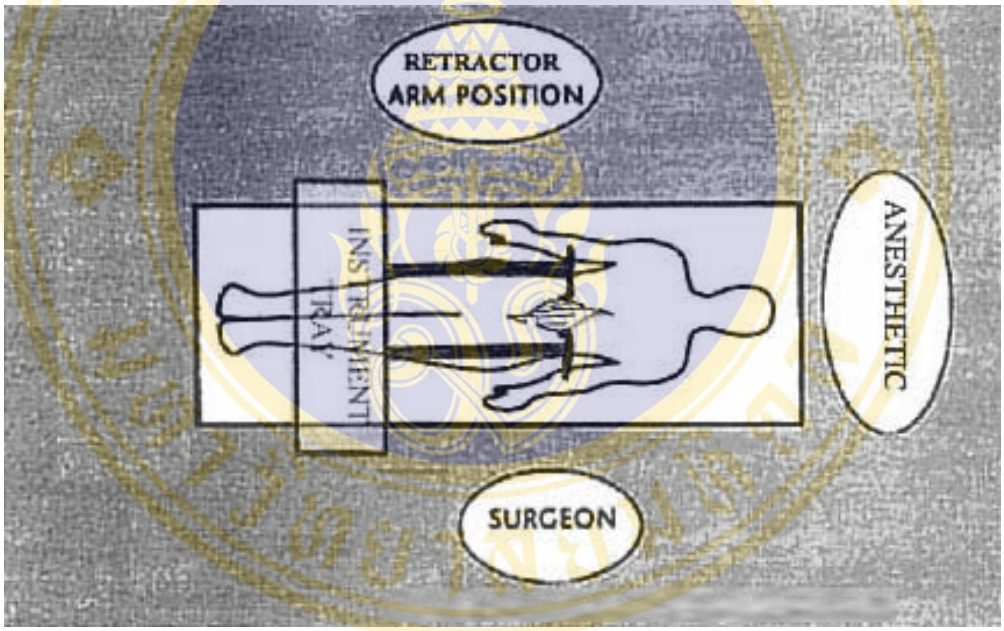

Figure 25 Retractor Robot position

CHAPTER IV
RESULTS AND DISCUSSION

Results of functional tests as performed in Chapter III for Laparoscope Unit and for Retractor Unit are tabulated in Tables 3 and 4 below.

VERBAL COMMAND		ACTION	RESPONSE	DESIGN SPECIFICATION
ENGLISH	THAI			
START	เริ่ม	System starts	immediate	-
STOP	หยุด	Movement stops	immediate	-
ROBOT UP	ขึ้น	Robot moves up	19.0 mm/s	20 mm/s
ROBOT DOWN	ลง	Robot moves down	19.5 mm/s	20 mm/s
ROBOT LEFT	ควงซ้าย	Collar rotates CCW	5.5 mm/s	5 mm/s
ROBOT RIGHT	ควงขวา	Collar rotates CW	5.5 mm/s	5 mm/s
UP	กล้องขึ้น	Collar raised up	4.5 mm/s	5 mm/s
DOWN	กล้องลง	Collar lowered down	5.5 mm/s	5 mm/s
LEFT	กล้องซ้าย	Collar moves left	4.5 mm/s	5 mm/s
RIGHT	กล้องขวา	Collar moves right	4.5 mm/s	5 mm/s

Table 3 Test Results of Laparoscope Unit

It was noted that robot responsed move readily to the verbal commands in English language when compared to the Thai verbal commands, most likely due to the fact that the Verbal Command Unit (Micro Intro Voice II) was primarily designed appropriately to the English-spoken words.

FOOTSWITCH COMMAND	ACTION	RESPONSE	DESIGN SPECIFICATION
Press ⇦	Arms moved left	2-3 mm/s	5 mm/s
Press ⇨	Arms moved right	2-3 mm/s	5 mm/s
Press ⇧	Arms raised up	19.0 mm/s	20 mm/s
Press ⇩	Arms lowered down	20.5 mm/s	20 mm/s

Table 4 Test Results of Retractor Arms Unit

The overall performances of the Verbal Command Robot so constructed for the controlling of a Laparoscope in aid of surgery were evaluated as fairly satisfactory in compliance with the design concept per project objectives and scope as stated in Paragraphs 1.2, 1.4. The work, although needed to improve on the speed of arms movement, can be regarded as satisfactory at the level of a prototype design.

The prototype system can be developed in future with the use of micro-circuitry technology in hardware construction for it to be compact and more convenient to handle. The software program can also be expanded to cover various other functions via the use of Expanded 32 ports which are spare communications ports at present.

Some features that need attention are suggested in principle for future developments of this prototype robot into a more practical and effective system as follows:

(i) Verbal Commands “Rotate Left / ควงซ้าย” and “ Rotate Right / ควงขวา “ in Table 3 should be replaced by “ Out / ออก “ for “Scope moved out” action and “ in/ เข้า“ for “Scope moved in”, respectively, in order to utilize the robot move effectively and more appropriately to the task.

(ii) Verbal Command Unit should be selected to respond better to Thai-spoken words, especially those involving some specific Thai vowels as in “ ขึ้น “, and “ หยุด “. This may not be necessary if verbal commands in English are quite acceptable in practice.

(iii) Movements of the Laparoscope based on Kinematics are likely to be improved if designed on the principle of Reverse Kinematics (24).

(iv) Speeds of robotics responses as fixed for various commands in the prototype design may be advantageously made changeable to various values as required by the use of variable-speed, Pulse Width Modulated (75).

(v) Micro-circuitry would be desirable if a more compact system is desired, together with additional functions that can be catered for through the expanded 32 ports still available for future use.

Moreover, since **safety** is an obvious concern for surgical robotics(4), regulatory agencies require that the safety be addressed for every clinical implementation. As with most complex computer controlled system, there is no accepted technique that can guarantee safety for all systems in every circumstance (5), (6). Various robotic systems approach the problem in different ways. One common technique is to include passive and active safety mechanisms in the mechanical design of manipulator. Moreover, a good autonomous mode of controlling a medical tool requires a meticulous consideration of man-machine interaction(7).

If this prototype system, so constructed and tested, is to be developed into a workable medical tool, it must meet the Food and Drug Authority’s requirements by including the ease in man-machine manipulation and the safety feature as previously discussed.

REFERENCES

1. Cutkosky MR, Srinivasan M, Salisbury JK, and Howe RD, eds. 1999. *Human and Machine Haptics*. Cambridge: MIT Press. In press
2. Khatib O, ed. 1992. *Robotic Review 2*, Cambridge: MIT Press
3. Taylor, RH, Stulberg D. 1996. Section 4 Robotics, In Report Intl. Workshop Robotics and Comp. Assisted Med. Interventions. 2nd , Bristol, England, June, ed. A DiGioia, T. Kanade, PNT Wells, Pittsburgh: Ctr. Ortho. Rsch., hadyside Hospital http://www.cs.cmu.edu/afs/cs/project/mrcas/www/rcami/Title_page.doc.html
4. Troccaz J, Delnondedieu Y, Poyet A. 1995. Safety issue in surgical robotics. In *Proc. IFAC Workshop Human-Oriented Design Adv. Robotics Sys*., Vienna, Sept. ed. P Kopacek. pp. 19-26. Oxford: Pergamon
5. Ng WS, Tan CK. 1996. On safety enhancements for medical robots. *Reliability Eng. & Sys. Safety* 54(1): 33-45. Amsterdam: Elsevier.
6. Davies B. 1998. The safety of medical robots. In *Proc. International Symposium on Robotics,* 29th, BirmingHam, April, ed. F. Redmill, T. Anderson, pp. 70-74. Birmingham: British Robot Assoc.
7. Bauer A, Lahmer, A Borner M. 1998b. Man-machine interaction – pitfalls in robotic orthopedic surgery. In *Proc. Comp. – Aided Ortho. Surg. Conf*., pp. 68. Pittsburgh: Ctr. Ortho. Rsch., Shadyside
8. R.J. Anderson and M.W. Spong. Bilateral Control of Teleoperators with Time Delay. IEEE Transaction on Automatic Control, 34 (5): 494~501, May 1989.
9. R.J. Anderson and M.W. Spong. Asymptotic Stability for Force Reflecting Teleoperators with Time Delay. International Journal of Robotics Research, 11(2): 153~148, April1992.
10. F. Arai, M. Tanimoto, T. Fukuda, K. Shimojima, H. Matsuura, and M. Negoro. Mul-timedia Telesurgery Using High Speed Optical Fiber Network and Its Applications to Intravascular Nerosurgery –System Configuration and Computer Networked Implementation. In Proceeding sof the IEEE

International Conference on Robotics and Automation, volume1, pages 878~883, 1996.

11. T. Arai, S. Hashino, E. Nakano, and K. Tani. Advanced Teleoperation with Configuration Differing Bilateral Master-Slave System. In Robotics Research, the Fourth International Symposium, pages 163~170, 1988.
12. T. Bazsar and G.J. Olsder. Dynamic Non-cooperative Game Theory. Academic Press, second edition, 1995.
13. T.L. Brooks. Telerobotic Response Requirements. In Proceedings of the IEEE International Conference on Systems, Manand Cybernetics, pages 113~120, 1990.
14. M.C. Cavusogluglu, J. Yan, and S.S. Sastry. Ahybrid System Approach to Contact Stability and Force Control in Robotic Manipulators. In Proceedings of the 12th IEEE International Symposium on Intelligent Control, 1997.
15. M. Cohn, L.S. Crawford, J.M. Wendlandt, and S.S. Sastry. Surgical Applications of Milli-Robots. Journal of Robotics Systems, 12 (6): 401 (416), June 1995.
16. M.B. Cohn, M. Lam, and R.S. Fearing. Tactile Feedback for Teleoperation. In Proceedings of the SPIE, volume 1833, pages 240~254, 1993.
17. J.E. Colgate. Robust Impedance Shaping Telemanipulation. IEEE Transactions on Robotics and Automation, 9 (4): 374~384, August 1993.
18. H. Das, H. Zak, W.S. Kim, A.K. Bejczy, and P.S. Schenker. Operator Performace with Alternative Manual Control Modes in Teleoperation. Presence, 1 (2): 201~218, Spring 1992.
19. O. Faugeras. Three Dimensional Computer Vision. MIT Press, 1993. Chapters 3, 6 and 7.
20. O. Faugeras and et. al. Real Time Correlation-Based Stereo Algorithm, Implementation and Applications. Technical Report INRIA Research Report No 2013, INRIA Sophia-Antipolis, France, 1993.

21 K. Furuta, K. Kosuge, Y. Shiote, and H. Hatano. Master-Slave Manipulator Based on Virtual Internal Model Following Control Concept. In Proceedings of the IEEE International Conference on Robotics and Automation, pages 567~572, 1987.

22. E. Graves. Vital and Health Statistics. Data from the National Health Survey No. 122. U.S. Department of Health and Human Services, Hyattsville, MD, 1993.

23. B.L. Gray and R.S. Fearing. A Surface Micromachined Microtactile Sensor Array. In Proceedings of the IEEE International Conference on Robotics and Automation, volume1, pages 1~6, 1996.

24. B. Hannaford. A Design Framework for Teleoperators with Kinesthetic Feedback. IEEE Transactions on Robotics and Automation, pages 426~434, August 1989.

25. B. Hannaford. Stability and Performance Tradeoffs in Bi-Lateral Telemanipulation. In Proceedings of the IEEE International Conference on Robotics and Automation, pages 1764~1767, 1989.

26. B. Hannaford, L. Wood, D.A. McAffee, and H. Zak. Performance Evaluation of a Six-Axis Generalized Force-Reflecting Teleoperator. IEEE Transactions on System, Man, and Cybernetics, 21 (3): 620~633, May/June 1991.

27. J. W. Hill, P.S. Green, J.F. Jensen, Y. Gorfu, and A.S. Shah. Telepresence Surgery Demonstration System. In Proceedings of the IEEE International Conference on Robotics and Automation, pages 2302~2307, 1994.

28. L.A. Jones and I.W. Hunter. Analysis of the Human Operator Controlling a Teleoperated Microsurgical Robot. In Proceedings of 6th IFAC/IFIP/IFORS/IEA Symposium on Analysis, Design and Evaluation of Man-Machine Systems, pages 593~597, 1995.

29 W.S. Kim, B. Hannaford, and A.K. Bejczy. Force-Reflection and Shared Compliant Control in Operating Telemanipulators with Time Delay. IEEE Transactions on Robotics and Automation, 8(2): 176~185, April 1992.

30 S. Lavallee, J. Troccaz, L. Gabarit, P. Cinquin, A.L. Benabid, and D. Hoffmann. Image Guided Operating Robot: A Clinical Application in Stereotactic Nuro-surgery. InR.H. Taylor, S. Lavallee, G. Burdea, and R.Mosges, editors, Computer Integrated Surgery: Technology and Clinical Applications.

MITPress, 1995.

31 C.A. Lawn and B. Hannaford. Performance Testing of Passive Communication and Control in Teleoperation with Time Delay. In Proceedings of the IEEE International Conference on Robotics and Automation, pages 776~783, 1993.

32. D.A. Lawrence. Stability and Transperancy in Bilateral Teleoperation. IEEE Trans-actions on Robotics and Automation, 9(5): 624~637, October 1993.

33. J. Lewin. Differential Games. Springer-Verlag, 1994.

34. J. Lygeros, D.N. Godbole, and S.S. Sastry. A Game Theoretic Approach to Hybrid System Design. Technical report, University of California, Berkeley, 1995.

35 J.K. Mills. Manipulator Transition to and from Contact Tasks: A Discontinuous Control Approach. In Proceedings of the IEEE International Conference on Robotics and Automation, pages 440~446, 1990.

36 R.M. Murray, Z. Li, and S.S. Sastry. A Mathematical Introduction to Robotic Manipulation. CRC Press, Inc., 1994.

37 G. Niemeyer and J.J.E. Slotine. Stable Adaptive Teleoperation. IEEE Journal of Oceanic Engineering, 16(1): 152~162, January 1991.

38. G.J. Raju, G.C. Verghese, and T.B. Sheridan. Design Issues in 2-port Network Models of Bilateral Remote Manipulation. In Proceedings of the IEEE International Conference on Robotics and Automation, pages 1316~1321, 1989.

39 A. Rovetta, R. Sala, X. Wen, and A. Togno. Remote Control in Telerobotic Surgery. IEEE Transactions on Systems, Man, and Cybernetics Part A: Systems and Humans, 26(4): 438~443, July 1996.

40 D.N. Roy. Applied Fluid Mechanics. Ellis Horwood Limited, 1988.

41 S.S. Sastry, M. Cohn, and F. Tendick. Millirobotics for Remote, Minimally-Invasive Surgery. Journal of Robotics Systems, to appear in 1997.

42 T.B. Sheridan. Telerobotics, Automation, and Human Supervisory Control. MIT Press, 1992.

43 T.B. Sheridan. Space Teleoperation Through Time Delay: Review and Prognosis. IEEE Transactions on Robotics and Automation, 9(5): 592~606, October 1993.

44. P.S. Schenker, H. Das, and T.R. Ohm. A New Robot for High Dexterity Microsurgery. In N.Ayache, editor, Computer Vision, Virtual Reality and Robotics in Medicine. First International Conference, CVRMed'95. Proceedings., pages 115~122, Berlin, Germany, 1995. Springer-Verlag.

45 R.H. Taylor, J. Funda, B. Eldridge, S. Gomory, K. Gruben, D. LaRose, M. Talamini, L. Kavoussi, and J. Anderson. A Telerobotics Assistant for Laparoscopic Surgery. IEEE Engineering in Medicine and Biology Magazine,, 14 (3): 279~288, May/June 1995.

46. R.H. Taylor, B.D. Mittlstadt, H.A. Paul, W. Hanson, P. Kazanzides, and et.al. An Image-Directed Robotics System for Precise Orthopaedic Surgery. IEEE Transactions on Robotics and Automation, 10 (3): 261~275, June 1994.

47. F. Tendick. Personal Communication, 1997.

48. F. Tendick, S. Bhoyrul, and L. Way. Comparison of laparoscopic imaging systems and conditions using a knot tying task. Journal of Image Guided Surgery, 2 (1), 1996.

49 R. Tombropoulos, A. Schweikard, J.C. Latombe, and J.R. Adler. Treatment Planning for Image Guided Robotic Radio surgery. In N. Ayache, editor, Computer Vision, Virtual Reality and Robotics in Medicine. First International Conference, CVRMed'95. Proceedings., pages 131~137, Berlin, Germany, 1995. Springer-Verlag.

50 L.W. Way, S. Bhoyrul, and T. Mori, editors. Fundamentals of Laparoscopic Surgery. Churchill Livingstone, 1995.

51 J. Wendlandt. Milli Robotics for Endoscopy. Memo M94/7, UC Berkley ERL, January 1994.

52 J. Wendlandt and S.S. Sastry. Designand Control of a Simplified Stewart Platform for Endoscopy. In Proceedings of the IEEE Conference on Decision and Control, volume1, pages 357~362, 1994.

53. J. Yan and S.E. Salcudean. Teleoperation Controller Design Using H-infinity Opti-mization with Application to Motion-Scaling. IEEE Transactionson Control Systems Technology, 4(3): 244~258, May 1996.

54. Y. Yokokohji and T. Yoshikawa. Bilateral Control of Master-Slave Manipulators for Ideal Kinesthetic Coupling-Formulation and Experiment. In Proceedings of the IEEE In ternational Conference on Robotics and Automation, pages 849~858, 1992.

55. Y. Yokokohji and T. Yoshikawa. Bilateral Control of Master-Slave Manipulators for Ideal Kinesthetic Coupling-Formulation and Experiment. IEEE Transactions on Robotics and Automation, pages 605~620, October 1994.

56. Z. Zhang and et.al. A Robust Technique for Matching Two Uncalibrated Images Through Recovery of the Unknown Epipolar Geometry. Technical Report INRIA Re-search Report No 2273, INRIA Sophia-Antipolis, France, May 1994.

57. L. Mettler, M. Ibrahim and W. Jonat, "One Year of Experience Working with the Aid of a Robotic Assistant the Voice-controlled optic holder AESOP in Gynaecological Endoscopic Surgery", *Human Reproduction*, Vol. 13, No. 10, 1998, pp. 2748-2750.

58. David Prewer, Les Kitchen. "A Simple Fast Edge-Based Visual Tracker". *Technical Report* 97/20, pp. 1-14. http://citeseer.nj.nec.com/59426.html

59. A. Azarbayejani and A. Pentland, "Real-time self-calibrating stereo person tracking using 3-D shape estimation from blob features", Proceedings of International Conference on Pattern Recognition , Aug. 1996, pp. 627—632.

60. Reddi, S. and G. Loizou, "Analysis of camera behavior during tracking", IEEE Transactions on Pattern Analysis and Machine Intelligence, volume 17 (1995), number 8, pp. 765 – 778.

61 M. E. Leventon, "Bayesian estimation of 3-d human motion from an image sequence" Technique report . July 1998. http://www.merl.com/reports/TR98-06/

62. Y. Wang, D. R. Uecker and Y. Wang, "Choreographed Scope Maneuvering in Robotically-Assisted Laparoscopy with Active Vision Guidance", IEEE Workshop on Application of Computer Vision, Saratoga, FL, Dec. 1996, pp. 187 – 192.

63. G. Wei, K. Arbter and G. Hirzinger, “Real Time Visual Servoing for Laparoscopic Surgery”, IEEE in Engineering and Biology, Jan. 1997, pp. 40 – 45.

64. C. Chen, S. Stitt and Y.F. Zheng, “Robotic Eye-in-Hand Calibration by Calibrating Optical Axis and Target Pattern”, Journal of Intelligent and Robotic System, 12, 1995, pp. 155-173.

65. R. Y. Tsai, “A Versatile Camera Calibration Technique for High- Accuracy 3D Machine Vision Metrology Using Off-the-Sheld TV Cameras and Lenses”, IEEE Journal of Robotics and Automation, Vol. RA-3, No. 4. Aug. 1987, pp. 323-344.

66. James D. Foley, Andries van Dam, Steven K. Feiner, John F. Hughes, Computer Graphics: Principles and Practice, Addison-Wesley 1995.

67. K.V. Asari, S. Kumar and D. Rashakrishnan, “Technique of Distortion Correction in Endoscopic images Using a Polynomial Expansion”, Medical &Biological Engineering & Computing, vol.37, 1999, pp 8-12.

68. W. E. Smith, N. Vakil and S. A. Maislin, “Correction of Distortion in Endoscope Images”, IEEE Transactions on Medical Imaging, Vol. 11. No. 1 1992, pp. 117- 122.

69. P. Wolf, Elements of Photogrammetry, Mcgraw-Hill Inc.1983.

70. KARL STORZ Endoscopy Canada Ltd, http://www.karlstorz.com/.

71. Ascension Technology Corporation, http://www.ascension-tech.com.

72. C.K. Lee, W.H. Pang., “A Brushless DC Motor Speed Control System Using Fuzzy Rules, “ Proceedings Power Electronics and Variable Speed Drives Conference, pp. 101~106, October 1994.

73. B.K. Bose., Modern Power Electronics and AC Drives, Prentice Hall, pp 483~492.

74. T. S Low et al., “Servo performance of a BLDC drive with instantaneous torq control”, Proceedings IEEE Control and Drives conference 1990, pp. 454~459.

75. Advance Motion Controls, PWM Servo Amplifiers 1999-2000 Catalog and Technical Manual., pp C-11~C-16.

75. Seattle Robotics Society – *What's a Servo?*
http://www.seattlerobotics.org/guide/servos.html

76. Marven C. & Ewers G. *A Simple Approach to Digital Signal Processing*, Chapter 6, John Wiley & Sons, 1996

78. Morton T. D. *Embedded Microcontrollers*. Prentice Hall, 2001

79. Kissell T. E. *Industrial Electronic – Applications for Programmable Controllers, Instrumentation & Process Control and Electrical Machines & Motor Controls*, Chapter 12 – AC & DC Motors, 2nd Ed. Prentice Hall, 2000

80. Motorola Semiconductor, *MC68HC912B32 Advanced Information*, Rev.3, Motorola Inc., 1999

80. Mohan N., Underland T.M & Robbins W.P., *Power Electronics – Converters, Applications and Design*. 2nd Ed. Chapter 13, John Wiley & Sons Inc. 1995

81. Jones D. W. Basic Stepping Motor Control Circuits. The University of Iowa – Department of Computer Science.
http://www.cs.uiowa.edu/~jones/step/circuits.html#bipolar

82. SGS Thompson. *L293D Data Sheet*, July 2003

APPENDIX A

APPENDICES
APPENDIX A

APPLICATION OF VISUAL TRACKING FOR ROBOT-ASSISTED LAPARO-SCOPIC SURGERY

Medical robotics and computer assisted surgery are new and promising fields of study, which aim to augment the capabilities of surgeons by taking the best from robots and humans.

In joint project between the Robotics and Intelligent Machines Laboratory of University of California at Berkeley, and the Department of Surgery of University of California at San Fransisco, a telesurgical workstation is being developed for use in laparoscopic surgery. The current design is a 6 DOF manipulator instrumented with a gripper controlled by a 6 DOF master manipulator.

Research on medical robotics at UC Berkeley includes (but is not limited to) the development of an endoscopic manipulator, early designs of millirobotic manipulators for laparoscopy, and studies on tactile sensing.

Laparoscopic surgery, or more generally endoscopic surgery, is a revolutionary techniqueinsurgery. They are minimally invasive, i.e. the operation is performed with instruments inserted through small incisions (~10 mm in diameter) rather than by making a large incision to expose the operation site. The main advantage of this technique is the reduced trauma to healthy tissue, which is the major reason for post-operational pain and long hospital stay of the patient. The hospital stay and rest periods, and therefore the operations' cost, are significantly reduced with minimally invasive operations, at the expense of more difficult techniques performed by the surgeon.

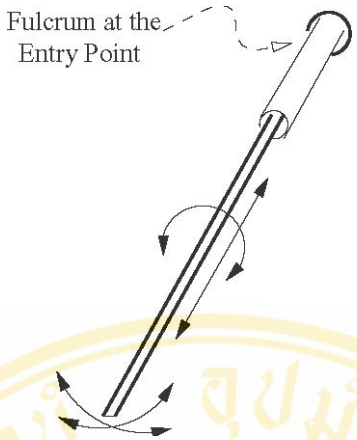

Figure A 4 DOF available in conventional laparoscopic instruments

Mainimally invasive operations include laparoscopy (abdominal cavity), thoracoscopy (chest cavity), arthroscopy (joints), pelviscopy (pelvis), and angioscopy (blood vessels). The first laparoscopic surgery was performed in 1985 by Muhe in (West) Germany. In the last decade, there was a quick shift from open surgery to laparoscopic surgery in simple operations, the most dramatic one being cholecystectomy (removal of gallbladder), of which 67 % were performed laparoscopically in the US in 1993.

In laparoscopic surgery, the abdominal cavity, which is expanded by pumping carbon dioxide inside to open a workspace, is observed with a laparoscope inserted through one of the incisions. The laparoscope it self is composed of a chain of lens optics to transmit the image of the operation site to the CCD camera connected to its outer end, and fiber optic cables to carry light to illuminate inside. A monoscopic image of the operation site is displayed on a TV screen. The instruments used for the operation are specially designed long and thin instruments and they are inserted through trocars put at the incision to air seal the abdomen. The instruments have only 4 DOF (see figure A), preventing the ability to arbitrarily orient the instrument tip, and trigger-like handles. The dexterity is significantly reduced because of the lost DOF's and motion reversal due to the fulcrum at the entry point

Motion reversal due to the fulcrum at the entry point. Force feedback is almost completely lost due to the friction at the air tight trocar and the stiffness of the inflated abdominal wall. There is no tactile sensation at all, which surgeons highly depend on in open surgery to locate arteries and tumors hidden in the tissue.

Minimally invasive surgery itself is telemanipulation as the surgeon is physically separated from the workspace. Therefore, telerobotics is the natural tool to extend capabilities in laparoscopic surgery. With the telesurgical workstation developed, the goal is to replace the manipulation and sensation capabilities of the surgeon which were lost due to minimally invasive surgery. A 6 DOF slave manipulator controlled through a spatially consistent and intuitive master will replace the dexterity, force feedback to the master will give back the fidelity of the manipulation, and tactile feedback will replace lost tactile sensation.

Other work in the literature on telesurgical systems for abdominal surgery include the telesurgical system for open surgery with 4 DOF manipulators developed at SRI International (laparoscopic version is also being developed), the telerobotic assistant for laparoscopic surgery developed by Tayloret.al., and the telesurgery experiments performed between JPL, California and Polytechnic University of Milan, Italy, and between Nagoya and Tokyo in Japan.

There are other successful medical applications of robotics including systems for orthopedic surgery, micro-surgery and stereotactic neurosurgery, eyesurgery, and radiotherapy.

Recently, laparoscopic surgery gained increasing popularity because of its minimally invasive nature. In laparoscopic surgery, a surgical operation can be performed with an endoscope and several long, thin, rigid instruments (see Figure 1) through several small

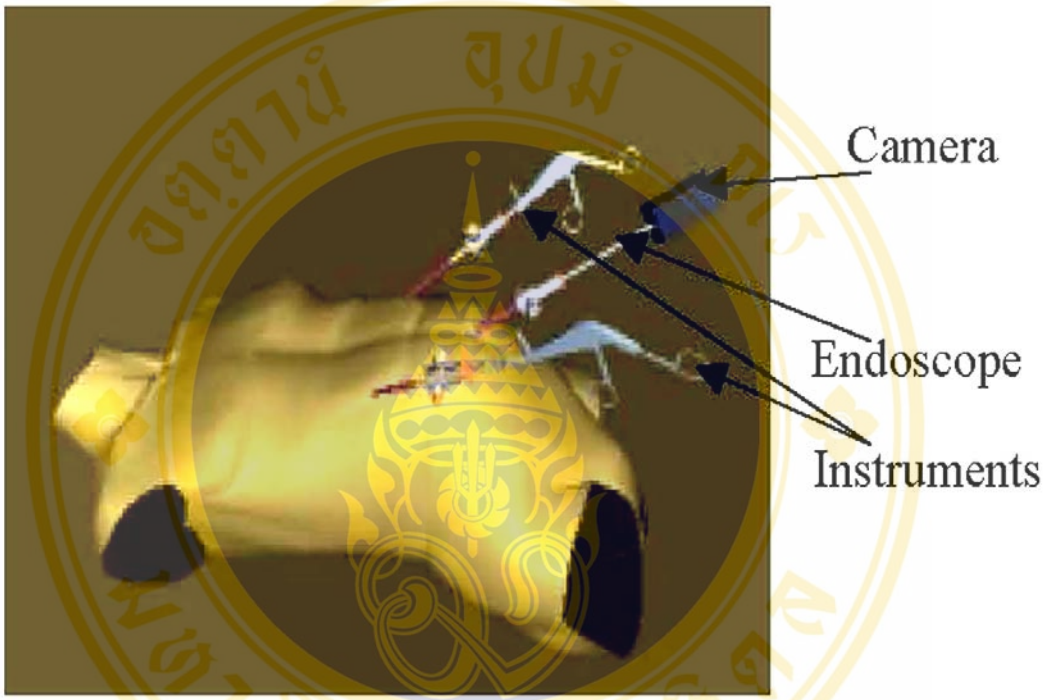

Figure 1. Tools needed for laparoscopic surgery.

incisions. Compared with traditional surgery, laparoscopic surgery provides less pain, faster recovery and small injuries. However, to control the surgeon's field of view, an assistant surgeon is needed to hold and manipulate the camera. During lengthy

procedures, accurate and on time adjustment of the camera cannot be guaranteed due to the fatigue of the camera assistant. Instead, using a robot to control the camera will result in less erroneous camera motion and can off-load routine tasks.

A typical laparoscopic surgery using robot camera assistant is shown in figure 2. The endoscope relays images of internal organs to a camera, and the images are displayed on a video screen placed in front of the surgeon. However, the lack of intelligence in the

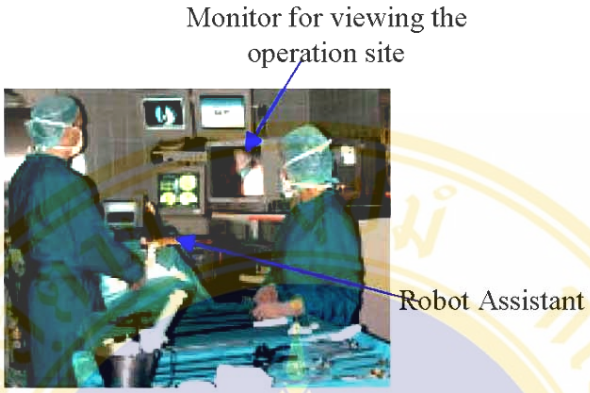

Figure 2. Laparoscopic surgery using a robot camera assistant.

design of current robot camera controllers presents a challenging problem. For example, the surgeon in general is often distracted by issuing positioning command to the robot manipulator via hand-held controllers, a foot pedal or other interface such as voice control, e.g., voice controlled robot AESOP.

To improve the current robot-assisted laparoscopic surgery system, we propose to use visual tracking techniques to enable automatic robotically control of the camera. In order to track the instrument, we need to know the three-dimensional (3D) positional information. In general, such 3D information can be obtained from stereo-endoscopy (the use of two separate optical channels, each with its own lens optics). However, this approach doubles the hardware, thus it is not widely accepted by clinicians. We propose a method that uses a single endoscope to obtain the 3D positional information of the instrument.

Visual tracking is an active research area addressed by many researchers. Prewer and Kitchen used edge correspondence to track the image features. Azarbayehani and Pentland obtained the 3D locations of the face and hands by tracking skin blobs. Reddi and Loizou used optical flow field to control the camera's motion to keep a target at the center of the camera's field of view. By using prior knowledge about how humans move, Leventon built a Gaussian probability model to reconstruct the 3D motion of a human figure from a monocular image sequence. However, only a few researchers addressed visual tracking in laparoscopic surgery: Wang et al. used color statistics to classify, group and label instrument directly, Wei et al. designed a marker and using color selection and color segmentation to detect and locate the marker.

Due to the diversity of the instruments, it is hard to track the tip of instruments directly as described in In this paper, we propose to design a marker and attach the marker to the tip of the instrument. When needed, visual tracking techniques can be

applied to track the marker as the instrument moves. Instead of using color information for visual tracking as proposed we use monochrome data for processing. Generally, monochrome image processing is quicker, simpler and robust. The 3D positional information of the marker then will be used to realize automatic tracking of the instruments.

There are many difficulties associated with using markers for instrument localization. First, images taken from the endoscope are distorted so it is difficult to obtain the correct measurement of the images. Second, tools may enter the endoscope field of view from different directions and at various angles. Finally, using images from mono-endoscope to reconstruct 3D spatial information is a challenging task. These problems will be addressed and solved in later parts of this paper.

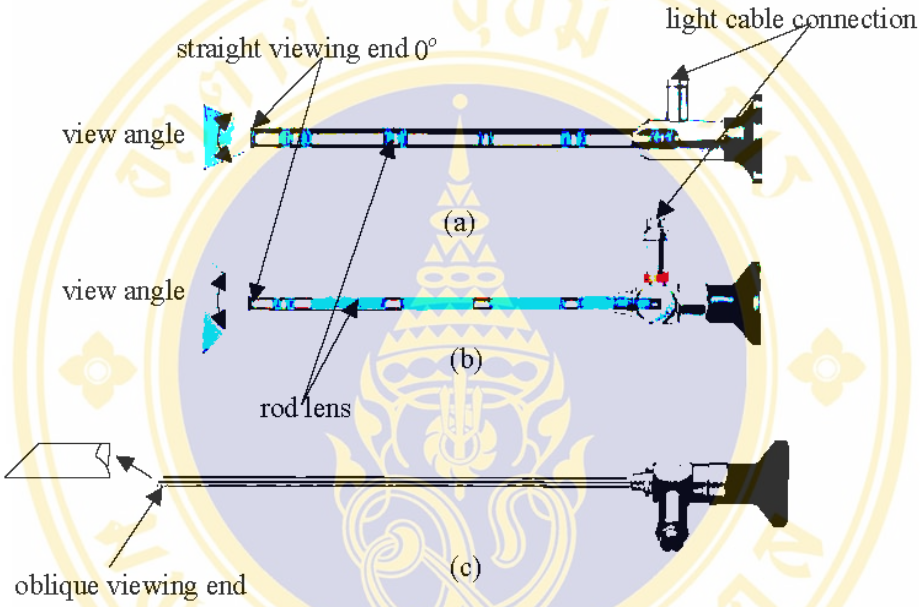

Figure 3. Rod Lens endoscope (a) An endoscope featuring a conventional lens system. Refraction occurs as light passes through small lenses seated at distant intervals. (b) A HOPKINS rod lens endoscope. The rod lenses are seated at close intervals, resulting in better light transmission and reduced diameter. (c) Forward-oblique Endoscope 45°.

The remainder of this paper is organized as follows: Section 2 presents a method for endoscope calibration. In section 3, marker design and tracking algorithm are discussed. In section 4, endoscope image distortion correction method is described in detail. To investigate the tracking results, the design and simulation of a camera manipulator are described in the section 5. Finally the experimental results are shown and future work is discussed.

2. Calibration Method

Defining the pixel-to-world mapping is known as camera calibration. Once the camera has been calibrated, we can transform the image pixel coordinates to their real-

world equivalents. Camera calibration is a critical first step in many applications such as dimensional measurement of mechanical parts, tracking, camera-on-robot configuration and robot vehicle guidance. Camera calibration has been investigated extensively by many researchers However, methods for camera calibration using rigid endoscope have not been addressed before.

In general, endoscope images have particular characteristics. The endoscope viewing angle, typically between $65° - 75°$, as shown in Figure 3, is narrow compare to the wide field of view of human eyes. Thus, vision is limited by the narrow endoscope field of view. To enlarge the field of view of endoscopes, wide-angle lens are employed in the endoscope. However wide-angle lenses intrinsically cause barrel distortion (i.e., transformation of straight line into curves). Barrel distortion cause objects in the image to be distorted along radial lines from the image center. This type of distortion is non-linear: image areas farther away from the center appear significantly smaller. This paper proposes a calibration method that assumes the image located within the small center area is distortion free.

Typical calibration parameters can be classified into two classes: extrinsic parameters and intrinsic parameters. This section presents methods for determining intrinsic parameters, namely, the effective focal length, the real image center and the scale factor. The extrinsic parameters, that is, the rigid body transformation from the world coordinate system to the camera coordinate system is discussed later.

Figure 4 illustrates the basic geometry of the camera model with (x, y, z) as the world coordinate system. In robotic system, this coordinate frame can be placed at the robot base. (x_c, y_c, z_c) is the camera coordinate system, $P(x, y, z)$ is the 3D coordinates of a

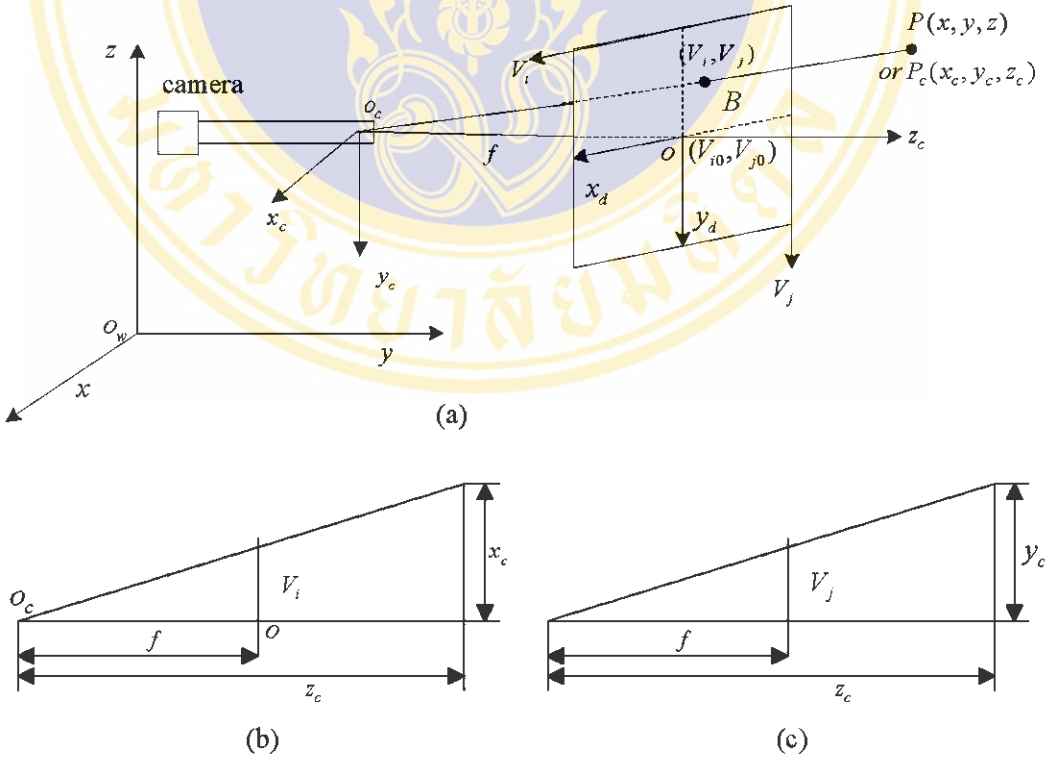

Figure 4. Camera geometry with perspective projection.

object P in the world coordinate system, $P(x_c, y_c, z_c)$ is the coordinate of point P in the camera coordinate system with its z_c axis the same as the optical axis. (x_d, y_d) (not shown in Figure 4) is the image coordinates of $P(x_c, y_c, z_c)$ projected into the image plane if a perfect pinhole model assumption is used [10]. However, since the unit for the coordinate used in the computer, (V_i, V_j), is the number of pixels in the frame memory, additional scale factors need to be specified that relate the camera coordinate system to the computer image coordinate system (using pixel units).

The focal length f is the distance between the image plane center, o, and the optical center, o_c. Here we define the image center as the point where the camera optical axis passes through the image plane. In theory, the image center should be the center of the image plane. However, in practice, especially in the endoscope image, the real image center is distorted due to the imperfect grind of endoscope lens.

In the following, first we propose a simple and fast method to obtain the real image center. Then, a method for calculating the calibration parameters such as the effective focal length and the scale factor. Figure 5 shows the calibration flow chart.

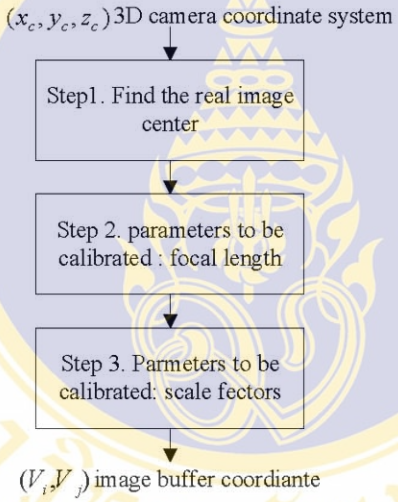

Figure 5. Three steps in endoscope calibration.

The first problem that needs to be addressed is the method for calculating the real image center. Since abdominal cavity is dark, an external light source is used, see Figure 3. A fiber optic cable transmits light to the side of the endoscope. The light source is evenly distributed through the rod lens. If we point the endoscope perpendicular to a white background, the light source forms a white circle in the image as shown in Figure 6. (a). Inspired by this feature, we propose a simple method to obtain the real image center by pointing the endoscope to a white background and recording the image. The center of the white circle in the image is defined as the real image center as seen in Figure 6. (b). Other work, such as Asari et 11], considered the distortion in endoscope image and proposed to use straight-line patterns. Then chose the intersection of lines that remain straight in the endoscope image as the real image center. However, their methods need

complex calculations. The feasibility of the proposed method for determining the real

(a) (b)

Figure 6. Endoscopic image (a) original gray scale image, (b) binary image (the image center has been marked).

image center is evaluated later in the experimental results section.

The second parameter to be calibrated is the effective focal length. As shown in Figure 4, the transformation from the 3D camera coordinate (x_c, y_c, z_c) to the image coordinate (V_i, V_j) based on the perspective projection with pinhole camera geometry yields the following equations:

$$\frac{\overline{oo_c}}{z_c} = \frac{f}{z_c} = \frac{(V_i - V_{i0})S_x}{x_c} = \frac{(V_j - V_{j0})S_y}{y_c}, \qquad (1)$$

$$x_c = \frac{z_c(V_i - V_{i0})S_x}{f}, \; y_c = \frac{z_c(V_j - V_{j0})S_y}{f},$$

where $\overline{oo_c}$ is the distance between the center of the image buffer to the center of the camera coordinate frame, (V_{i0}, V_{j0}) is the image center in the pixel unit, S_x, S_y are the scale factors that map (x_d, y_d) in the camera coordinate frame to (V_i, V_j) in the computer image coordinate frame. When V_i, V_j, X_c and Z_c are known parameters the effective focal length can be calculated from equation (1). Also, when f, V_i, V_j and x_c, y_c are known parameters, we can calculate the depth information, Z_c, of an object in

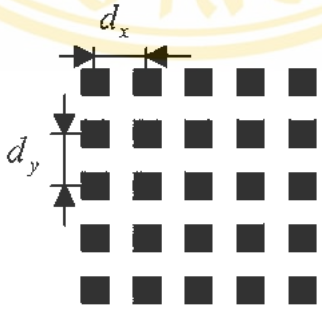

Figure 7. The pattern image for calibration.

the field of view. Scale factors S_x, S_y can be obtained using the following formula

$$x_d = (V_i - V_{i0})S_x,\ y_d = (V_j - V_{j0})S_y. \quad (2)$$

In general, manufacturers of CCD cameras supply the information of center-to-center distance between adjacent sensor elements in the Y direction (i.e., scale factor S_y) as a fixed value: $S_y = N_{fY} / d_y$, where N_{fY} is the number of pixels in the Y direction; d_y is the dimension of CCD in the Y direction. The scale factor S_x is an uncertain value due to various reasons, such as slight hardware timing mismatch between image acquisition hardware and camera scanning hardware, or the imprecision of the timing of TV scanning itself. Here we propose a simple and fast method to obtain the relationship between S_x and S_y.

By capturing an image of known dimension (e.g., the square grids, d_x and d_y are the actual center-to-center distance in millimeters of adjacent squares, see Figure 7), we can compute their corresponding, D_x and D_y, in pixel units in the computer image coordinate. The following relationship exists: $D_x = S_x d_x, D_y = S_y d_y$.

Solving for S_x, we get

$$S_x = S_y \times D_x / D_y. \quad (3)$$

In actual implementation, we can measure several squares' center-to-center distances and take the mean value to reduce the possible error in image processing.

3. Lens Distortion and Correction Methods

No lens can produce perfect images. Common imperfections are aberrations that degrade the quality or sharpness of the image and lens distortions that deteriorate the geometric quality (or positional accuracy) of the image. Endoscope image has a fundamental lens distortion due to the wide-angle design of the endoscope's objective lens. Wide-angle lenses are used in endoscope because they provide larger viewing fields. However, lens distortion will result in erroneous measurement for image positions in the resulting images. To eliminate the distortion effect, corrections should be applied to the measurement of the resulting endoscope images.

Lens distortions are classified as either radial or tangential. Radial distortion, as its

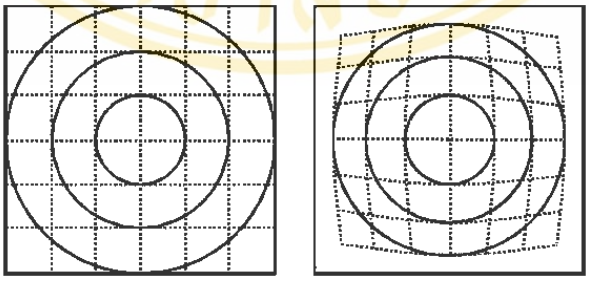

Figure 8. Barrel type distortion (The left image is an undistorted grid pattern, and the right image is the same pattern viewed after radial distortion).

name implies, causes image position to be distorted along radial line from the optical axis. Radial distortion includes barrel distortion, pincushion distortion or the combination of these two types. Tangential distortion is due to imperfect centering of the lens components and other manufacturing defects in a compound lens, and is also called decentering. That is, the optical center and the lenses are not strictly collinear. The pixel shift is away from the optical center and the new position lies at a new angle location as measured from the optical center. Tangential lens distortions are generally very small and are seldom corrected for.

Barrel type radial distortion is common in laparoscopic images, see Figure 8. Areas further from the center of the field of view appear smaller than they really are. In this paper, we only consider the barrel type distortion. We propose a distortion correction method that approximates the distortion curve by a polynomial and uses the least squares method to find the coefficients for this polynomial. With this experimentally determined polynomial, we can correct the endoscope image accordingly.

3.1 Radial Lens Distortion Model

The radial lens distortion model consists of two image planes. The distorted image plane is represented by (V_i', V_j'), while the distortion correction image plane is represented by (V_i, V_j). Their corresponding centers are represented by (V_{i0}', V_{j0}') and (V_{i0}, V_{j0}). The center of the distortion-correction image can be chosen arbitrarily. Unlike the method proposed by that selects these two centers at different locations, in this paper, we select both centers the same as the real image center. The real image center is defined as the point where straight lines remain straight as they pass through this point in the distorted image plane.

Using a polar coordinate system with its origin at the real image center (V_{i0}, V_{j0}), a point P' in the distorted image plane can be represented as

$$r' = \sqrt{(V_i' - V_{i0}')^2 + (V_j' - V_{j0}')^2},$$
$$\theta = \arctan\left(\frac{V_j' - V_{j0}'}{V_i' - V_{i0}'}\right), \tag{4}$$

where magnitude, r', is the distance of P' to the center (V_{i0}', V_{j0}'). The corresponding point, P', in the corrected image plane is P. Point P can be represent in polar coordinate as (r, θ). Because we assume that the distortion is pure radial, the polar angle is unchanged in the distorted and corrected image planes. Hence: $\theta = \theta'$.

The objective of the distortion model is to find the relationship between P and P'. As shown in Figure 9, the relationship between r and r' is

$$r' = r - \Delta r, \tag{5}$$

where Δr can be represented as an odd-ordered polynomial series :

$$\Delta r = k_1 r + k_2 r^3 + k_3 r^5 + k_4 r^7 + \ldots \tag{6}$$

where $k_i (i = 1,2,3...)$ are the expansion coefficients. After obtaining the coefficients, the new pixel location in the corrected image plane can be calculated as:

$$V_i' = V_i - \Delta V_i = V_i(1 - \frac{\Delta r}{r}) = V_i(1 - k_1 - k_2 r^2 - k_3 r^4 - ...)$$
$$V_j' = V_j - \Delta V_j = V_j(1 - \frac{\Delta r}{r}) = V_j(1 - k_1 - k_2 r^2 - k_3 r^4 - ...). \quad (7)$$

To obtain the polynomial series for mapping the distorted image to the distortion correction image, first, we need to obtain the coefficients for the polynomial.

3.2 Coefficients Estimation

The polynomial coefficients define the shape of the curve. They can be calculated by nonlinear regression analysis, such as the least squares method, to obtain the best curve fit to a given data set (obtained from experiments). A pattern image (see Figure 7) was used to obtain the given data set. Since we assume that the distortion is pure radial, the distortion is circularly symmetric. Without the loss of generality, testing squares that lie in the horizontal or vertical of the image can represent the general distortion pattern for the whole image. For a given data set $S = \{C_1, C_2, ..., C_i, ...C_N\}$, let there be N columns of testing squares, for each $C_i(r_i, \Delta r_i)$, r_i represents the radial distance between the center of the square from the real image center, Δr_i is the distortion at a radial distance r_i. Consider the polynomial series of degree $2M+1$:

$$\Delta r_i = k_0 r_i + k_1 r_i^3 + k_2 r_i^5 + ... + k_j r_i^{2j+1} + ..., \quad j = 0,...M \quad (8)$$

The deviation of a point from the above equation is

$$F_i = y_i - \sum_{j=0}^{M} k_j r_i^{2j+1}. \quad (9)$$

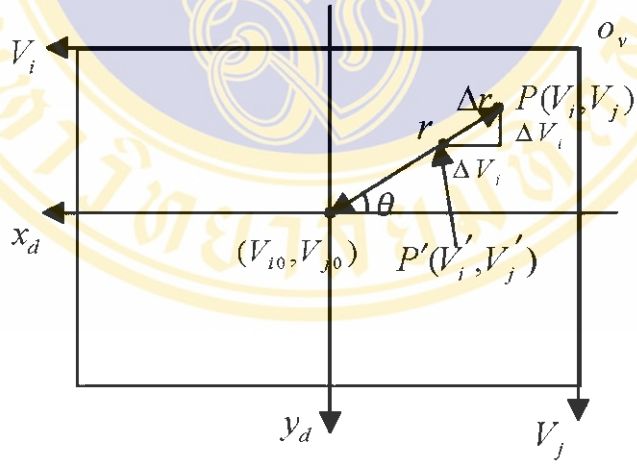

Figure 9. Components of Radial Distortion. The image point (V_i, V_j) is radically displaced by Δr to the new position (V_i', V_i').

The least squares problem is then to find the values of k_j, $j = 0,..,M$, so as to minimize

$$\sum_{i=1}^{N}[y_i - (\sum_{j=0}^{M} k_j r_i^{2j+1})]^2 \quad (10)$$

Hence, k_j can be calculated by

$$\frac{\partial F_i}{\partial k_j} = 0, \qquad for \quad j = 0,1,...,M. \quad (11)$$

From equation (9), $M+1$ simultaneous equations are obtained and represented in the matrix form:

$$AK = Y. \quad (12)$$

where

(a) (b)

Figure 10. (a) The original image, (b) the image after distortion correction (using forward mapping).

$A = [r_i^{2j+1}]_{(N+1)\times(M+1)}$, $for\ i = 0,..N,\ j = 0,...,M$,

$K = [k_0, k_1, ..., k_M]^T$,

$and\ Y = [y_0, y_1, ..., y_N]^T$.

Equation (12) can be calculated as

$$K = (A^T A)^{-1} A^T Y. \quad (13)$$

The matrix K consists of most probable values for unknowns, $k_0, k_1, ..., k_M$.

Once the expansion coefficients are computed, all pixels from the distorted image are mapped onto the corrected image. However, the direction of mapping is one problem to be considered. One approach is mapping from the distorted image plane to the corrected image plane using the formula of $r = r' + \Delta r'$ or

$$r = k_1' r' + k_2' r'^3 + k_3' r'^5 + k_4' r'^7 + ... \quad (14)$$

where r' is the radial distance measured in the distorted image plane. r is the radial distance measured in the corrected image plane. However, this method of mapping will result in blank pixels in the corrected image due to the non-linear expansion of the image. The original image has to be mapped into a new enlarged image. See Figure 10 (b),

notice there are many blank pixels in the image, especially in the peripheral areas. This problem can be avoided by using an inverse-mapping method, that is, mapping from the corrected image plane to the distorted image plane. The coefficient estimation method described in equation (7) used the inverse mapping method. In equation (7), r was measured in the corrected image plane. Thus, for every pixel in the corrected image plane, the corresponding location in the distorted image is obtained using the polynomial (8). The information (e.g., gray level) for that pixel location is assigned to the pixel in the corrected image plane. In the event that the pixel positions calculated using inverse mapping are non-integers, we simply round them to the closest integers. Because the corrected image enlarged the distorted image in barrel type radial distortion, several pixels in the corrected image may possibly find the same pixel in the original image. In this manner, all pixels in the corrected image plane can find their corresponding pixel values, thus generating a complete undistorted image.

4. Marker Design

As mentioned in the introduction section, researchers have proposed several types of tracking methods such as optical flow (the optic flow field is the 2D distribution of apparent velocities that associated with the variation of brightness patterns on the projection), feature points correspondence and model-based tracking. In our application, due to the diverse design of instruments, it is difficult to locate the instrument directly. To solve this problem, a black strip marker is designed. The marker is attached to the tip of instruments, which is then identified for the tracking task.

In general, the tracking task includes recognizing markers and calculating its relative position in the camera coordinate system. In real surgery, the instrument may enter the field of view from different positions and at different angles, using shape analysis and pattern matching would be infeasible, for there is no fixed shape suited for tracking. Instead, the image contrast information is used alone for instrument segmentation to locate the marker's position in the image. Two factors should be considered in the marker design. For one thing, in real-time image tracking, the marker should be simple and easy to locate. For the other, the marker's size should be chosen according to the size of the instruments.

Considering the above constrains, we design the marker as shown in Figure 11. The strips in Figure 11 are the designed markers. They are of the same size, each with the

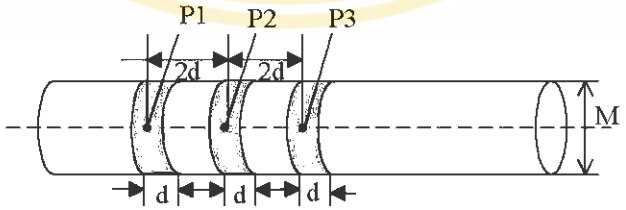

Figure 11. The designed marker.

width of d ($M/3 < d < M/2$). The diameter of the instrument is M. Points $P1, P2$ and $P3$ are the centers of each strip projected onto the image plane. These strips' center-to-center distance is $2d$.

Designing the marker in this shape has several advantages. First, the shape of the marker is simple and its contrast with the instruments and background is large; thus, it is easy to identify the marker. Second, the tool's diameter M is used to acquire depth information. Regardless how the instrument rotates along its axis (see the dotted line in Figure 11), we can always find two peripheral points on the marker that can represent the tool's diameter. Finally, even if an organ or other instruments block one or two strips, we can still get the instrument positional information form the remaining strips (at least one strip should be in the endoscope field of view).

When needed, the tracking task is to move camera so as to position an instrument feature, such as markers, at the desired location of the endoscope field of view and also keep the depth of the chosen instrument feature as a given value as the instrument moves.

Considering Figure 11, during the tracking procedure, one of the points among $P1, P2$, and $P3$ is located, the located point has not been blocked and is the closest to the tip of the instrument. To determine which point is the closet one to the tip, we can compare their diameter M value in the image. We assume that in laparosocopic surgery, generally the tip of the instrument is the point that is the furthest away from the endosocpe; thus, the smallest M is the one closed to the tip of the endoscope. Based on the change of the chosen point in V_i and V_j directions in the image plane and the calibration parameters described in section 2, we can calculate the displacement in real world unit to which the endoscope should be moved. From the change of diameter M in the image plane, the depth information of the marker can also be obtained using formula (1). This information is utilized as feedback for manipulating the endoscope so as to keep the tip of the instrument at a desired position in the endoscope field of view.

5. Endoscope Holder Design

In laparosocopic surgery, the endoscope is inserted into the abdominal cavity through a trocar. Constrains at the pivot point only allow four degrees of freedom for

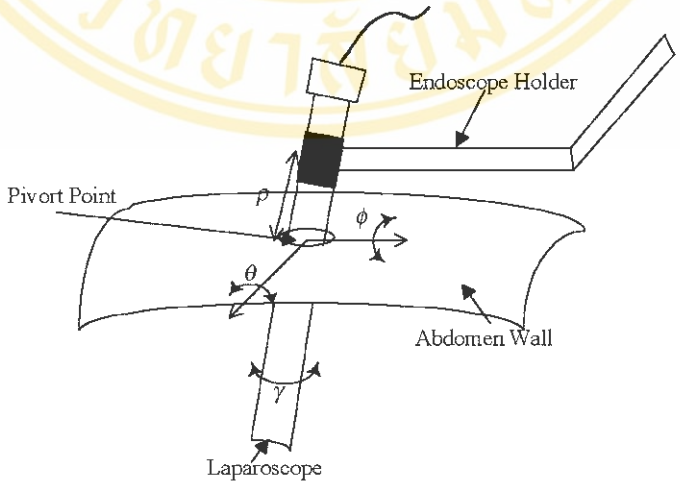

Figure 12. 4 DOF constraints imposed by the pivot point on the endoscope.

manipulating the endoscope, that is, three degree of freedom of angular movement (θ, ϕ, γ) around the incision point and one translational degree of freedom ρ in or out the incision point (see Figure 12). These spherical movement constrains should be carefully considered prior to the design of the endoscope holder.

Considering Figure. 12, we notice that rotation, γ, is only used to adjust the orientation of the image. Generally this angle will not change during the surgery. Based on this observation, the endoscope holder design can be simplified as 3DOF design with two rotational DOF and one translational DOF.

For robot manipulators, there are two types of joints, P: prismatic (prismatic joints exhibits sliding or linear motion) and R: revolute (revolute joints exhibit rotary motion about an axis). The endoscope holder has to have spherical movements. Among different combinations of prismatic and revolute joints, 3DOF RRP produces a spherical coordinate robot, which fits the purpose of this work. Another notable problem is that the designed endoscope holder should grantee the fixed position at the pivot point.

Considering all the constraints stated above, a designed endoscope holder is illustrated in Figure 13. This design satisfies the kinematic constrains. To ensure that the endoscope holder will not change its position at the incision point, we can adjust point, P, to the same height as the incision point. The world coordinate frame, (x, y, z), is set at the base of the endoscope holder. Generally, the camera is mounted at the end of the endoscope outside the abdomen. The endoscope transmits the image as seen at the tip of the endoscope inside the abdomen. Hence, we can set the camera coordinate frame, (x_c, y_c, z_c), at the center of the tip of the endoscope.

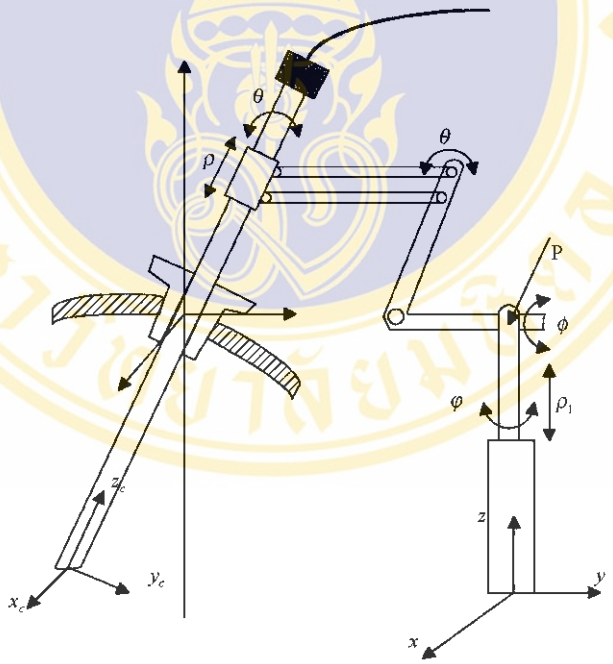

Figure 13. The designed scope holder.

The tracking task is to obtain the three displacement parameters, $\Delta\theta, \Delta\phi$ and ρ, based on the image features. These parameters are used to control the endoscope holder. As shown in Figure 14, here the desired position for the marker is chosen as the image center (V_{i0}, V_{j0}). When tracking, first, we determine the errors, ΔV_i and ΔV_j, between the current marker location and the desired location, and then transform them to real world coordinates using the calibration parameters described in section 2. Second, the following formula exists for small angles: $\Delta\alpha = \Delta d / \rho$. Replace Δd with ΔV_i and ΔV_j, $\Delta\alpha$ with $\Delta\theta$ and $\Delta\phi$, we obtain:

$$\Delta\theta = \Delta V_i / \rho$$
$$\Delta\phi = \Delta V_j / \rho \qquad (14)$$

The translation parameter, ρ, is calculated from the current diameter M in the image plane using formula (1). Last, the endoscope can be adjusted accordingly to keep the instrument at a desired location under the endoscope field of view.

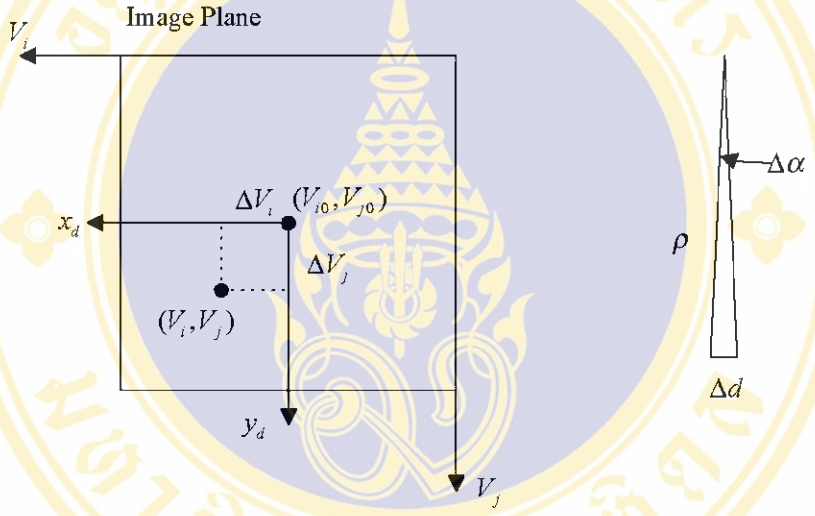

Figure 14. The geometric approach for obtaining three displacement parameters.

6. Experimental Results

To evaluate the proposed method, several types of experiments are conducted. In this section, we describe the camera calibration, endoscope image distortion-correction, endoscope holder simulation and visual tracking results separately.

An electronic endoscopy system, comprising a Karl Storz endos‹ [12] is used in capturing the image. A testing pattern-image containing a rectangular array of black squares of 4×4 mm in size, separate by 4mm in the horizontal and vertical direction (see figure 7) is used for calibration and distortion correction purpose.

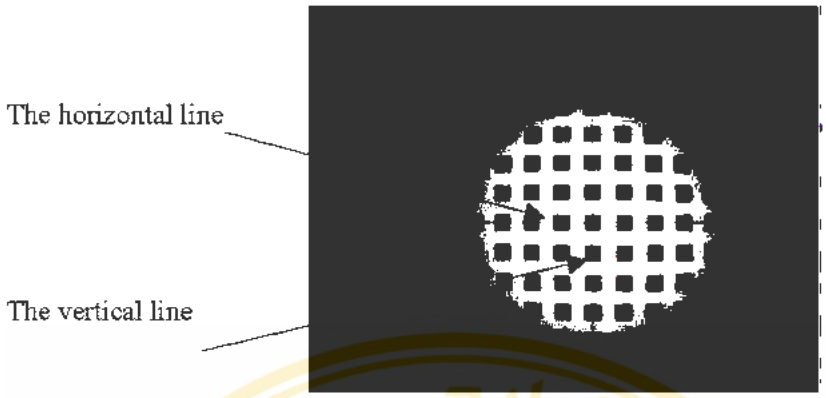

Figure 15. Verify the proposed center determination method.

6.1 Calibration Results

A discussion of the calibration parameters, which are the real image center, the scale factors, and the focal length, and how they are obtained, is found in this section.

1) Locate the real image center.

Before the experiment, a grid pattern is used to evaluate the feasibility of the proposed center determination method. First, the real image center is located by the proposed method. Then the software draws two crossed long lines with their intersections at the real image center using an overlay image. Third, place the pattern image under the ensoscope field of view. The pattern image should be placed by picking one square in the pattern image and aligning its sides with the two marked long lines. At the same time, align the chosen square's center with the real image center (see Figure 15). As we can see in figure 15, lines passing through real image center remain straight in the endoscope image. Numerical analysis also shows that for one row of squares that travel along the horizontal line, their centers have the same V_j coordinates. For one column of squares that travel along the vertical line, their centers have the same V_i coordinates, while other columns or rows of squares do not have this feature. It shows the proposed method is feasible.

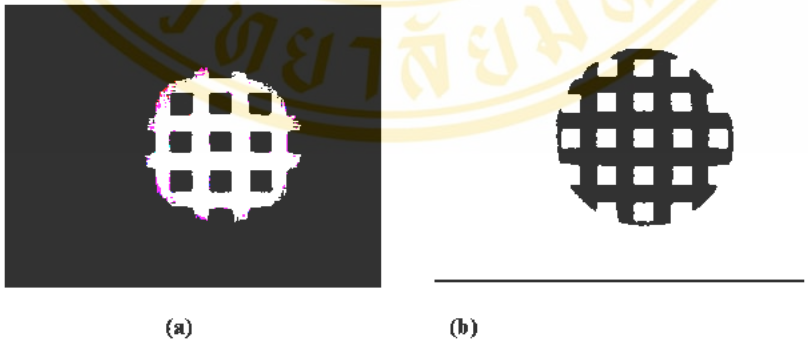

Figure 16. (a) Original gray scale image, (b) Binary image, the blob center have been marked.

Applying this method, the real image center could be obtained as follows. An image is recorded by pointing the endoscope perpendicular to a white background. The captured image is then processed by binarization using a threshold. The center of the white circle in the binarized image is chosen as the real image center (see Section 2, Figure 6).

2) Obtaining image coordinates of the calibration points.

The centers of squares are chosen as the points for calibration. Because this work is only interested in obtaining the intrinsic parameters, we only need to measure the adjacent square's center-to-center distance. Their values in the world coordinate unit are known.

Image coordinates of the calibration points are computed as follows:

a) Acquire a gray scale image (see Figure 16 (a)).

b) Threshold the image and calculate the center of every blob (see Figure 16 (b)). Because the threshold value is not critical and the illumination system is kept stable in our application (It can also be selected automatically by analysis of intensity histograms if necessary).

3) Calculating camera intrinsic parameters.

This section describes steps for calculating camera intrinsic parameters as well as the calculated intrinsic parameters of the endoscope used in this work.

a) Scale factors.

In this step, first we examine the validity of the assumption that the distortion in the center area is negligible. The closer the endoscope is to the object, the more distorted the image appears. After obtaining the real image center, the test grid is placed perpendicularly 50mm (the typical range for endoscope surgery is 40mm-100mm) away from the endoscope, with the center of one square at the real image center. Figure 16 shows the original gray scale endoscope image and the image after being binarized and marked the center of each blob. To reduce the influence of lens distortion, we use the 9 central squares for calculation. As shown in Table 1, from the coordinates of the center of

Table 1 V_i, V_j coordinates of the center of 9 squares in the central area (pixel unit)

(298, 196)	(363, 168)	(430, 169)
(297, 234)	(364, 234)	(431, 234)
(297, 300)	(363, 301)	(431, 300)

these 9 squares, their corresponding V_i or V_j coordinates are only at most 1 pixel difference. Given the first column in the table as an example, the coordinates of the three points along V_i direction are 298, 297, 297, only one pixel's difference from each other. This difference is negligible for our current application. We use mean values of the center-to-center distance between adjacent squares along V_i and V_j directions to calculate the scale factors.

$$\frac{S_x}{S_y} = \frac{66.67}{65.83} = 1$$

b) Focal length.

Considering the above steps, we note that the scale factors in V_i and V_j directions are almost the same. In this task, we do not need to calculate the value of focal length in the world coordinate unit, the focal length can be calculated as:

$$f = \frac{(V_i - V_{i0})Z_c}{X_c} = \frac{66.67 \times 50}{8} = 416.7 \text{(pixel)}$$

3) Calibration Data

The depth information can be obtained by using the calculated focal length and equation (1) as described in Section 2. The image of the markers are record at various distances from the endoscope (40, 60, 70, 80 and 90 mm). The experimental data are shown in Table 2. Errors in this depth measurement experiment comes from different sources, such as the image processing error, the accuracy of physically measured distance, and the actual angle of the laparoscope with the experimental plane (we assume it as 90°).

Table 2. Experimental data via the proposed algorithm.

No.	Actual distance (mm)	Calculated distance (mm)	Errors (mm)
1	40	42.5	-2.5
2	60	60.5	-0.5
3	70	69.4	0.6
4	80	78.1	1.9
5	90	88.2	1.8

6.2 Distortion Correction Results

For the proposed distortion correction procedure, the same calibration chart containing a rectangular array of black squares is used.

The testing chart is placed perpendicularly to the camera's optical axis. Figure 17(a) shows the captured image. We compute the polynomial coefficients using the method proposed in Section 3. The corrected image is shown in Figure 17(b). The image is

(a) (b)

Figure 17. (a) Distorted image of testing image, (b) corrected image corresponding to (a) using inverse mapping.

magnified after correction, and lines are straightened especially in the peripheral part.

The least total error reduces when the order of the polynomial becomes higher. Nonetheless, with the increase of the order of polynomial, the computation time also increases. The variation in least-square total error was negligible beyond the 3rd polynomial order (see Table 3), therefore, we pick the polynomial order to be 3 as a compromise between computation time and error.

Table 3. Variation in least total error with respect to order of expansion polynomial .

Polynomial order n	1	3	5	7
Least square total error	1.9909	0.1445	0.04196	0.04113

The relationship between the radial distance of the testing points (in the experiment, we chose squares lies in the same row) from the real image center before and after distortion correction is shown in Table 4. Note that the calculated value has a decimal part. Since the image buffer accepts integer pixel locations, the floating number is rounded to its closest integer. After the distortion correction, the radial distance is more evenly distributed and closer to the actual radial distance.

Table 4. The radial distance of testing points from the real image center before and after distortion correction.

Idea Radial Distance(pixel)	22	56	84	112	140
Radial Distance (pixel) (before correction)	22	55	82	108	134
Radial Distance (pixel) (after correction)	22.4009 (22)	56.0093 (56)	84.0326 (84)	111.6783 (112)	140.1538 (140)

The above figures and experimental results show that the proposed distortion correction method yields satisfactory results for visual and computer analysis.

6.3 Endoscope Holder Simulation Results

To visualize and validate the endoscope holder design. OpenGL was used to simulate the animated control of the endoscope holder through the data obtained from the image tracking process.

Using Visual C++ split window techniques; the simulated endoscope holder and the real endoscope image captured in real time are shown simultaneously in Figure 18. The left side of the image shows the endoscope image while the right side shows the animated endocope holder (the small block represents the mark attached to the instrument). The endoscope holder moves according to the positional information obtained from the marker that attached in the instrument indicated in the left image. The endoscope holder can be controlled in real time by moving the tool under the endoscope.

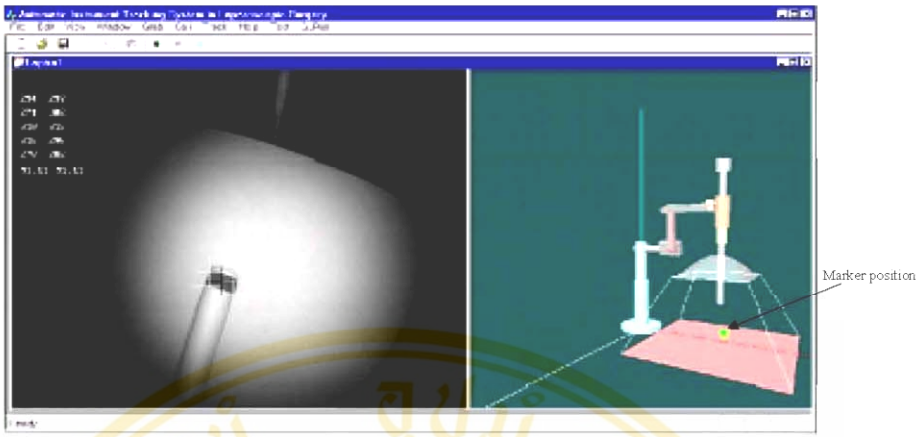

Figure 18. Endoscope holder simulation result.

6.4 Tracking Results

To estimate errors in automated instrument localization and tracking with the proposed method, several measurement methods are applied to evaluate the results. Besides direct measurement, pcBird system (a position and orientation measurement system) is also used to obtain positional data for comparison with the tracking results.

Figure 19 shows the experimental setup. The endoscope is fixed into a stand in the visual tracking experiment. The pcBird comprises a transmitter, a receiver (sensor). The pcBird measures the position and orientation of a sensor by transmitting a pulsed DC magnetic field measured by the sensor. From the measured magnetic field characteristics, the chip computes the sensor's position and orientation with respect to the center of the transmitter. In the experiment, the sensor is mounted in the upper part of a tool, while the

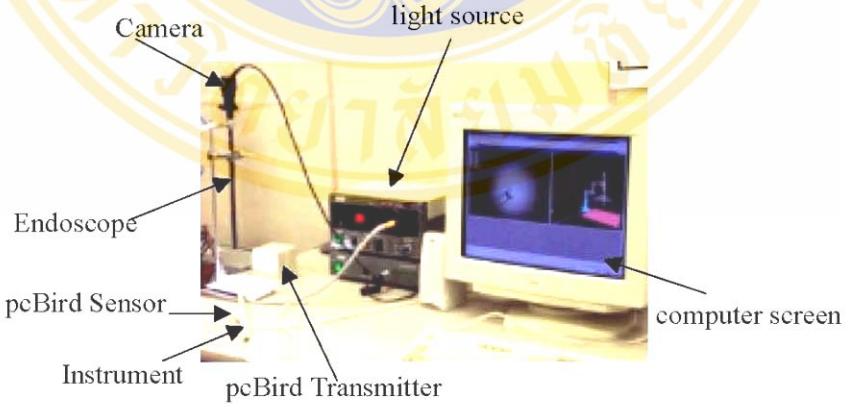

Figure 19. Experimental setup for the tracking experiment

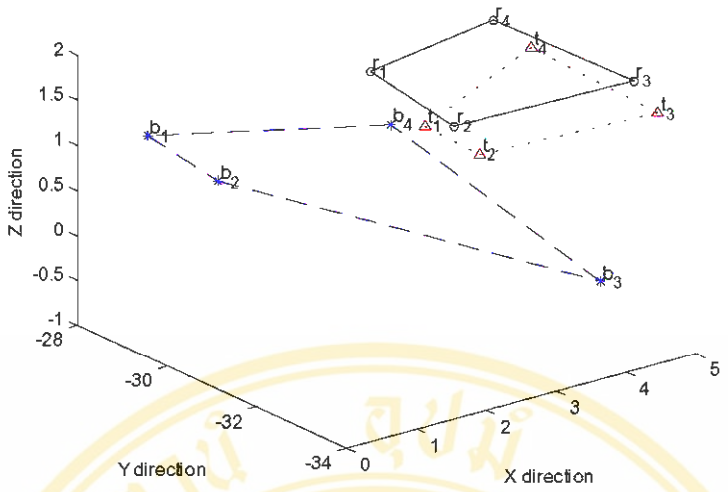

Figure 20. Comparison of tracking results (initial b represent the pcBird tracking results, t represents the proposed tracking results, r represents the ruler measured real positions).

maker is attached to the tip of the tool. Since the relative position of the sensor and the marker is fixed, the marker's position can be derived from the sensor's position. Thus, the marker's 3D position obtained from the pcBird and from the proposed image tracking method can be compared.

We define a world coordinate frame at the center of the transmitter. The camera coordinate frame is defined at the tip of the endoscope. Four points with different location are given for the experiment. We place the tool at the given location and let the center of the marker (select one strip of the marker) overlap with the given points. In this experiment, we capture ten frames in each location. The mean tracking error is defined as the average difference over a whole sequence between the actual measured position and the position obtained from the proposed tracking methods. A similar approach is applied to the pcBird position and orientation measurement system. The results are shown in Figure 20 and Table 5. The error is measured in terms of cm and in the x, y and z directions. From Figure 20, the visual tracking results are better than the pcBird position and orientation measurement system. One reason is related to the restrictions in using the pcBird. The pcBird is supposed to be used in a non-metallic environment. However the operating room environment cannot guarantee this restriction. The errors for both tracking methods are affected by imprecise manual placement of the marker at the known position.

Table 5. Average Error in Instrument Tracking

Sequence No. (10 frames)	Mean tracking error (cm)					
	x direction		y direction		z direction	
	pcBird	Image Tracking	pcBird	Image Tracking	pcBird	Image Tracking
1	- 2.0817	- 0.0286	1.7060	- 1.2817	-0.6661	-0.2999
2	- 1.9400	- 0.1123	2.2452	- 0.7557	-0.7152	-0.1177
3	- 0.3100	- 0.2132	0.2786	- 0.8689	-2.2257	-0.1177
4	- 0.9635	0.0200	0.7644	- 0.8301	-1.1250	-0.1177

7. Concluding Remarks

In this paper, some novel ideas of using visual tracking to realize automated instrument localization and endoscope maneuvering in robot-assisted laparoscopic surgery are presented. Implementation methods are described in detail. Good experimental results demonstrate the feasibility of the proposed methods. Some more experiments can be conducted in future work in the visual tracking part, such as, testing the tracking accuracy when the tools enter the endoscope field of view from different angles.

In our proposed method, we use the intensity information of the image for the marker localization, the specular reflection due to lights projected into the shining objects does not affect the tracking results. This is because in gray scale images, the intensity difference between the shining objects and the marker is even larger than surroundings, which is a desired feature for locating the marker.

The general goal of this work is to further improve the existing laparoscopic surgery system, to build a human – machine interface for the surgeon to automatically manipulate the endoscope. The system can be applied to surgical training simulators and telepresence (telepresence systems are used in medicine to manipulate equipment at a remote site. The surgeon has the sense of actually being at the site performing the procedure).

Our future research goal is to utilize this technique together with other sensors, such as laser sensors to reconstruct the surface of the surgical site, so to overcome the lack of 3D depth cue of the current laparoscopic surgery systems. The research will benefit the development of the laparoscopic surgery system in the long run.

APPENDIX B

APPENDIX B

UC BERKELEY TELESURGICAL WORKSTATION OF MILLIROBOT

The Berkeley/UCSF Telesurgical Workstation is a master-slave teleoperation system with two 6 DOF robotic manipulators. The slave manipulator is composed of two parts. The first part is the gross positioning stage which is located outside the body. It is responsible for positioning the millirobot, which is the second part. The gross stage controls the same 4 DOF as those available in conventional laparoscopic instruments. It has a parallel structure, where three linear joints hold a small platform that carries the tool arm and the motor rotating it. All four actuators of this part are DC servo motors. The linear joints are actuated by leadscrews connected to the electric motors. (See figure 2.1)

The millirobot has a 2 DOF wrist located inside the body, and a gripper. It is 10 mm in diameter. Wrist to gripper length is 10 cm, and the tool arm is 24 cm up to the wrist. The millirobot is actuated by hydraulic actuators. Each joint is actuated by a pair of bladders which are inflated with water. The water section is separated from the rest of the hydraulic circuit, utilizing hydraulic fluid, via a set of manifolds. The millirobot is designed to be disposable, and to avoid problems in case of leaks in hydraulics, the bladders will be driven by sterile saline solution.

Performance goals in the design of the millirobot are given in table 2.1. These values are estimated for a suturing task, force and movement requirements for driving a needle through tissue and tying a knot. Table 2.2 gives the experimental measurement results with the actual robot, which are well within the design goals. The specifications adopted for the second version of the system are given in table 2.3.[1]

The master manipulator is a 6 DOF serial robot. A commercial 4 DOF force

Parameter	Value
Dimension: overall diameter	10-15 mm max
Dimension: wrist joint to grasper	100 mm max
Force: at the point of needle, for driving the needle through tissue	1.47 N min
Torque: about grasper axis, for driving needle (assumes curved needle, 15 mm from grasper to needle tip)	2.2 N.cm min
Force: gripping, while driving needle	5 N min
Force: knot tightening tension	2.2 N min
Range of motion: gripper jaw opening	2-3 mm min
Range of motion: rotation about grasper axis, to drive plus allowance for inclined work surface	180–270 degrees min
Range of motion: wrist flexion, for driving needle	90 degrees min
Range of motion: wrist pronation	180 degrees min
Bandwidth	5 Hz min

Table 2.1: Performance goals for the millirobot

Parameter	Measured Value	Target Value
Gripping force	15 N	5 N min
Grasper opening width	6 mm	2–3 mm min
Wrist roll torque	8.8 N.cm	2.2 N.cm min
Wrist roll range of motion	285 degrees	180–270 degrees min
Wrist flexion (yaw) torque	30 N.cm	10-15 N.cm
Bandwidth	~6 Hz	5 Hz

Table 2.2: Millirobot test results

Parameter	Target Value
Wrist joint to grasper length	50 mm max
Gripping force	40 N min
Grasper opening width	8 mm min
Grasper speed: full close in	0.5 sec max
Wrist roll torque	100 N.mm min
Wrist roll range of motion	270 degrees min
Wrist roll speed	540 degrees/sec min
Wrist flexion (yaw) torque	300 N.mm min
Wrist flexion range of motion	90 degrees min
Wrist flexion speed	360 degrees/sec min
Life time	6 months min

Table 2.3: Performance goals for the second version of the millirobot

Figure 2.1: Slave manipulator of the Berkeley / UCSF laparoscopic workstation

Reflecting joystick (Immersion Impulse Engine 3000) with 3 actuated axes is equipped with an additional 2 DOF (one actuated) and stylus handle. There are position measurements in all 6 joints and the 4 actuated joints give force feedback in trauslational directions and the roll axis, where the force is important while driving a needle through tissue. (See figures 2.2 and 2.3)

Figure 2.2: Master manipulator of the Berkeley / UCSF laparoscopic workstation

Figure 2.3: Close-up view of the master manipulator

APPENDIX C

APPENDIX C

KINEMATICS

The master and slave manipulator structures were described in chapter 2. For the control of the system, inverse kinematics of the slave manipulator and forward kinematics of the master manipulator are needed. In this chapter, the explicit solutions of these problems will be derived.

For the kinematic analysis, the product of exponentials formulation is used. Refer to [29] for a full treatment of this formulation.

3.1 Slave Manipulator Inverse Kinematics

To simplify the inverse kinematics calculations, slave kinematics can be divided into two parts: the serial portion inside the body and parallel portion outside the body. The serial part is composed of the fulcrum, which is modeled with a spherical joint and a translational joint, and the 2 DOF wrist. The parallel part of the slave consists of the three arms holding the base of the tool arm, and the tool arm itself. (See figure 3.1)

In the inverse kinematics calculations, first the serial part will be solved, which will give the angles of the wrist joints and the desired configuration of the parallel part. Then the parallel part will be solved to calculate the lengths of the linear joints and the tool arm rotation.

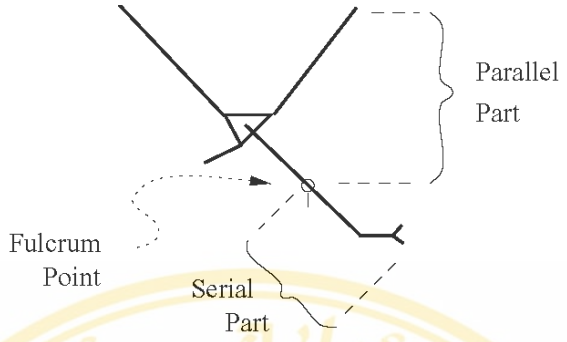

Figure 3.1: Parallel and serial parts of the slave robot

3.1.1 Serial Part

Using the naming convention and the zero configuration shown in figure 3.2, the kinematic configuration of the serial part is characterized by the following twists $\in se(3)$:

$$\xi_{s1} = \begin{bmatrix} 0 \\ 0 \\ 0 \\ 0 \\ 0 \\ 1 \end{bmatrix}, \xi_{s2} = \begin{bmatrix} 0 \\ 0 \\ 0 \\ 0 \\ 1 \\ 0 \end{bmatrix}, \xi_{s3} = \begin{bmatrix} 0 \\ 0 \\ 0 \\ 1 \\ 0 \\ 0 \end{bmatrix}, \xi_{s4} = \begin{bmatrix} 0 \\ 0 \\ 1 \\ 0 \\ 0 \\ 0 \end{bmatrix}, \xi_{s5} = \begin{bmatrix} 0 \\ 0 \\ 0 \\ 0 \\ 1 \\ 0 \end{bmatrix}, \xi_{s6} = \begin{bmatrix} 0 \\ 0 \\ 0 \\ 0 \\ 0 \\ 1 \end{bmatrix} \tag{3.1}$$

and the reference configuration:

$$g_s(0) = \begin{bmatrix} & & & 0 \\ & I_{3\times3} & & 0 \\ & & & 0 \\ 0 & 0 & 0 & 1 \end{bmatrix} \in SE(3) \tag{3.2}$$

which gives the forward kinematics map as:

$$g_s(\theta_s) = e^{\hat{\xi}_{s1}\theta_{s1}} e^{\hat{\xi}_{s2}\theta_{s2}} e^{\hat{\xi}_{s3}\theta_{s3}} e^{\hat{\xi}_{s4}\theta_{s4}} e^{\hat{\xi}_{s5}\theta_{s5}} e^{\hat{\xi}_{s6}\theta_{s6}} g_s(0) \tag{3.3}$$

The inverse kinematics of the serial part is straightforward as it is a kinematically simple configuration. Given the desired configuration

$$g_d = \begin{bmatrix} & R_d & & p_d \\ 0 & 0 & 0 & 1 \end{bmatrix} \in SE(3) \tag{3.4}$$

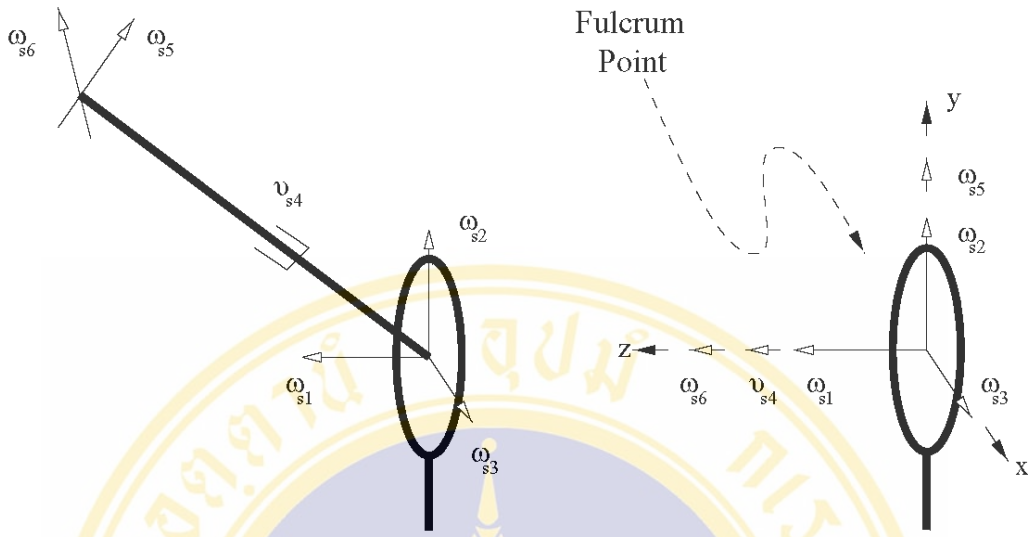

Figure 3.2: Naming convention and the zero configuration of the serial part

θ_{s4} is calculated as:

$$\theta_{s4} = ||p_d|| \tag{3.5}$$

Also observing that the origin $[\ 0 \quad 0 \quad 0 \quad 1\ ]^T$ is invariant under $e^{-\hat{\xi}_{s3}\theta_{s3}} e^{-\hat{\xi}_{s2}\theta_{s2}} e^{-\hat{\xi}_{s1}\theta_{s1}}$:

$$g_s^{-1}(\theta) \begin{bmatrix} 0 \\ 0 \\ 0 \\ 1 \end{bmatrix} = \begin{bmatrix} \theta_{s4} \sin(\theta_{s5}) \cos(\theta_{s6}) \\ -\theta_{s4} \sin(\theta_{s5}) \sin(\theta_{s6}) \\ -\theta_{s4} \cos(\theta_{s5}) \\ 1 \end{bmatrix} \tag{3.6}$$

θ_{s5} and θ_{s6} can be solved as

$$\theta_{s6} = atan2(-\beta_y, \beta_x) \tag{3.7}$$

and

$$\theta_{s5} = atan2(\mp\sqrt{\beta_x^2 + \beta_y^2}, -\beta_z) \tag{3.8}$$

where

$$\beta = g_d^{-1} \begin{bmatrix} 0 \\ 0 \\ 0 \\ 1 \end{bmatrix} \tag{3.9}$$

Here, note that θ_{s5} has two solutions, and θ_{s6} can have any value when $\theta_{s5} = 0$, which is a singular configuration. Then,

$$e^{\hat{\xi}_{s1}\theta_{s1}} e^{\hat{\xi}_{s2}\theta_{s2}} e^{\hat{\xi}_{s3}\theta_{s3}} = g_d e^{-\hat{\xi}_{s6}\theta_{s6}} e^{-\hat{\xi}_{s5}\theta_{s5}} e^{-\hat{\xi}_{s4}\theta_{s4}} \tag{3.10}$$

which will be used in the solution of the parallel part, since ξ_{s1}, ξ_{s2}, and ξ_{s3} form the fictitious ball joint at the entry point.

3.1.2 Parallel Part

The parallel part of the platform consists of three arms, connected to a triangular base which holds the millirobot. Two of the arms have 6 DOF, whereas the third one has only five. In all of the arms, only 1 DOF, the translational joint, is actuated. The solution of the inverse kinematics for the parallel part requires finding the lengths of these translational joints and calculating the rotation of the tool arm. We will first proceed to solve the inverse kinematics of the 5 DOF arm, then use this to calculate the lengths of the prismatic joints in the other two arms, and the rotation.

Specification of the Configuration

Figure 3.3 gives a side view of the parallel part, showing the joint naming conventions and various point and coordinate frames used in the calculations. In the figure, joints 1–5 are on the 5 DOF arm, and joint 6 is the rotation of the tool arm. The serial part of the inverse kinematics gives the direction $\hat{n}$, which is determined from the spherical joint at the fulcrum, as:

$$\hat{n}_f = e^{\hat{\xi}_{s1}\theta_{s1}} e^{\hat{\xi}_{s2}\theta_{s2}} e^{\hat{\xi}_{s3}\theta_{s3}} \begin{bmatrix} 0 \\ 0 \\ 1 \\ 0 \end{bmatrix} \tag{3.11}$$

and the length d:

$$d = \theta_{s4} \tag{3.12}$$

As notation, the subscripts of points and vectors denote the coordinate frames in which they are expressed. The subscripts of the homogeneous transforms denote which coordinate frames they transform. Also, $< \cdot, \cdot >$ is used to denote inner product.

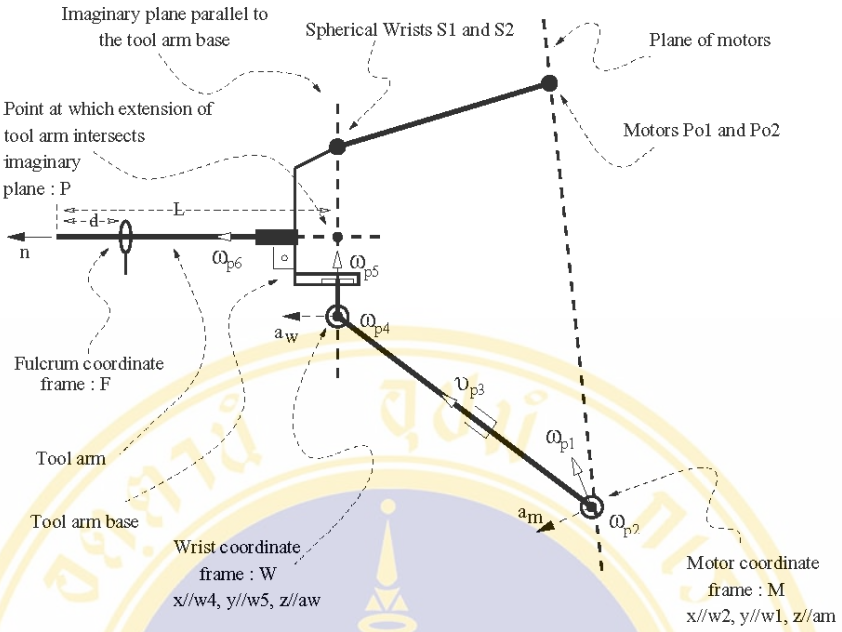

Figure 3.3: Kinematic diagram of the side view of parallel section

The forward kinematics of the 5 DOF arm, choosing the zero configuration as W overlapped with M, are:

$$g_{mw}(\theta_p) = e^{\hat{\xi}_{p1}\theta_{p1}} e^{\hat{\xi}_{p2}\theta_{p2}} e^{\hat{\xi}_{p3}\theta_{p3}} e^{\hat{\xi}_{p4}\theta_{p4}} e^{\hat{\xi}_{p5}\theta_{p5}} g_{mw}(0) \tag{3.13}$$

where,

$$\xi_{p1} = \begin{bmatrix} 0 \\ 0 \\ 0 \\ 0 \\ 1 \\ 0 \end{bmatrix}, \xi_{p2} = \begin{bmatrix} 0 \\ 0 \\ 0 \\ 1 \\ 0 \\ 0 \end{bmatrix}, \xi_{p3} = \begin{bmatrix} 0 \\ 0 \\ 1 \\ 0 \\ 0 \\ 0 \end{bmatrix}, \xi_{p4} = \begin{bmatrix} 0 \\ 0 \\ 0 \\ 1 \\ 0 \\ 0 \end{bmatrix}, \xi_{p5} = \begin{bmatrix} 0 \\ 0 \\ 0 \\ 0 \\ 1 \\ 0 \end{bmatrix}, g_{mw}(0) = I_{4\times4} \tag{3.14}$$

The homogeneous transform between the M and F coordinate frames (g_{mf}), W coordinates of the spherical wrists S_1 and S_2, and M coordinates of the centers of the other two motors P_{o1} and P_{o2} are all known as they are constant.

The point at which extension of the tool arm intersects the (imaginary) plane passing through the wrists on the tool base is defined as P. Note that P has W coordinates

of the form:

$$p_w = \begin{bmatrix} 0 & p_{wy} & 0 & 1 \end{bmatrix}^T \tag{3.15}$$

and equations 3.11 and 3.12 give

$$p_f = -(L-d)\hat{n}_f + \begin{bmatrix} 0 \\ 0 \\ 0 \\ 1 \end{bmatrix} \tag{3.16}$$

where L is the length of the tool arm.

Solution of the Inverse Kinematics

First, the unknowns $\theta_{p1} \ldots \theta_{p5}$ are solved using the following equations:

- The z axis of W points in the same direction as $\hat{n}$:

$$g_{mw} \begin{bmatrix} 0 \\ 0 \\ 1 \\ 0 \end{bmatrix} = g_{mf}\hat{n}_f \tag{3.17}$$

$$\begin{bmatrix} \sin(\theta_{p1})\cos(\theta_{p2}+\theta_{p4})\cos(\theta_{p5}) + \cos(\theta_{p1})\sin(\theta_{p5}) \\ -\cos(\theta_{p5})\sin(\theta_{p2}+\theta_{p4}) \\ \cos(\theta_{p1})\cos(\theta_{p2}+\theta_{p4})\cos(\theta_{p5}) - \sin(\theta_{p1})\sin(\theta_{p5}) \\ 0 \end{bmatrix} = \hat{n}_m \tag{3.18}$$

- The origin of W and the point P lie on the imaginary plane passing through the wrists on the base, which is perpendicular to $\hat{n}$:

$$< g_{mw} \begin{bmatrix} 0 \\ 0 \\ 0 \\ 1 \end{bmatrix}, g_{mf}\hat{n}_f > = < g_{mf}p_f, g_{mf}\hat{n}_f > \tag{3.19}$$

$$\theta_{p3}(n_{mz}\cos(\theta_{p1})\cos(\theta_{p2}) + n_{mx}\cos(\theta_{p2})\sin(\theta_{p1}) - n_{my}\sin(\theta_{p2})) = < p_m, \hat{n}_m > \tag{3.20}$$

- The transform of p_w through g_{mw} is the same as transform of p_f through g_{mf}, as they are coordinates of the same point, P:

$$g_{mw}p_w = g_{mf}p_f \tag{3.21}$$

$$\begin{bmatrix} \sin(\theta_{p1})(\theta_{p3}\cos(\theta_{p2}) + p_{wy}\sin(\theta_{p2}+\theta_{p4})) \\ p_{wy}\cos(\theta_{p2}+\theta_{p4}) - \theta_{p3}\sin(\theta_{p2}) \\ \cos(\theta_{p1})(\theta_{p3}\cos(\theta_{p2}) + p_{wy}\sin(\theta_{p2}+\theta_{p4})) \\ 1 \end{bmatrix} = p_m \tag{3.22}$$

Note that although there are 7 equations (3.18,3.20, and 3.22) in 5 unknowns, some of them are dependent. That is why these equations can be solved.

θ_{p1} can be immediately solved from the first and third rows of the equation (3.22):

$$\theta_{p1} = atan2(p_{mx}, p_{mz}) \tag{3.23}$$

Note that the term multiplying $\sin(\theta_{p1})$ and $\cos(\theta_{p1})$ is always positive in the physically possible workspace of the manipulator.

Then, eliminating $\sin(\theta_{p5})$ from first and third rows of equation (3.18) and solving for $\cos(\theta_{p2}+\theta_{p4})\cos(\theta_{p5})$:

$$\cos(\theta_{p2}+\theta_{p4})\cos(\theta_{p5}) = n_{mz}\cos(\theta_{p1}) + n_{mx}\sin(\theta_{p1}) \tag{3.24}$$

Then, $\theta_{p2}+\theta_{p4}$ can be solved using the second row of equation (3.18) and equation (3.24):

$$\theta_{p2}+\theta_{p4} = atan2(-n_{my}, n_{mz}\cos(\theta_{p1}) + n_{mx}\sin(\theta_{p1})) \tag{3.25}$$

Here, note that $\cos(\theta_{p5})$ cannot be zero practically.

Assuming $\theta_{p3} \neq 0$, which is also practically true, first $\theta_{p3}\cos(\theta_{p2})$ can be solved from third row of equation (3.22):

$$\theta_{p3}\cos(\theta_{p2}) = \frac{p_{mz}}{\cos(\theta_{p1})} - p_{wy}\sin(\theta_{p2}+\theta_{p4}) \tag{3.26}$$

and then used to calculate θ_{p2} using the second row of equation (3.22):

$$\theta_{p2} = atan2(p_{wy}\cos(\theta_{p2}+\theta_{p4}) - p_{my}, \frac{p_{mz}}{\cos(\theta_{p1})} - p_{wy}\sin(\theta_{p2}+\theta_{p4})) \tag{3.27}$$

If $\cos(\theta_{p1}) \approx 0$, to avoid division by zero, $\theta_{p3}\cos(\theta_{p2})$ can be solved from row 1 of equation (3.22):

$$\theta_{p3}\cos(\theta_{p2}) = \frac{p_{mx}}{\sin(\theta_{p1})} - p_{wy}\sin(\theta_{p2}+\theta_{p4}) \tag{3.28}$$

giving

$$\theta_{p2} = atan2(p_{wy}\cos(\theta_{p2}+\theta_{p4}) - p_{my}, \frac{p_{mx}}{\sin(\theta_{p1})} - p_{wy}\sin(\theta_{p2}+\theta_{p4})) \tag{3.29}$$

Then, θ_{p3} can be calculated from equation (3.20):

$$\theta_{p3} = \frac{< p_m, \hat{n}_m >}{n_{mz}\cos(\theta_{p1})\cos(\theta_{p2}) + n_{mx}\cos(\theta_{p2})\sin(\theta_{p1}) - n_{my}\sin(\theta_{p2})} \tag{3.30}$$

Here, note that as θ_{p3} and the right hand side of equation 3.20 cannot be zero, there will not be division by zero.

Then θ_{p5} can be solved from the first row of (3.18), by first replacing $\cos(\theta_{p2}+\theta_{p4})\cos(\theta_{p5})$ calculated earlier. A little manipulation, using the facts that $\cos(\theta_{p1}) \neq 0$ practically, and $\theta_{p5} \in (-\pi/2, \pi/2)$, yields:

$$\theta_{p5} = \arcsin(n_{mx}\cos(\theta_{p1}) - n_{mz}\sin(\theta_{p1})) \tag{3.31}$$

It is also possible to get a formula in $atan2(\cdot,\cdot)$ for higher precision, using the second row of equation (3.18) or the formula for $\cos(\theta_{p2}+\theta_{p4})\cos(\theta_{p5})$ derived in equation (3.24) above, depending on the value of $\theta_{p2}+\theta_{p4}$. For $\sin(\theta_{p2}+\theta_{p4}) \neq 0$:

$$\theta_{p5} = atan2(n_{mx}\cos(\theta_{p1}) - n_{mz}\sin(\theta_{p1}), \frac{-n_{my}}{\sin(\theta_{p2}+\theta_{p4})}) \tag{3.32}$$

and for $\sin(\theta_{p2}+\theta_{p4}) \approx 0$:

$$\theta_{p5} = atan2(n_{mx}\cos(\theta_{p1}) - n_{mz}\sin(\theta_{p1}), \frac{n_{mz}\cos(\theta_{p1}) + n_{mx}\sin(\theta_{p1})}{\cos(\theta_{p2}+\theta_{p4})}) \tag{3.33}$$

Once p_m and g_{mw} are known, remaining unknowns, the other two lengths and the rotation, can be easily solved:

$$l_1 = ||g_{mw}s_{1w} - p_{o1m}|| \tag{3.34}$$

$$l_2 = ||g_{mw}s_{2w} - p_{o2m}|| \tag{3.35}$$

$$\alpha = g_{mw}^{-1} e^{\hat{\xi}_{s1}\theta_{s1}} e^{\hat{\xi}_{s2}\theta_{s2}} e^{\hat{\xi}_{s3}\theta_{s3}} \begin{bmatrix} 1 \\ 0 \\ 0 \\ 0 \end{bmatrix} \tag{3.36}$$

$$\theta_{p6} = atan2(\alpha_y, \alpha_x) \tag{3.37}$$

If $\cos(\theta_{p1}) \approx 0$, to avoid division by zero, $\theta_{p3}\cos(\theta_{p2})$ can be solved from row 1 of equation (3.22):

$$\theta_{p3}\cos(\theta_{p2}) = \frac{p_{mx}}{\sin(\theta_{p1})} - p_{wy}\sin(\theta_{p2}+\theta_{p4}) \tag{3.28}$$

giving

$$\theta_{p2} = atan2(p_{wy}\cos(\theta_{p2}+\theta_{p4}) - p_{my}, \frac{p_{mx}}{\sin(\theta_{p1})} - p_{wy}\sin(\theta_{p2}+\theta_{p4})) \tag{3.29}$$

Then, θ_{p3} can be calculated from equation (3.20):

$$\theta_{p3} = \frac{< p_m, \hat{n}_m >}{n_{mz}\cos(\theta_{p1})\cos(\theta_{p2}) + n_{mx}\cos(\theta_{p2})\sin(\theta_{p1}) - n_{my}\sin(\theta_{p2})} \tag{3.30}$$

Here, note that as θ_{p3} and the right hand side of equation 3.20 cannot be zero, there will not be division by zero.

Then θ_{p5} can be solved from the first row of (3.18), by first replacing $\cos(\theta_{p2}+\theta_{p4})\cos(\theta_{p5})$ calculated earlier. A little manipulation, using the facts that $\cos(\theta_{p1}) \neq 0$ practically, and $\theta_{p5} \in (-\pi/2, \pi/2)$, yields:

$$\theta_{p5} = \arcsin(n_{mx}\cos(\theta_{p1}) - n_{mz}\sin(\theta_{p1})) \tag{3.31}$$

It is also possible to get a formula in $atan2(\cdot,\cdot)$ for higher precision, using the second row of equation (3.18) or the formula for $\cos(\theta_{p2}+\theta_{p4})\cos(\theta_{p5})$ derived in equation (3.24) above, depending on the value of $\theta_{p2}+\theta_{p4}$. For $\sin(\theta_{p2}+\theta_{p4}) \neq 0$:

$$\theta_{p5} = atan2(n_{mx}\cos(\theta_{p1}) - n_{mz}\sin(\theta_{p1}), \frac{-n_{my}}{\sin(\theta_{p2}+\theta_{p4})}) \tag{3.32}$$

and for $\sin(\theta_{p2}+\theta_{p4}) \approx 0$:

$$\theta_{p5} = atan2(n_{mx}\cos(\theta_{p1}) - n_{mz}\sin(\theta_{p1}), \frac{n_{mz}\cos(\theta_{p1}) + n_{mx}\sin(\theta_{p1})}{\cos(\theta_{p2}+\theta_{p4})}) \tag{3.33}$$

Once p_m and g_{mw} are known, remaining unknowns, the other two lengths and the rotation, can be easily solved:

$$l_1 = ||g_{mw}s_{1w} - p_{o1m}|| \tag{3.34}$$

$$l_2 = ||g_{mw}s_{2w} - p_{o2m}|| \tag{3.35}$$

$$\alpha = g_{mw}^{-1} e^{\hat{\xi}_{s1}\theta_{s1}} e^{\hat{\xi}_{s2}\theta_{s2}} e^{\hat{\xi}_{s3}\theta_{s3}} \begin{bmatrix} 1 \\ 0 \\ 0 \\ 0 \end{bmatrix} \tag{3.36}$$

$$\theta_{p6} = atan2(\alpha_y, \alpha_x) \tag{3.37}$$

3.2 Master Manipulator Forward Kinematics

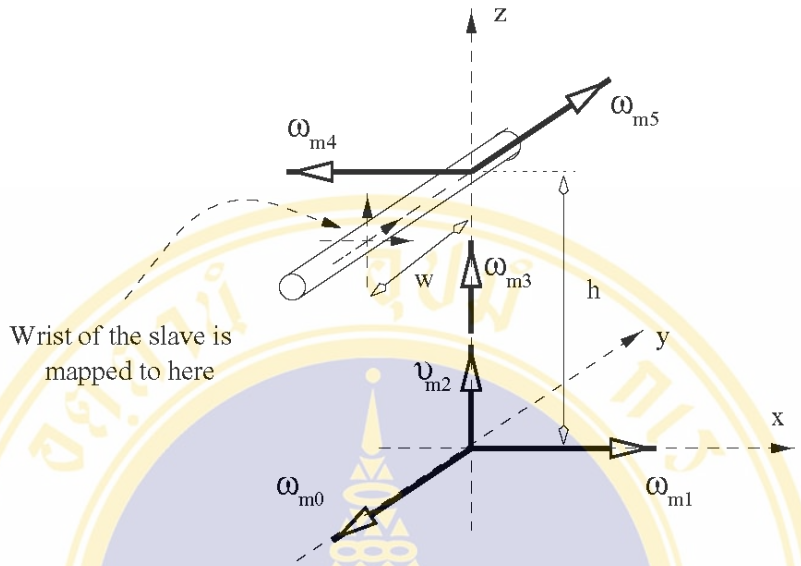

Figure 3.4: Naming convention and the zero configuration of the master manipulator

The master manipulator is a simple serial structure. Using the naming convention and the zero configuration shown in figure 3.4, the kinematics of the serial part is characterized by the following twists:

$$\xi_{m0} = \begin{bmatrix} 0 \\ 0 \\ 0 \\ 0 \\ -1 \\ 0 \end{bmatrix}, \xi_{m1} = \begin{bmatrix} 0 \\ 0 \\ 0 \\ 1 \\ 0 \\ 0 \end{bmatrix}, \xi_{m2} = \begin{bmatrix} 0 \\ 0 \\ 1 \\ 0 \\ 0 \\ 0 \end{bmatrix}, \xi_{m3} = \begin{bmatrix} 0 \\ 0 \\ 0 \\ 0 \\ 0 \\ -1 \end{bmatrix}, \xi_{m4} = \begin{bmatrix} 0 \\ -h \\ 0 \\ -1 \\ 0 \\ 0 \end{bmatrix}, \xi_{m5} = \begin{bmatrix} h \\ 0 \\ 0 \\ 0 \\ -1 \\ 0 \end{bmatrix} \tag{3.38}$$

and the zero configuration:

$$g_m(0) = \begin{bmatrix} & & & 0 \\ & I_{3\times3} & & -w \\ & & & h \\ 0 & 0 & 0 & 1 \end{bmatrix} \tag{3.39}$$

which gives the forward kinematics map as:

$$g_m(\theta_m) = e^{\hat{\xi}_{m0}\theta_{m0}} e^{\hat{\xi}_{m1}\theta_{m1}} e^{\hat{\xi}_{m2}\theta_{m2}} e^{\hat{\xi}_{m3}\theta_{m3}} e^{\hat{\xi}_{m4}\theta_{m4}} e^{\hat{\xi}_{m5}\theta_{m5}} g_m(0) \tag{3.40}$$

$$= \begin{bmatrix} c_5\ (c_0\, c_3 + s_0\, s_1\, s_3) + (-(c_1\, c_4\, s_0) + (-(c_3\, s_0\, s_1) + c_0\, s_3)\ s_4)\ s_5 \\ -(c_1\, c_5\, s_3) + (-(c_4\, s_1) + c_1\, c_3\, s_4)\ s_5 \\ c_5\ (c_3\, s_0 - c_0\, s_1\, s_3) + (c_0\, c_1\, c_4 + (c_0\, c_3\, s_1 + s_0\, s_3)\ s_4)\ s_5 \\ 0 \\ c_4\ (-(c_3\, s_0\, s_1) + c_0\, s_3) + c_1\, s_0\, s_4 \\ c_1\, c_3\, c_4 + s_1\, s_4 \\ c_4\ (c_0\, c_3\, s_1 + s_0\, s_3) - c_0\, c_1\, s_4 \\ 0 \\ c_5\ (-(c_1\, c_4\, s_0) + (-(c_3\, s_0\, s_1) + c_0\, s_3)\ s_4) - (c_0\, c_3 + s_0\, s_1\, s_3)\ s_5 \\ c_5\ (-(c_4\, s_1) + c_1\, c_3\, s_4) + c_1\, s_3\, s_5 \\ c_5\ (c_0\, c_1\, c_4 + (c_0\, c_3\, s_1 + s_0\, s_3)\ s_4) - (c_3\, s_0 - c_0\, s_1\, s_3)\ s_5 \\ 0 \\ -(h\, c_1\, s_0) - \theta_2\, c_1\, s_0 + w\, c_3\, c_4\, s_0\, s_1 - w\, c_0\, c_4\, s_3 - w\, c_1\, s_0\, s_4 \\ -(w\, c_1\, c_3\, c_4) - h\, s_1 - \theta_2\, s_1 - w\, s_1\, s_4 \\ h\, c_0\, c_1 + \theta_2\, c_0\, c_1 - w\, c_0\, c_3\, c_4\, s_1 - w\, c_4\, s_0\, s_3 + w\, c_0\, c_1\, s_4 \\ 1 \end{bmatrix} \tag{3.41}$$

and the body Jacobian of the manipulator as:

$$\begin{bmatrix} -((h+\theta_2)\ c_4\, c_5\ (c_1\, c_3\, c_4 + s_1\, s_4)) - (w + h\, s_4 + \theta_2\, s_4)\ (-(c_4\, c_5\, s_1) + c_1\ (c_3\, c_5\, s_4 + s_3\, s_5)) \\ -((h+\theta_2)\ c_1\, c_4\, s_3) \\ (h+\theta_2)\ c_4\ (c_1\, c_3\, c_4 + s_1\, s_4)\ s_5 - (-w - h\, s_4 - \theta_2\, s_4)\ (-(c_4\, s_1\, s_5) + c_1\ (-(c_5\, s_3) + c_3\, s_4\, s_5)) \\ c_4\, s_1\, s_5 - c_1\ (-(c_5\, s_3) + c_3\, s_4\, s_5) \\ -(c_1\, c_3\, c_4) - s_1\, s_4 \\ c_4\, c_5\, s_1 - c_1\ (c_3\, c_5\, s_4 + s_3\, s_5) \\ (h+\theta_2)\ {c_4}^2\, c_5\, s_3 + (w + h\, s_4 + \theta_2\, s_4)\ (c_5\, s_3\, s_4 - c_3\, s_5) \\ -((h+\theta_2)\ c_3\, c_4) \\ -((h+\theta_2)\ {c_4}^2\, s_3\, s_5) + (-w - h\, s_4 - \theta_2\, s_4)\ (c_3\, c_5 + s_3\, s_4\, s_5) \\ c_3\, c_5 + s_3\, s_4\, s_5 \\ c_4\, s_3 \\ c_5\, s_3\, s_4 - c_3\, s_5 \end{bmatrix}$$

$$\begin{bmatrix} c_4\, s_5 & -(w\, c_4\, c_5) & w\, s_5 & 0 \\ -s_4 & 0 & 0 & 0 \\ c_4\, c_5 & w\, c_4\, s_5 & w\, c_5 & 0 \\ 0 & -(c_4\, s_5) & -c_5 & 0 \\ 0 & s_4 & 0 & -1 \\ 0 & -(c_4\, c_5) & s_5 & 0 \end{bmatrix} \tag{3.42}$$

where c_i and s_i denote $\cos(\theta_{mi})$ and $\sin(\theta_{mi})$ respectively.

APPENDIX D

APPENDIX D

AESOP 2000

COMPUTER MOTION, INC.
130-B Cremona Drive
Goleta, CA 93117
United States

PHONE: 805-968-9600
FAX: 805-685-9277

SALES
PHONE: 800-479-0685
FAX. 805-685-9277

AESOP® 2000 Robotic Visualization System for Endoscopy

Starting with endoscopic harvesting of the IMA, the all new **AESOP® 2000** will assist you through the evolution of minimally invasive cardiac surgery. The voice-activated robotic arm allows you to maneuver your endoscope and position it with pinpoint accuracy-wherever you need it. And it provides a rock-steady image for as long as you want it.

The **AESOP® Robotic Visualization System for Endoscopy** was first introduced in October 1994. The safety record speaks for itself. The AESOP family of robotic assistants is the first to receive FDA approval and has successfully assisted in over 35,000 minimally invasive surgical procedures, including mitral valve placement and harvesting of the IMA, in over 350 hospitals around the world.

For more information, please browse the Company's Web site at http://www.computermotion.com/

FEATURES

- Direct Surgeon Control with Voice Commands
- Rock-Steady Endoscopic Images
- Articulating Arm Specially Designed for Maximum Flexibility
- Returns the Endoscope to Precise Positions Stored in Memory
- An Invaluable Resource that is available 24 hours a day
- AESOP 2000 can be used in a broader range of MIS Procedures
- Easy System Setup and intra-operative adjustment
- Saves Time and Money

This document contains forward-looking statements concerning the Company's business and products. Actual results may differ materially depending on a number of risk factors, including the risks of obtaining regulatory approval and physicians and/or payers acceptance of the Company's products. Other risks inherent in the Company's business are described in the Company's Securities and Exchange Commission filings, including its Registration Statement of Form S-1 and Quarterly Reports on Form 10-Q. The Company undertakes no obligation to revise the forward-looking statements contained herein to reflect events or circumstances to reflect the occurrence of unanticipated events.

For more information on AESOP, please contact Computer Motion at (805) 968-9600 or browse the Company's Web site at http://www.ctsnet.org/%20www.ComputerMotion.com

COMPUTER MOTION
The Leader in Medical Robotics

TECHNICAL REFERENCE INFORMATION

PRODUCT SPECIFICATIONS (cont.)

System Input Power Requirements:

Voltage:	100/230 VAC switchable
Frequency:	50 to 60 Hz
Current:	3A AC max

General Specifications:

Designed & Tested to:

EN55011/A1	EN61000-4-6
EN61000-4-2	IEC 601-1
EN61000-4-3	IEC 601-1-1
EN61000-4-4	IEC 601-1-2
EN61000-4-5	IEC 601-2-18
	UL 2601

CE mark in accordance with Medical Device Directive 93/42/EEC

CE 0482

Classification:

Class I, Type B, Ordinary Equipment for Continuous Operation

PRODUCT WARNINGS

WARNING: To reduce the risk of electric shock disconnect the endoscope prior to use of a cardiac defibrillator.

WARNING: To reduce the risk of electric shock do not remove the cover. There are no user-serviceable components inside. Refer servicing to qualified personnel only.

WARNING: Risk of explosion if used in the presence of flammable anesthetics.

WARNING: Tissue damage may result if the distal tip of the endoscope is used to probe tissue while the scope is controlled by the Positioning Arm.

WARNING: If the AESOP 2000 System exhibits an unexpected movement, depress and hold the Manual Mode Button. Depressing and holding the Manual Mode Button will cause the System to enter into Manual Mode operation and all motors will become disabled.

COMPUTER MOTION
The Leader in Medical Robotics

TECHNICAL REFERENCE INFORMATION

PRODUCT SPECIFICATIONS (cont.)

Maximum Speed: 3" per second in horizontal direction at tip of Positioning Arm at 15" radius.

Maximum Tilt:
- Positioning Arm with respect to Mount: ±15°
- Positioning Arm from Vertical: ±25°

Number of Re-View™ Memory Positions:
- 3 Re-View memory positions available using Voice Control Interface
- 4 Re-View memory positions available on the Hand Control
  (Positions 1, 2, and 3 are the same as the Voice Control positions.)
- 2 Re-View memory positions available on the Foot Control

Operating Table Rail Dimensions:

U.S.:	International:
.23" to .4" thickness	6mm to 10mm thickness
1.10" to 1.15" height	24.4mm to 25.6mm height

Universal Mount Adaptors available for rail heights: 25mm, 28mm, 30mm, 32mm, 38mm
(Adaptors are for use with Universal Mount Body.)
Rail height tolerance for Mount Adaptors: ±0.5mm

Endoscope Requirements:
- Short Collars available for scope sizes: 5mm, 5.5mm, 10mm, 11mm and 12mm
- Barrel Diameter Tolerance: ±0.1mm
- Custom Collar sizes available upon request

Environmental Specifications:

Operating Temperature:	10° to 40° C
Humidity:	20 to 95% RH
Altitude:	-1,000 to 15,000 feet above sea level
Vibration:	0.2 g, 25 to 500 Hz
Shock:	Positioning Arm: 5g 11 ms half-sine - recoverable position, no damage; Controller: 2 g, 11 ms half-sine
Electrosurgical Compatibility:	Compatible with all known units

Non-Operating/Shipping/Storage:

Temperature:	-30 to +55° C
Humidity:	10 to 95% RH
Altitude:	-1,000 to 40,000 feet above sea level
Vibration:	1 g, 25 to 500 Hz
Shock:	10 g, 11 ms half-sine - no damage
Packaged Drop:	6", any face or corner

COMPUTER MOTION
The Leader in Medical Robotics

TECHNICAL REFERENCE INFORMATION

PRODUCT SPECIFICATIONS

Component Weights:

System Cart:	140 lb
Positioning Arm:	37.5 lb
Controller:	15 lb
Headset Microphone:	.25 lb
Hand Control:	1 lb
Foot Control (optional):	5 lb

Component Sizes:

System Cart:	25"W x 18"D x 40.5"H
Positioning Arm:	Trunk: 6" Dia x 24"H
	Upper Arm: 3" Dia x 18"L
	Forearm: 2" Dia x 14"L
Controller:	11"W x 13"D x 5.5"H
Hand Control:	2.5"W x 4"D x <1"H
Foot Control (optional):	8"W x 8"D x 2"H

Motion Extents: Top view of Positioning Arm

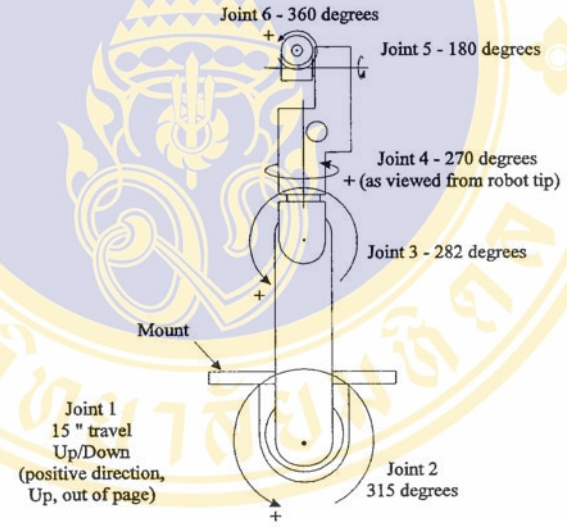

COMPUTER MOTION
The Leader in Medical Robotics

TECHNICAL REFERENCE INFORMATION

REFERENCE ILLUSTRATION

1. Arm Drape
2. Tightening Knobs
4. Endoscope
5. 3-D Manual Mode Button
6. Drape Tapes
7. Forearm
7a. Locking Lever
8. Elbow
8a. Second Elbow
9. Upper Arm
9a. Lower Limit Button
10. Shoulder
10a. Volume Control
11. Mounting Bracket
12. Body
13. Vertical Adjustment Knob
14. Positioning Arm Cable

Foot Control (Optional)

15. Tongue
16. Out Button
17. Circular Pad
18. Re-View Button "A"
19. Foot Control Cable
20. Re-View Button "B"
21. In Button

System Cart

22. Drawer
23. Horseshoe Bracket
24. Fingers
25. Horseshoe Release Button
26. Horseshoe Slide Handle
27. Steering Handle
28. Height Adjustment Crank

Endoscope Collar/Collar Holder (Detail A)

29. Insertion Post
30. Positioning Arm Red Dot
31. Insertion Post Hole
32. Collar Holder
33. Collar Holder Black Arrow
34. Collar Holder Red Dot
35. Hexagonal Spindle
36. Endoscope Collar
37. Gear
38. Mount Levers
39. Tilt Knob

Hand Control (Detail C)

40. Hand Control Cable
41. Set Limit Button
42. Re-View Buttons
43. Circular Pad
44. Out Button
45. In Button

Controller (Details D, E, F)

Detail D

46. Hand Control Cable Coupling
    [or Optional Foot Control Cable Coupling]
48. Positioning Arm Cable Coupling
49. Headset Extension Cable
50. Headset Microphone Jack

Detail E

51. On/Off Switch
52. Ready Light
53. Cable Error Light
54. System Error Light
55. Hand Control Jack
    [or Optional Foot Control Jack]
57. Positioning Arm Jack

Detail F

58. Serial Port
59. Power Cable
60. Grounding Post
61. Power Socket Inlet

Miscellaneous

62. Collar Tool
63. Headset Microphone
64. Microphone Extension Connection
65. PVC Eject Button

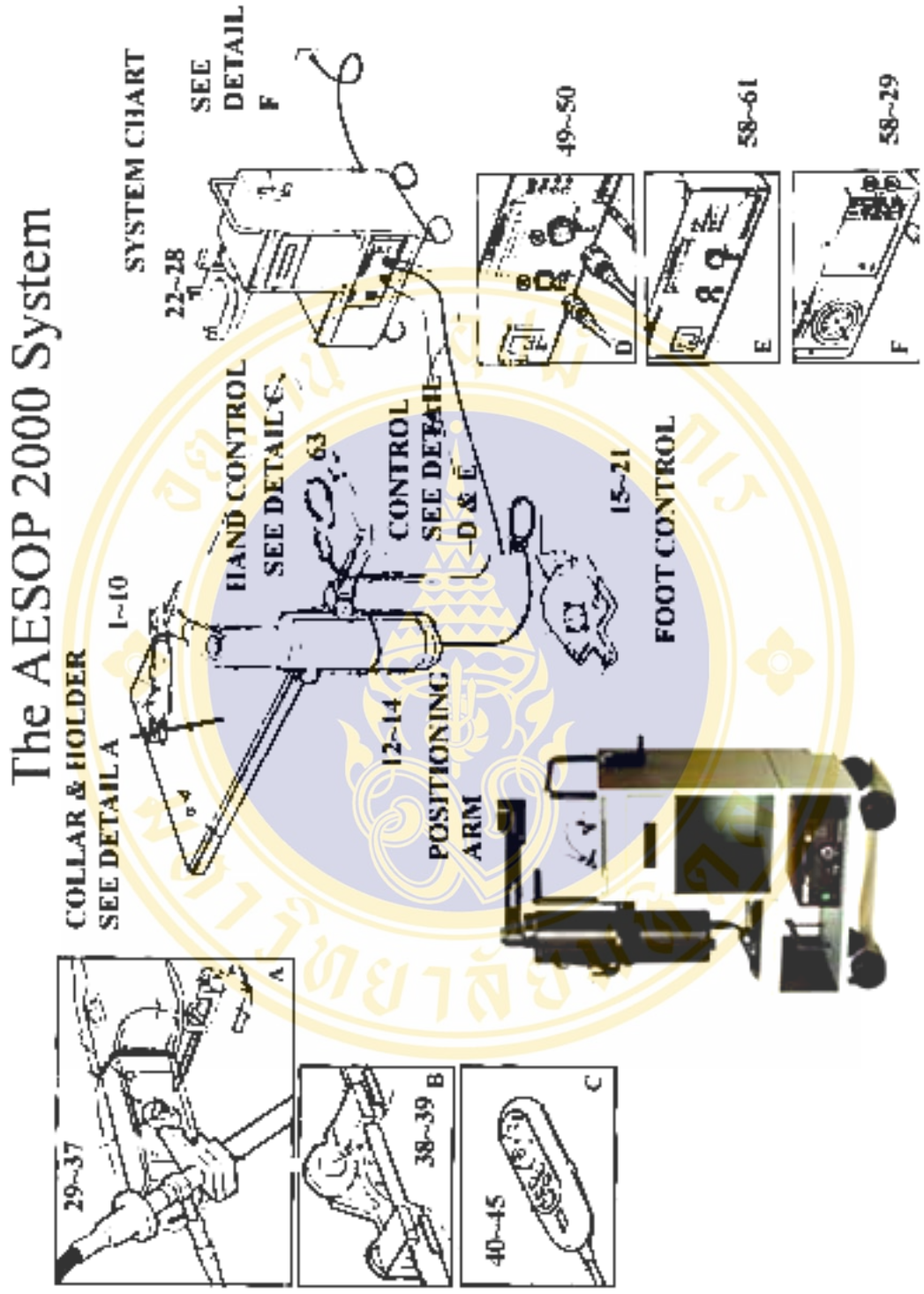

BIOGRAPHY

NAME Mr. Chookiet Nakornnarathorn

ADDRESS 61 Moo 6 Soi. Settakit 7 Mubaan Settakit
Petchakasem Rd. Laksong Bangkae Bkk. 10160
Tel. 02-808-1100 Mobil. 01-838-5941

BIRTHDATE May 26, 1970

PLACE OF BIRTH Wat Trimitvitayaram Bkk.

EDUCATION BACKGROUND

1975-1981 Primary School at ChuelibjingKuang (Chinese School)

1982-1985 Secondary School at Trimitvitayalai School

1986-1988 Pre-University at Trimitvitayalai School

1990-1993 South-East Asia University (Bachelor's degree of Electronics Engineer) Thesis "The Pocket Eprom Programmer"

1998-2003 Mahidol University (Master's degree of Biomedical Engineer) Thesis "A Verbal-Command Robot To Control A Laparoscope In Aids of Surgery: A Prototype Design"

JOB EXPERIENCE

Mar-May, 1993 Technician at ETT Co., Ltd.

Nov-Oct, 1994-1995 Process Engineer at Densei (Thailand) Co., Ltd.

Dec-Apr, 1995-1997 Control Engineer at Chase Enterprise (Siam) Co., Ltd.

Aug-Apr, 1997-2002 Production Engineer at SVI Co., Ltd.

May, 2002-Present Engineer at AFG Asia Satellite Co., Ltd.